

1-1-1983

A study of the effects of consolidation (compaction) on the remanent magnetism of argillaceous sediments.

Frank Reginald Hall

Follow this and additional works at: <http://preserve.lehigh.edu/etd>

 Part of the [Geology Commons](#)

Recommended Citation

Hall, Frank Reginald, "A study of the effects of consolidation (compaction) on the remanent magnetism of argillaceous sediments." (1983). *Theses and Dissertations*. Paper 2334.

This Thesis is brought to you for free and open access by Lehigh Preserve. It has been accepted for inclusion in Theses and Dissertations by an authorized administrator of Lehigh Preserve. For more information, please contact preserve@lehigh.edu.

A STUDY OF THE EFFECTS OF CONSOLIDATION (COMPACTION)
ON THE REMANENT MAGNETISM OF ARGILLACEOUS SEDIMENTS

by

Frank Reginald Hall

A Thesis

Presented to the Graduate Committee
of Lehigh University
in Candidacy for the Degree of

Master of Science

in

Geological Sciences

Lehigh University

1983

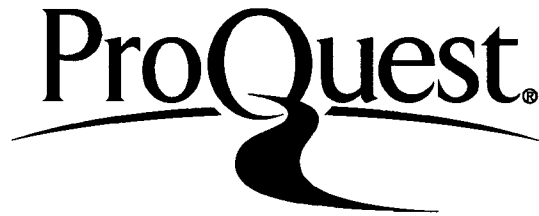
ProQuest Number: EP76610

All rights reserved

INFORMATION TO ALL USERS

The quality of this reproduction is dependent upon the quality of the copy submitted.

In the unlikely event that the author did not send a complete manuscript and there are missing pages, these will be noted. Also, if material had to be removed, a note will indicate the deletion.



ProQuest EP76610

Published by ProQuest LLC (2015). Copyright of the Dissertation is held by the Author.

All rights reserved.

This work is protected against unauthorized copying under Title 17, United States Code
Microform Edition © ProQuest LLC.

ProQuest LLC.
789 East Eisenhower Parkway
P.O. Box 1346
Ann Arbor, MI 48106 - 1346

A Certificate of Approval

a) This thesis is accepted and approved in partial fulfillment of the requirements for the degree of Master of Science.

May 9, 1983
(date)

Professor in Charge

Chairman of Department

Figures		Page
19	Inclination, Declination and Intensity <u>vs.</u> 1- $\Delta H/H$ (marine sediment).....	73
20	Inclination, Declination, and Intensity <u>vs.</u> % Water (marine sediment).	79
21	Inclination, Declination, and Intensity <u>vs.</u> Depth of Burial (marine sediment).....	83

DEDICATION

This thesis is dedicated to the one man, without whom this work would not be complete. He is my first advisor, and I will always look to him for strength and guidance. His constant drive helped me see this to completion. This thesis is lovingly dedicated to my father: Mr. Alexander Alphonso Hall.

Thanks Pops!

Acknowledgements

I am indebted to many people for their assistance in making this thesis a reality. Special thanks are due to Dr. Kenneth P. Kodama, my friend and advisor, for his capable, generous, and enthusiastic guidance through this study. I am also grateful to Dr. Charles Denham and Dr. Dennis Kent for their helpful suggestions and the use of their laboratories. Dr. Joseph Liddicoat, Dr. Lisa Tauxe, and Dr. Dann Spariosau also provided many helpful suggestions for which I am most grateful. Special thanks are also due Mr. Raymond Hall and the U.S. Geological Survey of Woods Hole for their assistance. The writer is also very grateful to Dr. A. Lee Meyerson who made mud a part of my life and has always been generous of his time and encouragement. Finally, thanks are due to my family for their patience and encouragement. I am grateful to my father, Professor Alexander Hall, for typing and proof-reading the manuscript. Special thanks to my mother, Mrs. Warrenie Hall, for her patience and encouragement. Thanks Emila for your company during many hours in the laboratory.

Financial support for this project was provided by the U.S. Geological Survey.

Table of Contents

	Page
Abstract.....	1
Introduction.....	5
Consolidation Theory.....	12
Methods.....	20
Results and Discussion.....	37
Synthetic Sediment.....	38
Marine Sediment.....	70
Model of Compaction Effect.....	87
Summary.....	89
Bibliography.....	90
Appendices	
A. Scanning Electron Micrographs.....	94
B. Depth vs Pressure Table (from Hamilton, 1959).102	
C. Consolidometer Calibration Table.....104	
D. Tables of Experimental Data.....106	
Vita.....	118

List of Figures

Figure	Page
1 The Theoretical Model of the Compaction Effect.....	9
2 Four Possible Orientations of Clay Grains	14
3 Post-Compaction Orientation of Clay Grains.....	16
4 Cumulative Percent <u>vs.</u> Particle Size	21
5 The Karol-Warner Model 350 Consolidometer	29
6. Force <u>vs.</u> Dial Gauge Reading	31
7. %Water <u>vs.</u> $1-\Delta H/H$ (all samples).....	35
8 Inclination <u>vs.</u> $1-\Delta H/H$ (synthetic sediment).....	39
9 Inclination, Theoretical Inclination, and Inclination Corrected for Rebound <u>vs.</u> $1-\Delta H/H$ for samples S3(A), S4(B) and S5(C).....	42
10 Declination <u>vs.</u> $1-\Delta H/H$ (synthetic sediment).....	46
11 Intensity ($10^{-9}Am^2$) <u>vs.</u> $1-\Delta H/H$ (synthetic sediment)	49
12 Inclination, Declination, and Intensity <u>vs.</u> % Water (synthetic sediment).....	51
13 Inclination <u>vs.</u> Depth of Burial (synthetic sediment).....	55
14 Intensity <u>vs.</u> Depth of Burial (synthetic sediment)	59
15 Declination <u>vs.</u> Depth of Burial (synthetic sediment).....	62
16 Change in Inclination <u>vs.</u> Initial Inclination (synthetic sediment).....	64
17 Demagnetization Curves for Samples L1, L2, L4 ..	68
18 Inclination <u>vs.</u> $1-\Delta H/H$ for Samples S3 and S4 ...	71

Abstract

An experiment was designed to study the effects of consolidation (compaction) on the remanent magnetism of wet sediments. The sediments, a kaolinitic rich clay with a mean particle size of 2.7μ , an initial water content of $\sim 100\%$ and an admixture of needle shaped magnetite ($< 0.03\%$ dry weight) with a length to width ratio of 6:1, and a marine carbonate ooze with a mean particle size of 8.8μ , an initial water content of $\sim 175\%$, and a carbonate content of 53% were poured into an acrylic tube, given an anhysteretic remanent magnetization with a peak A.C. field of 100 mT and a D.C. field of 5×10^{-2} mT (the earth's magnetic field with the vertical component nulled by Helmholtz coils) measured in a cryogenic magnetometer and compacted in a Karol-Warner model #350 consolidometer. Consolidation was performed in six successive steps in pressure (loads): 1.34, 2.74, 6.19, 14.34, 28.70, and 57.30 kg/cm^2 , respectively. After each step in pressure, the sample was allowed to rebound by backstepping each load, removed from the consolidometer, measured for its magnetic remanence, then returned to the consolidometer for further consolidation. The pressures attained corresponded to the depths of burial of 25, 55, 110, 225, 415, and 725 meters respectively.

The results of the experiment suggest that consolidation causes a shallowing of magnetic inclination, with

the largest change occurring with sediments having an initial inclination of 45° , no change in magnetic declination, and a decrease in magnetic intensity with most of this decrease occurring in the first 300 meters of burial.

The two sediments showed different trends of change of magnetic inclination. Both sediments had an initial large jump (shallowing). However, further consolidation resulted in a continuing shallowing of inclination for the synthetic sediment, linearly related to the change in volume, while the marine sediment had a sharp steepening of the magnetic vector. After the change in height was $\sim 50\%$, both sediments again showed similar trends in shallowing. Rebound does not appear to affect the resulting magnetic vector.

The difference in the trends of inclination shallowing of the two sediments is believed to be a body effect. Whereas, the compaction of the synthetic sediment can be modeled by simple consolidation theories; the composition of the marine sediment makes it a more complex system.

The experiment was altered for six of the marine samples. Instead of stopping the consolidation procedure after each load, these samples were continuously consolidated until a desired pressure was attained. Thus, only two

magnetic readings were made for each of these samples: the initial measurement before consolidation and the measurement after the desired load was reached. The pattern of change in magnetic inclination of these samples was similar to the pattern for the samples analyzed by the other method. This suggests that the method of consolidation is not important when considering consolidation effects.

Three samples, after compaction, were stepwise demagnetized by alternating field demagnetization to test the hypothesis that consolidation will only affect larger, lower coercivity grains and leave untouched the smaller, higher coercivity grains. The inclination of one sample (L1) increased during progressive demagnetization. However, the inclinations of the other samples (L2 and L4) remained constant during the analysis. Although there is a suggestion that the smaller grains escape compactive forces, this cannot be concluded from these analyses.

A rotational grain model is used to explain the results. As compaction begins, water content is high and the frictional contact between the grains is low. The clay grains move from a random state to one of preferred orientation, with the flat part of the plate rotating to the horizontal plane. This movement of the grains imposes a force on the magnetic grains resulting in rotation to the horizontal.

As the volume decreases the magnetic grains, aligned in the same direction, move closer together. This results in a decrease in magnetic intensity.

Introduction

To understand the processes that affect the ability of sediments to successfully record the earth's magnetic field, it is important to understand diagenesis (Larsen and Chilingar, 1967). Among the most significant aspects of diagenesis which could affect the magnetization of sediment is consolidation (compaction), which results from increasing overburden pressure. This thesis reports on an experimental study of the effects of overburden pressure on the magnetism of argillaceous sediments.

Early laboratory studies of sediment magnetism dealt largely with syn-depositional processes (King and Rees, 1966; Verosub, 1977). As sediment was deposited, the declination of the earth's magnetic field was accurately recorded. However, the magnetic inclination recorded was generally shallower than the field inclination (McNish and Johnson, 1938). This shallowing is referred to as an "inclination error" (King, 1955), and follows the general equation:

$$\tan I_o = f \tan I_f$$

where I_o is the recorded sediment inclination, I_f is the field inclination and f is a constant for the particular sediment.

Griffiths, et al (1960) discovered a larger inclination

error associated with sediments deposited along a bed having a slope (bedding error). This error follows the equation:

$$\tan I_o = \frac{2 \cos \phi}{1 + \cos \phi} \tan I_f$$

where ϕ is the average angle through which the grains roll.

Rees (1961) concluded that the motion of water currents on the top of sediments can result in errors similar to the bedding error.

Some authors have found evidence for inclination errors in the field (McNish and Johnson, 1948; Opdyke, 1961; Irving, 1969; Noel, 1981). McElhinny (1973) does not believe that these errors are important because of post-depositional changes occurring within the sediment.

Harrison (1966) concluded that deep-sea sediment cores from the Pacific Ocean accurately recorded the earth's magnetic field. He attributed this result to the stirring action of Brownian motion and bioturbation causing the magnetic grains to realign themselves with the earth's magnetic field.

Kent (1973) found that deposited slurries, stirred in a known field, accurately recorded the field inclination. A piston core studied by Kent (1973), which had strong evidence for bioturbation, showed no inclination error.

Although it can not be concluded that bioturbation is necessary for inclination errors to be removed, it does appear to have some importance in deep-sea cores.

The water content of a sediment appears to determine when a sample will acquire a remanence. The depth, within the sediment column, where the remanence is acquired is termed the lock-in depth (Verosub, 1977). Bioturbation generally occurs where the water content is highest (Hamilton, 1976). Kent (1973) suggested that lock-in is possible at high water contents. Khramov (1968) discovered that deposited sediments with water contents >70% were affected by changes in a magnetic field after deposition while sediments with water contents <30% felt no changes in the magnetic field. Verosub et al (1979) monitored the magnetism of various types of wet sediments with initial water contents ranging from 560% to 60%. They noted no change in magnetism for the samples used except for one sample: a terrigenous clay with an initial water content of 370%. They concluded that the water contents of the sediments were initially too low to yield changes as the samples dried.

Barton and McElhinny (1970) deposited sediments slowly over a period of nine months. They reported an accurate recording of the applied field with a remanence, having water contents as high as 90%. Although a small

inclination error of $>10^{\circ}$ was noted, they suggested that this was a result of the partial drying of the sediment.

Løvlie (1974) performed depositional experiments where magnetic field reversals were simulated during deposition. His experiments demonstrated a "down-core" displacement of the zone where the reversal took place, i.e., the sediments older than the actual reversal recorded the reversal. His experiments also showed an increase in magnetic intensity in sites of higher temperature during deposition.

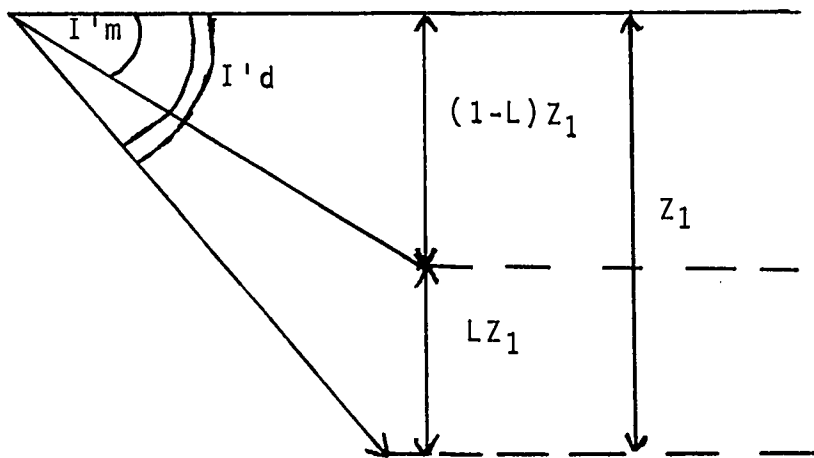
Factors controlling the paleomagnetic accuracy of sediments have been explained experimentally by various authors.

Blow and Hamilton (1978) performed depositional experiments using silty clays deposited in two modes: grain by grain settling of the sediment in a column, and as slurries. In their experiments, sediments were deposited in still water and, after deposition, allowed to settle under their own weight. Over time, each of the deposits acquired an inclination error ranging from 19.4° to 41.7° , with the smaller error associated with the slurry deposit. The model they developed to explain the effects of compaction on the magnetic record is shown in Figure 1.

Henshaw and Merrill (1976) noticed a decrease in magnetic intensity of sediments allowed to dry in the presence of a magnetic field. By using magnetic grains of

Figure 1 - The Theoretical Model of the Compaction Effect

The model proposed by Blow and Hamilton (1980) is given by the equation: $\tan I'm = (1-L)Z_1 \tan I'd$, where $I'd$ is the original inclination, $I'm$ is the compactive inclination, Z_1 is the original sample height, and $(1-L)$ is the ratio of the change in sample height.



known shapes and sizes in a synthetic sediment, they noticed a difference in the amount of change in magnetic intensity associated with the differing grains and suggested that grain shape affects the accuracy of paleomagnetic signal.

Tucker (1980) performed laboratory analyses monitoring the change in magnetism as sediments dried. He noticed a range of water contents (65% to 75%) through which the magnetism of the sediment is locked-in. He modeled his results as rotation of magnetic grains in voids when water content is high and the frictional contact of the grains is low. As the water content decreases, the frictional contact increases. A point is reached where the frictional contact cannot be overcome by the magnetic field acting on the grains.

Previous depositional experiments (Kent, 1973; Løvlie, 1974; Blow and Hamilton, 1976; Verosub, et al, 1979; Tucker, 1980) have dealt with surface or near surface (upper 15 meters of sediment) acquisition of DRM. Only a few studies have attempted to model what occurs after overburden is applied.

Otofuji and Sasajima (1980) attempted to model post-depositional processes by consolidating in a centrifuge. They suggested that the density of the sediment rather than time is significant in determining what the post-depositional

remanence can be. However, Otofujii and Sasajima could not accurately measure the change in sample height by centrifuging because they could not account for any rebound that may have occurred in the sample (Reike and Chilingarian, 1974).

Hamano (1980) studied post-depositional remanent magnetization by slowly compacting sediments in a consolidometer regulated by allowing water to enter a vessel at the top of his machine. His sediments successfully recorded the magnetic field. His analysis is a good model of the PDRM process at sediment depths of 15 meters or less.

The experiments reported here attempt to model consolidation effects at much greater depths (down to 700 meters). A consolidometer is used to apply a load to a previously magnetized wet clay with magnetite intermixed. The procedure used has the advantage of being able to continuously measure the change in sample height and the pressure applied to the sample. The experiment allows the determination of changes in water content during analysis.

Consolidation Theory

To understand the way sediments compact, consolidation theories have been proposed (Reike and Chilingarian, 1974). Because coarse grained sediments consolidate

differently than fine grained sediments, and because the material used in these experiments is clay, the following discussion will deal with the consolidation of clay sediments.

Rieke and Chilingarian (1974) state that clay particles can deposit with four possible orientations (Figure 2):

1) unflocculated dispersed, 2) unflocculated with edge-to-edge contacts, 3) flocculated-dispersed, and 4) flocculated with edge-to-edge contacts. When initially deposited, these four different orientations will have random arrangement, with a high porosity. The deflocculated-dispersed arrangements will tend to be most closely packed with the lowest initial porosity of the four orientations. As overburden pressure is applied to the clay sediment, pore volume decreases as water is expelled from the pore spaces. The clay particles move closer together, and will take a preferred orientation with the flat area of the clay aligning itself parallel to the horizontal (Figure 3).

Aylmore and Quirk (1960) proposed the turbostatic orientation of clays. In this structure, clays are grouped into domains and pore spaces occur between domains of clay groups. Domains consist of a series of parallel plates of clay minerals (Aylmore and Quirk, 1960). These domains are arranged in a random order, or what has been referred to as "turbostatic groups" (Aylmore and Quirk, 1960).

Figure 2 - Four Possible Orientations of Clay Grains

Given by Reike and Chilingarian (1974), they are
1) unflocculated-dispersed, 2) unflocculated with edge-
to-edge contacts, 3) flocculated-dispersed, and 4)
flocculated with edge-to-edge contacts.

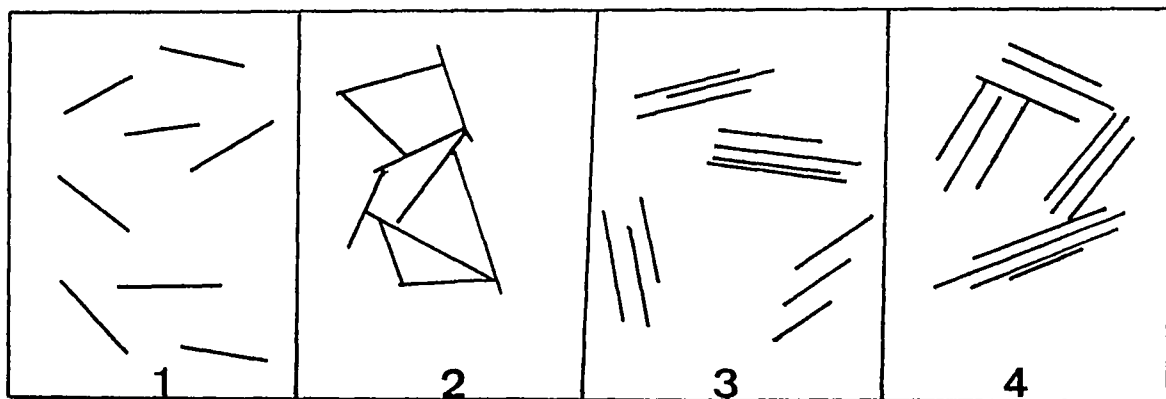
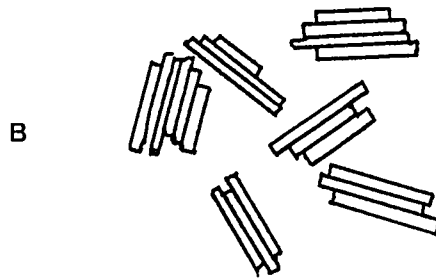
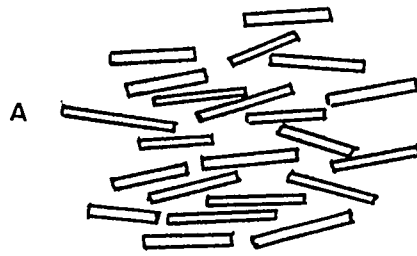


Figure 3 - Post-Compaction Orientation of Clay Grains

After compaction, clay grains move from a previously random arrangement to a preferred orientation, with the flat part of the plates moving to the horizontal plane. A. non-turbostatic structure, B. turbostatic structure. (from Meade, 1968).



Müeller (1967) states that agillaceous sediments, with an initial porosity of 80%, will undergo very rapid water expulsion and grain reorientation to a depth of 500 meters below the sediment surface. Below 500 meters, the rate of water expulsion and grain reorientation slows greatly.

In a study of marine cores, Hamilton (1976) found that the initial reduction in porosity at depths less than 100 meters below the sea floor was less than suggested from consolidation models, and that the rapid reduction in porosity occurred at depths as great as 600 meters for terrigenous deposits.

With electron microscopy of clays under applied loads, Bryant, et al (1974) showed that the grain orientation went from random at zero pressure to preferred orientation at higher pressure. Bowles (1968) studied the microstructure of Gulf of Mexico clays and showed the tendency for preferred orientation with depth of core.

Meade (1968), while studying sediments of central California demonstrated that some clays undergo changes in porosity faster than others. He found that kaolinite and illite undergo changes in porosity faster than montmorillonites. Meade also showed that the rate of sediment compaction is a function of the types and amounts of absorbed cations on the clays, the interstitial water electrolyte concentration, acidity of the solution and temperature.

Studies off Oregon (Carson, 1977) have demonstrated that areas of high tectonic activity may have a faster water expulsion rate than areas of low tectonic activity because water is squeezed out by forces of tectonism.

Methods

The sediments used in this experiment were a synthetic clay and a marine calcareous ooze with an initial carbonate content of 53%.

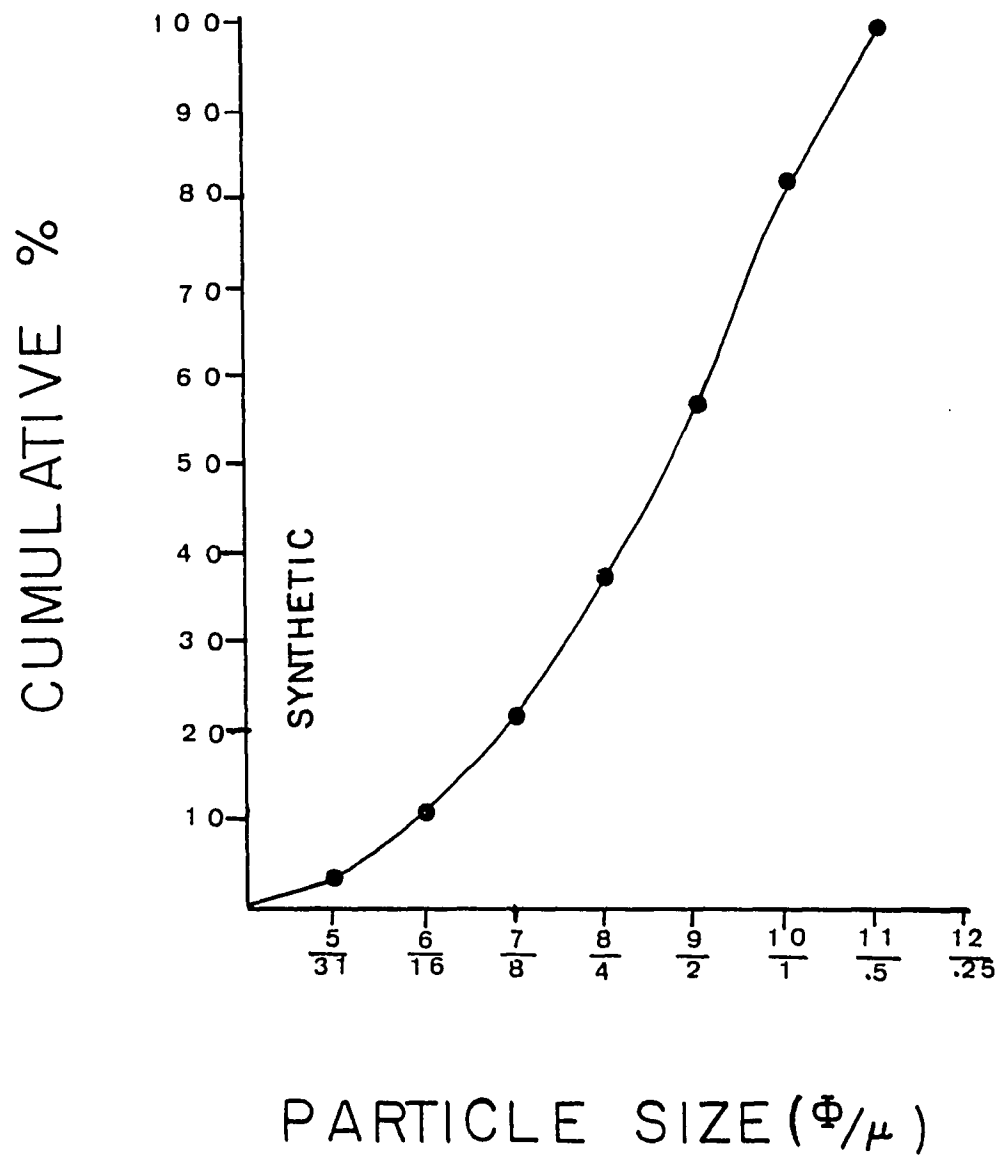
The synthetic sediment was basically a mixture of quartz and kaolinite commercially designated as "½ Champion and ½ Challenger". It is distributed by Spinks Clay Company, Tennessee. Particle size analysis of the sediment (Coulter Counter, Model TA II) shows it to have a mean particle size of 8.5ϕ (2.7μ), with only 0.1% of it being larger than 4ϕ (63μ) (Figure 4). The grain size analysis was performed without the addition of magnetite.

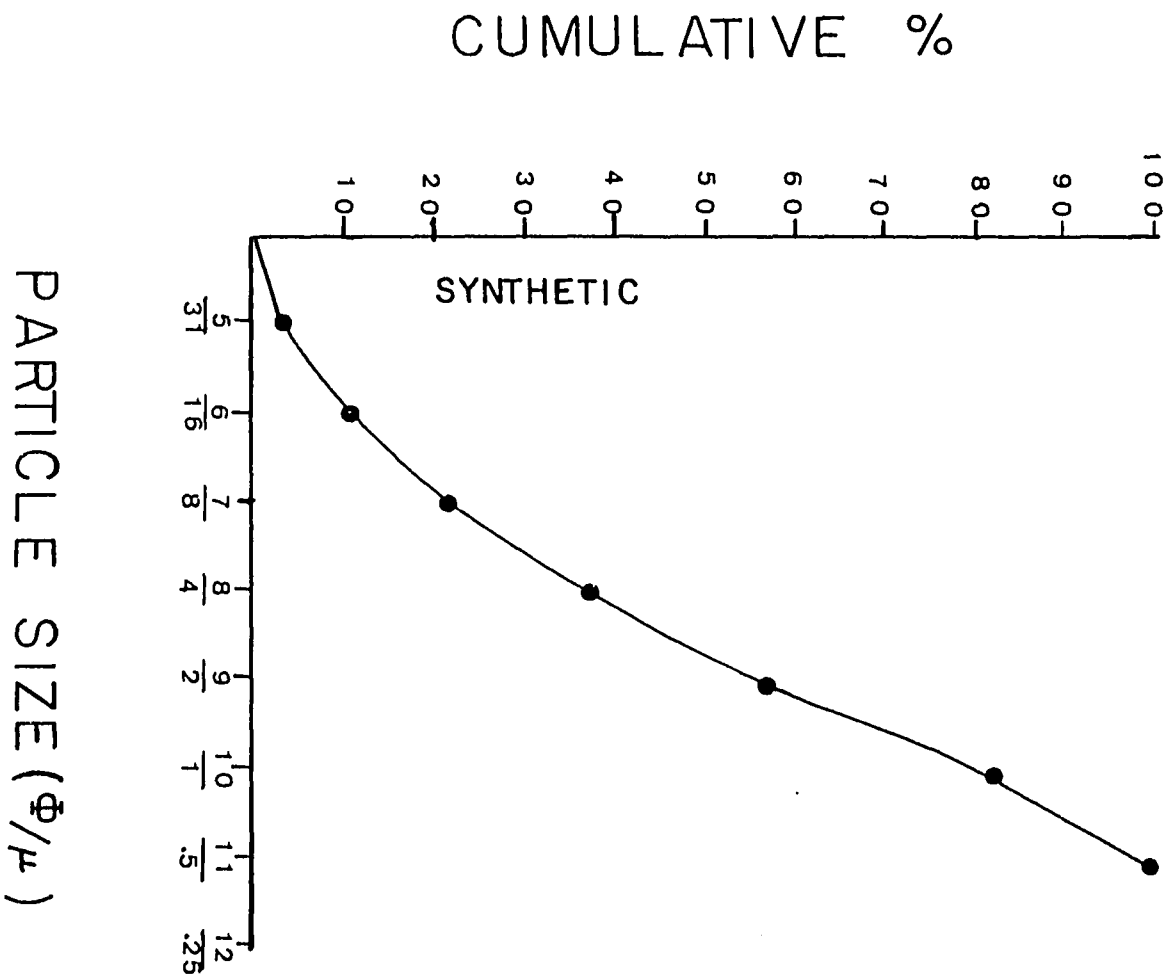
Needle-shaped magnetite was added to the dry sediment to make it magnetic. The magnetite has an average length of 0.45μ on its long axis (Pfizer Chemical Company, Data Sheet, 1979) and a length to width ratio of approximately 6:1. The amount of magnetite added to the sample did not exceed 0.03% dry weight in order to prevent the sample from becoming too magnetic for the cryogenic magnetometer and to reduce the effect of magnetic interactions between grains.

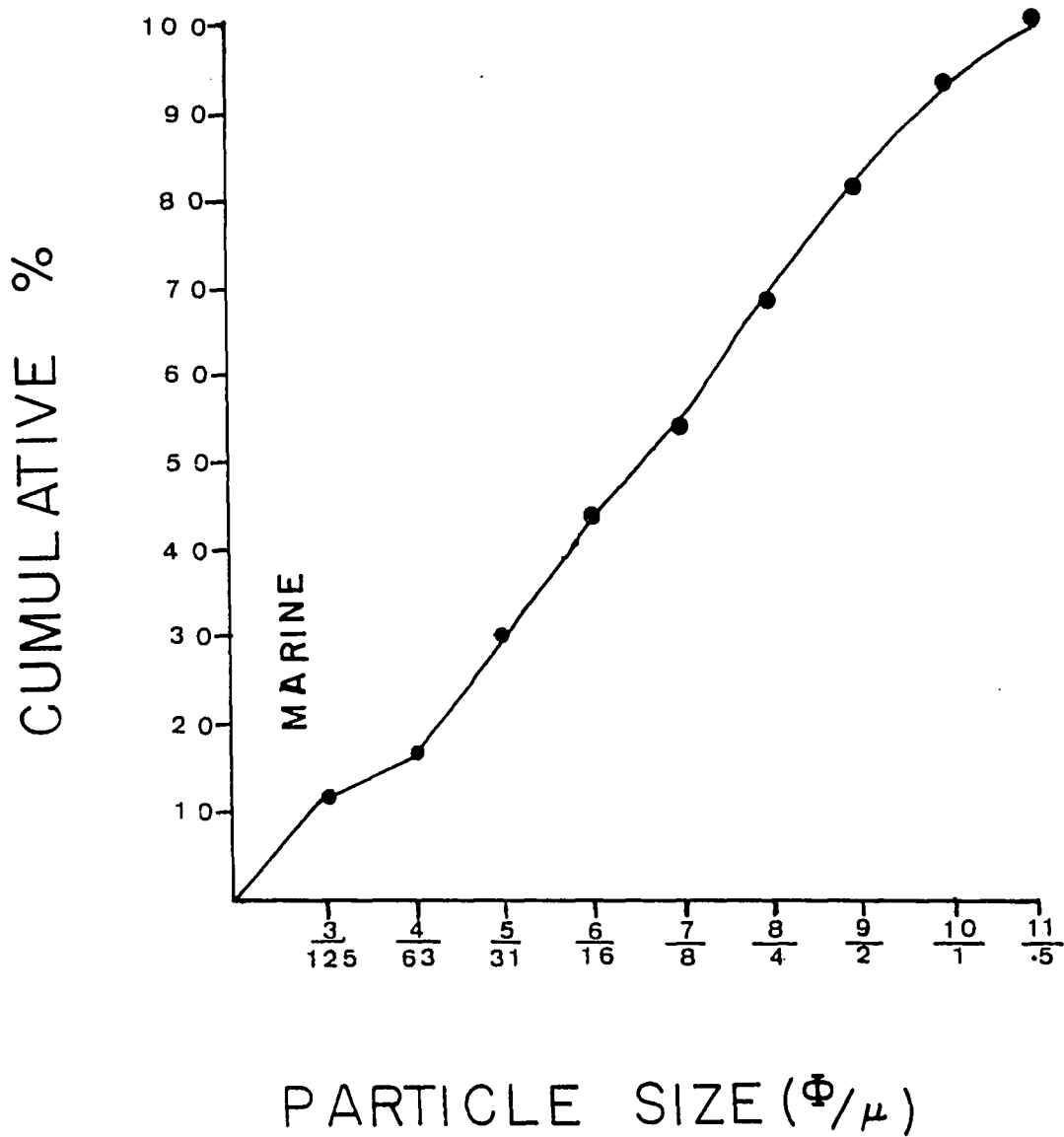
Before the magnetite and sediment were mixed, the magnetite was dispersed using a #230 U.S. Standard Sieve to reduce the clumping together of magnetic grains. They were combined as dry powders.

Figure 4 - Cumulative Percent vs. Particle Size

The synthetic sediment has a mean size of 2.7 μ and the marine sediment has a mean size of 8.8 μ . Less than 1% of the synthetic sediment is larger than 63 μ , while 15% of the marine sediment is larger than 63 μ , and consists predominately of foraminifera and foraminiferal fragments.







Distilled water was added to this mixture bringing its water content to approximately 100%, where water content is defined as $(W_w - W_d)/W_d$. W_w is the weight of the wet sediment and W_d is the weight of the sediment dried at 100°C for 24 hours.

A second sediment was a core from Timor Islands. It was mixed with distilled water to a water content of ≈160%. The marine sediment had a mean particle size of 8.8μ(6.8φ), with 15% of it being larger than 4φ. The coarse fraction (>64μ) consists mostly of foraminifera and foraminiferal fragments. Coccolith plates are abundant and easily seen with the SEM (Plate 3). Magnetite was not added to the marine sediment.

An acrylic tube 2.54 cm in inner diameter, with a wall thickness of 0.32 cm, and a length of 6.4 cm was used to house the artificially magnetic sediment during the experiments. A snugly fitting non-magnetic porous stone was placed into the bottom of the tube. The wet sediment was poured into the tube. A non-magnetic rod, usually a blunt pencil, was placed in the tube and moved in an up and down motion. This procedure removed air pockets that were formed during the pouring process

A second loosely fitting porous stone was gently placed on top. The tolerance of the second porous stone

and the tube wall must allow the stone to slide freely through the tube but not be so great that the sediment will flow out of the tube when the consolidation procedure begins. For this experiment, a tolerance of not more than 0.0765 mm was found to be best.

The porous stones used in this experiment were compressed pellets of carborundum and diatomaceous earth. They tended to acquire remanences during the anhysteretic remanent magnetization application even though they were composed of nonmagnetic materials. This remanence was probably due to small magnetic particles emplaced in the stone during machining. The stones were soaked and boiled in hydrochloric acid. However, the remanence was not removed. The remanence was two orders of magnitude (10^{-11} Am^2) less magnetic than the remanence acquired by the synthetic sediment (10^{-9} Am^2). Thus the magnetic effect of the stones during the measurement would be insignificant.

The porous stones used with the synthetic sediment were magnetically only one order of magnitude less than the marine sediment (10^{-10} Am^2). Hence, two acrylic plugs of 0.625 cm diameter with holes running through them were made to be used in the place of the porous stones.

A piece of filter paper is placed between the porous stones and the sediment. This is necessary to prevent the sediment from clogging the porous stones.

The sample was given an anhysteretic remanent magnetization (ARM) (Stacey and Banerjee, 1974) by a peak alternating field of 100 mT applied in the presence of the horizontal component of the earth's magnetic field (approximately 0.05 mT): the vertical component having been nulled by Helmholtz coils.

Blow and Hamilton (1978) suggest that a sample magnetized parallel or perpendicular to the axis of consolidation should not undergo any change in magnetization during consolidation because no torque would be applied to the sample's magnetization to cause it to rotate. The greatest change due to compaction would occur when the initial inclination is 45° (Denham, C., personal communication). Hence, the samples were magnetized between the angles of $\sim 20^{\circ}$ to $\sim 70^{\circ}$ from the horizontal.

If the sample did not acquire the proper magnetic inclination during the ARM process, the procedure was repeated until the proper inclination was achieved.

The measurements of the sample magnetization was made using a Super-Conducting Technology 2-Axis cryogenic magnetometer. A sample holder was fashioned by taking a Coulter Counter Accuvette, which has a round top and a square bottom, and epoxying a square piece of plastic the size needed to fit the sample holder of the magnetometer to the bottom. A line was drawn down one of the faces of

the sample holder and the length of the acrylic tube for the purpose of sample orientation.

The sample was consolidated at six successive steps of pressure: 1.34, 2.74, 6.19, 14.34, 28.7, 57.30 kg/cm². After the sediment was consolidated to each of the successive steps in pressure, it was allowed to rebound in the consolidometer. Pressure was released by backstepping to each point of pressure until the initial pressure of 1.34 kg/cm² was achieved. The sample was removed from the consolidometer, when there was no more change in sample height, and placed inside the magnetometer for measurement. The sample was then returned to the consolidometer and subjected to a pressure of 1.34kg/cm². This procedure was followed to estimate the amount of rebound that occurred while the sample was out of the consolidometer being measured for magnetic properties.

During the course of this experiment, it was decided to alter the consolidation procedure for the marine sediment. Instead of performing magnetic measurements after each successive step in pressure, the sample would remain in the consolidometer until the consolidation was completed to a given pressure step. Thus, for each sample, only two magnetic measurements were made: the initial measurement before consolidation, and the final measurement after consolidation.

The consolidometer used is a Karol-Warner Model 350 Consolidometer (Figure 5). The unit works by applying force to the bottom plate, which moves upward towards a fixed crossbar. The sample to be consolidated rests between the movable plate and the crossbar. Air pressure provides the force for consolidation. The pressure is regulated by three valves. The first valve controls the amount of air entering the unit. A dial gauge is used to determine the magnitude of the force being applied. The second valve allows air to flow to the movable plate. The third valve releases the air pressure.

The consolidometer was calibrated using a Balwin Model 60 cs Tensile Test Machine. It consists of a large bar which is lowered onto an object to apply a range of forces (from 0 to 60,000 pounds) to an accuracy of 0.1%.

To calibrate the consolidometer, the crossbar of the tensile test machine was lowered so as to rest just above the movable plate of the consolidometer. The tensile test machine's electronic stress gauge would read zero pounds. When the compressed air is allowed into the consolidometer, the movable plate would move upward, strike the crossbar of the tensile test machine, and thus apply a force to the crossbar. The electronic stress gauge would read this as though the tensile test machine was applying the force and would allow calibration of the consolidometer's pressure

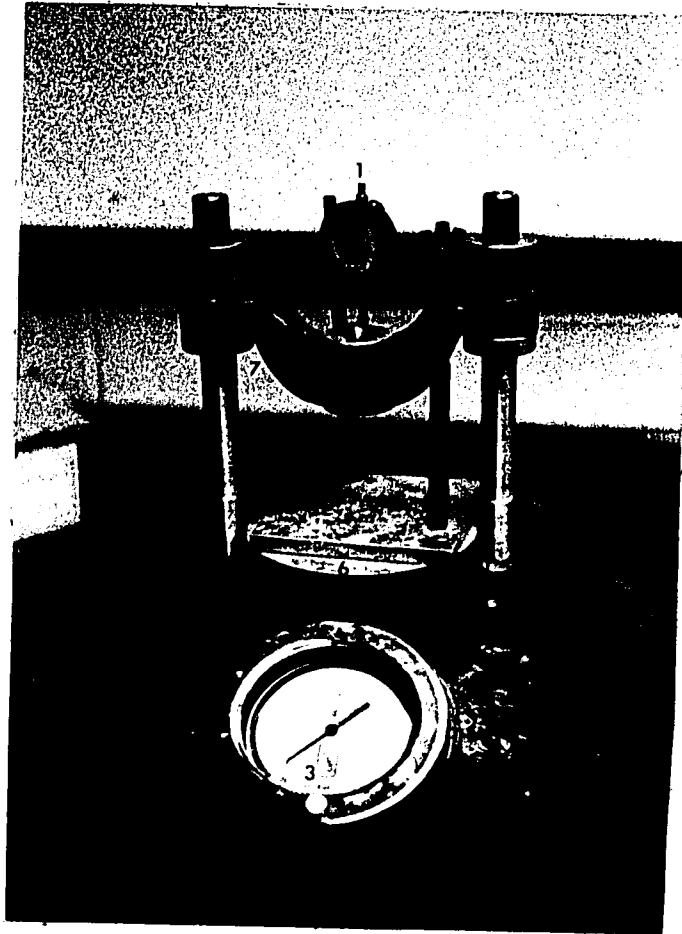


Figure 5 - The Karol-Warner Model 350 Consolidometer

- 1) the gauge used to determine sample height,
- 2) the first intake valve, 3) the pressure gauge,
- 4) the second intake valve which allows air to go to the movable base plate, 5) the outtake valve, 6) the movable base plate, and 7) the fixed cross bar.

gauge. Figure 6 is the calibration curve for the consolidometer.

The procedure for laboratory consolidation is similar to the ASTM standard procedure (1970) with a few modifications (see also Bowles, 1970). The modifications were necessary because the sample holder must be able to fit into a cryogenic magnetometer with an aperture size of 3.81 cm (Woods Hole's magnetometer).

The sample to be consolidated was placed between the movable plate and the crossbar of the consolidometer. To assure equal pressure distribution and water escape during consolidation, a loose fitting acrylic plug, with holes running through it and a steel ball (1.27 cm diameter) placed into the divot at the center of the plug, was placed between the sample and the crossbar. A large porous stone was placed under the sample.

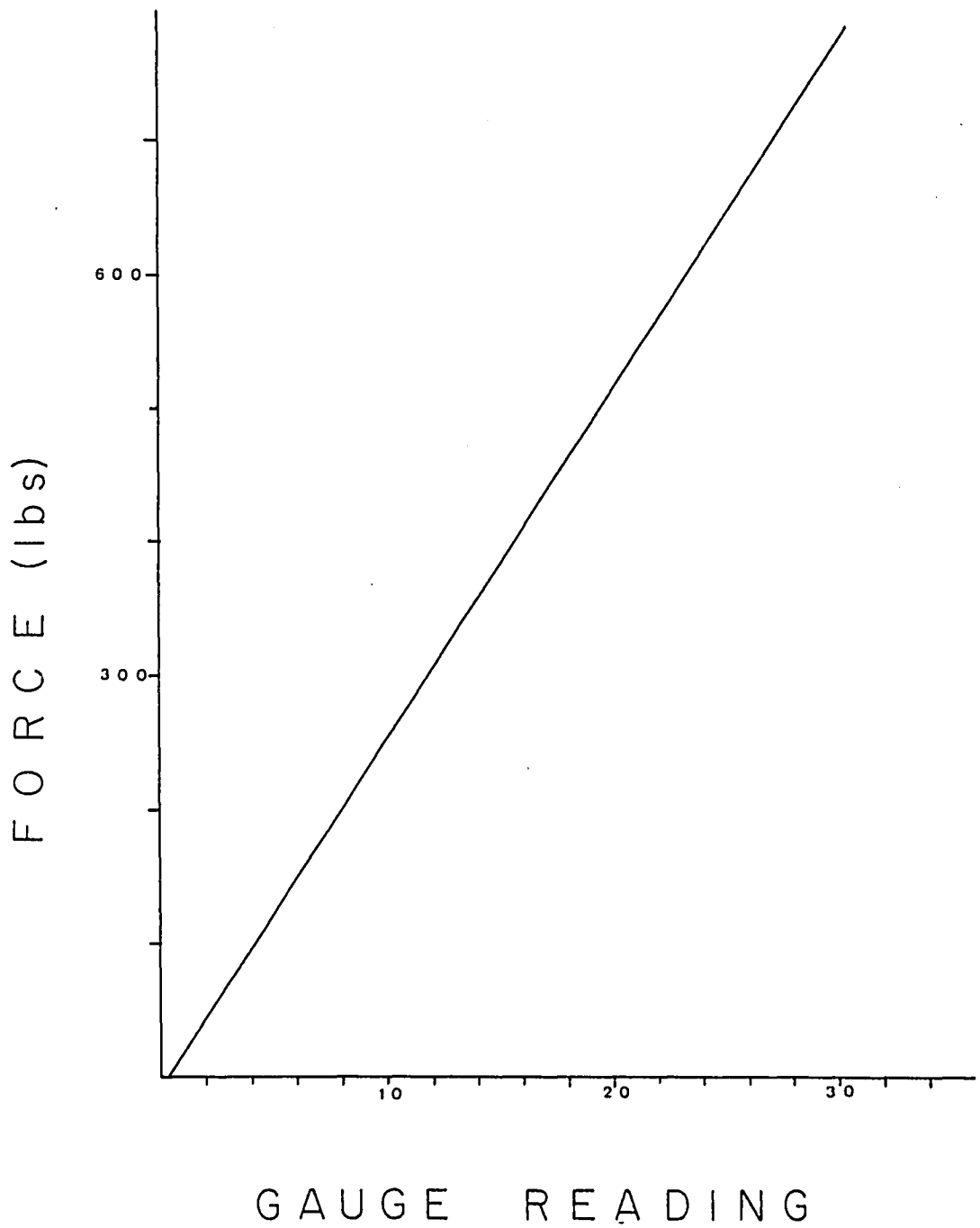
A Scherp-Tumico Model B1-1 test gauge was used to measure the change in sample height. This gauge has an accuracy of $\pm 2.54 \times 10^{-4}$ cm. The sample height (H) associated with each load was calculated by:

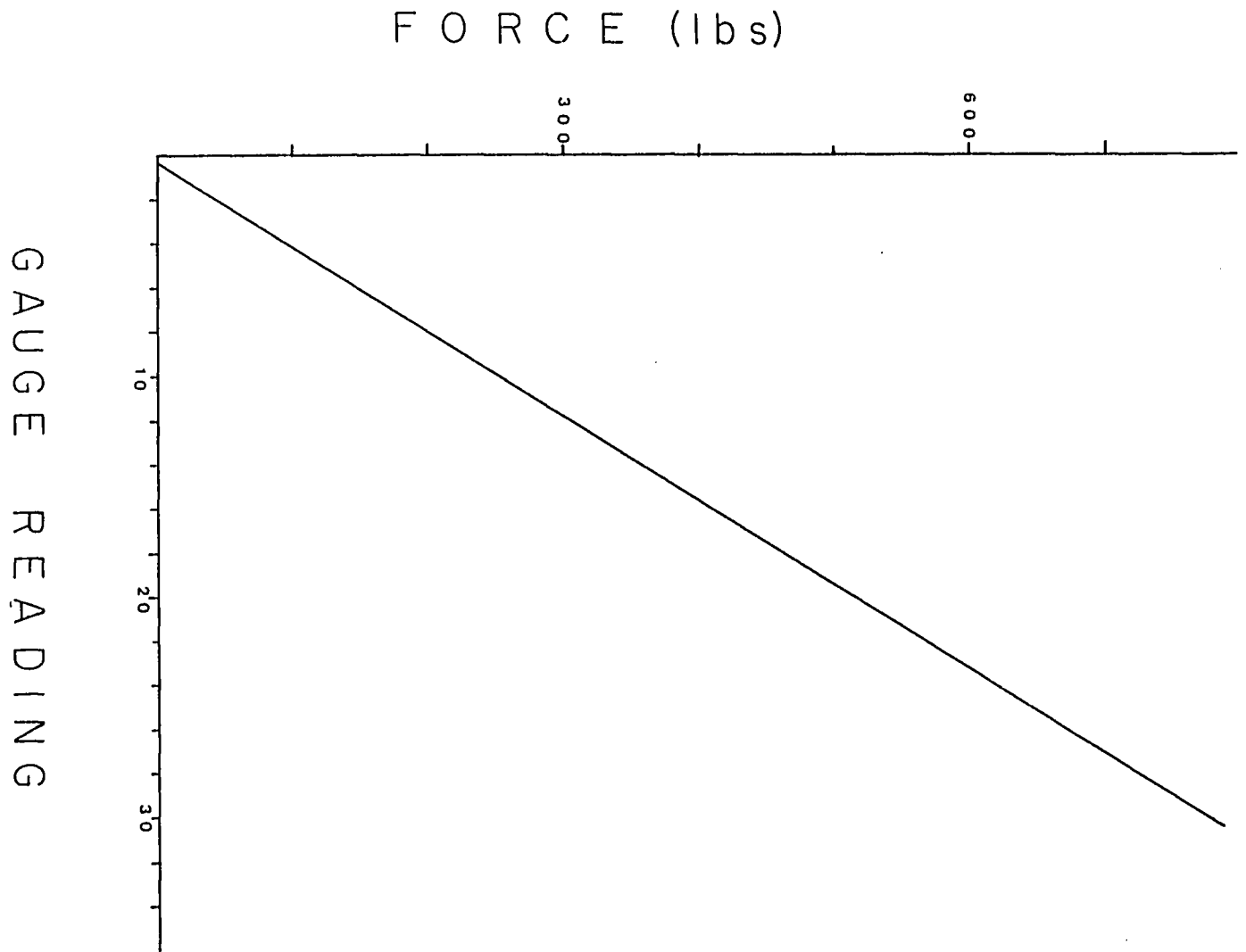
$$H = H_0 - \left(\sum_{n=1}^n H_c - \sum_{n=0}^{n-1} H_r \right)$$

Where H_0 is the original height, H_c is the height caused by compaction, H_r is the height caused by rebound and n is the load number.

Figure 6 - Force (pounds) vs. Dial Gauge Reading

The calibration curve for the consolidometer was calculated using a Baldwin 60 cs tensile test machine.





Some of the synthetic sediment was examined with a scanning electron microscope (SEM) in an attempt to see the effects of consolidation on the alignment of clay grains and to see how the magnetic grains were distributed in the clay (Plates 2-4). Compacted and uncompacted clays were allowed to dry in air at room temperature for a period of one to two days. Small pieces of each were placed onto SEM studs and coated with gold to ground the samples. They were then placed inside the SEM and pictures were taken.

The results of this experiment were disappointing. The clays, by the drying process alone, aligned themselves. It was difficult, if not impossible, to differentiate between the compacted and uncompacted sediments.

When high energy electrons strike a sample, x-rays are emitted at wavelengths characteristic of the individual atoms hit by the beam (Skoog and West, 1971). This concept is utilized in x-ray dispersive techniques to determine the composition of materials. When the electron beam of the SEM strikes a magnetite grain, the amplitude of the Fe-peak will suddenly increase above some background level. The K-Vex analyzer with the SEM was used in an attempt to locate magnetite in the sediment.

Except for one grain, the Fe-peak never became higher

than background level. The grain was large ($\approx 40\mu$) and euhedral in shape (Plate 6). This is not considered to be characteristic of the magnetite in the sediment. Its size conforms to grains of the multidomain type (McElhinny, 1976). The grains that were of interest are the single and pseudosingle domain grains which are believed to be the grains which carry the remanent magnetism of the sediments (Stacey and Banerjee, 1974)

To estimate the percent water, It is assumed that the loss of volume of sample results only from the loss of water during the consolidation procedure. The total volume, V , equals the sum of the volume of water, V_w , and the volume of sediment, V_s . The volume of sediment is constant because the porous stones prevent the escape of sediment. The change in volume can be given by:

$$\Delta V = \Delta V_w + V_s$$

If the porous stones are too loose, the sediment will ooze out of the tube when pressure is applied. When this occurred, the sample was discarded and a new sample prepared. Figure 7 is the graph of the percent water change for all samples.

The depth of burial equivalent to the load applied was calculated using the depth vs. pressure table of Hamilton (1958) (Appendix 1) calculated for shale.

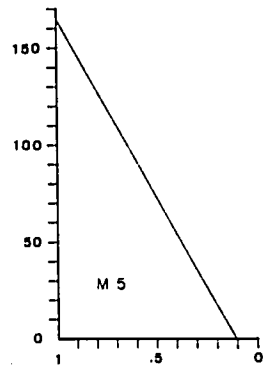
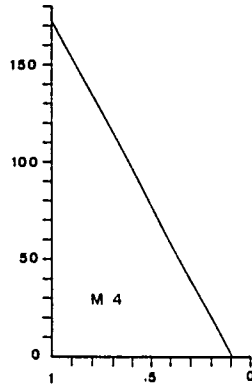
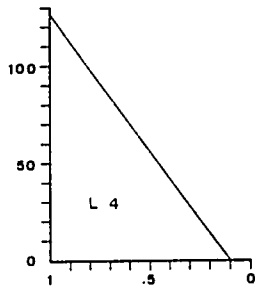
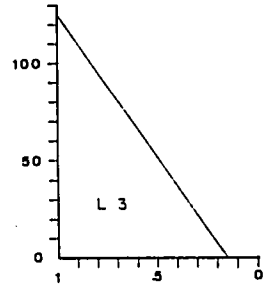
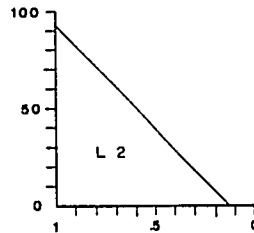
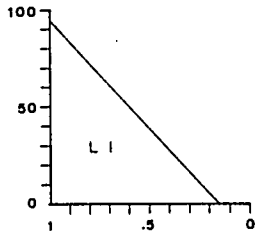
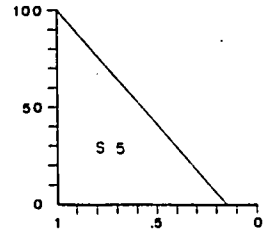
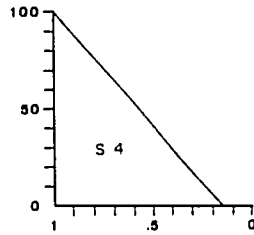
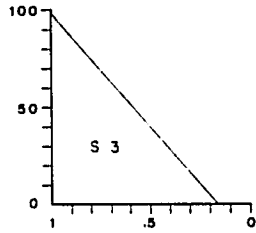
Figure 7 - % Water vs. $1-\Delta H/H$ (all samples)

The procedure for calculating the % water is outlined in the text. A line is drawn connecting the % water in the beginning and the end of the analyses.

Figure 7 - % Water vs. $1-\bar{\Delta}H/H$ (all samples)

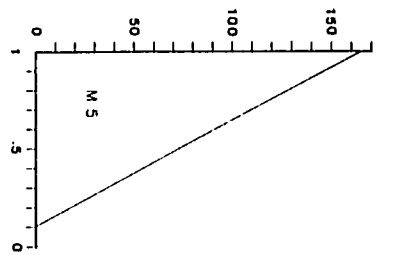
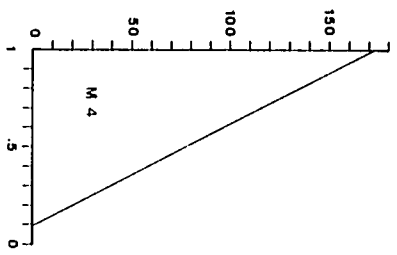
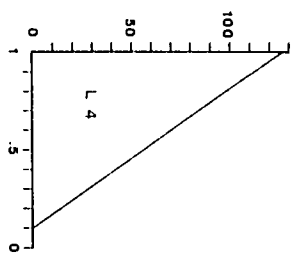
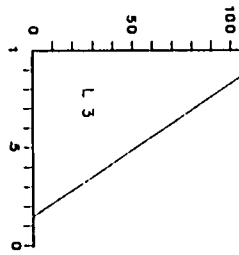
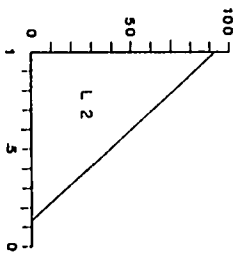
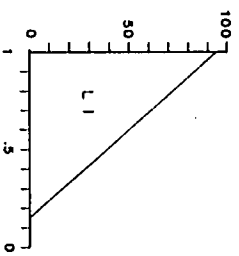
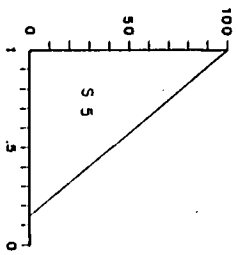
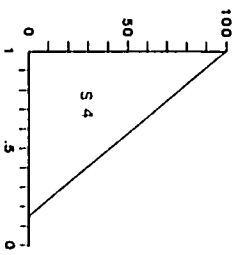
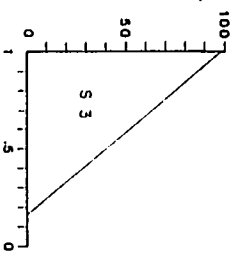
The procedure for calculating the % water is outlined in the text. A line is drawn connecting the % water in the beginning and the end of the analyses.

% WATER



$$1 - \Delta H / H$$

% WATER



$1 - \Delta H / H$

Results and Discussion

The data is presented in graphical form within the text with data tables in the appendices.

Seven analyses were performed from the synthetic sediment, three samples (S3, S4, and S5) from the first batch of sediment prepared and measured at Woods Hole Oceanographic Institute (WHOI). Four samples (L1, L2, L3, and L4) from the second batch of sediment were analyzed at Lamont Doherty Geological Observatory (LDGO).

The two batches of sediment did not consolidate the same amount even though they were made from the same material. This was expected. Keller (1976) reported on three short sediment cores taken 20 cm apart in the Gulf of Mexico. Although they showed the same horizons down core, their individual physical properties differed. Thus the differences in consolidation patterns of the two batches were expected. However, the changes in magnetic remanences were similar, and are grouped together.

The marine sediment had eight analyses performed, all at WHOI. Two of the samples (M4 and M5) were analyzed in a fashion similar to the synthetic samples. Six samples were analyzed by not stopping the consolidation until a particular load was reached (Mc samples). The change in magnetic remanence of the marine samples is markedly different from the synthetic sediment and are grouped separately.

Synthetic Sediment

Figure 7 is a graph of magnetic inclination vs. $1-\Delta H/H$, rebound excluded. This shows a shallowing of the magnetic vector of all samples as consolidation proceeded. There was a large jump in the magnetic inclination as the initial pressure was applied. This probably results from the sudden shock imposed on the sediment column. It is during this initial loading that the largest volume change occurs, and the grains go from random orientation to a state of preferred alignment. The rapid pace of this change is believed to cause the resulting initial jump in the inclination.

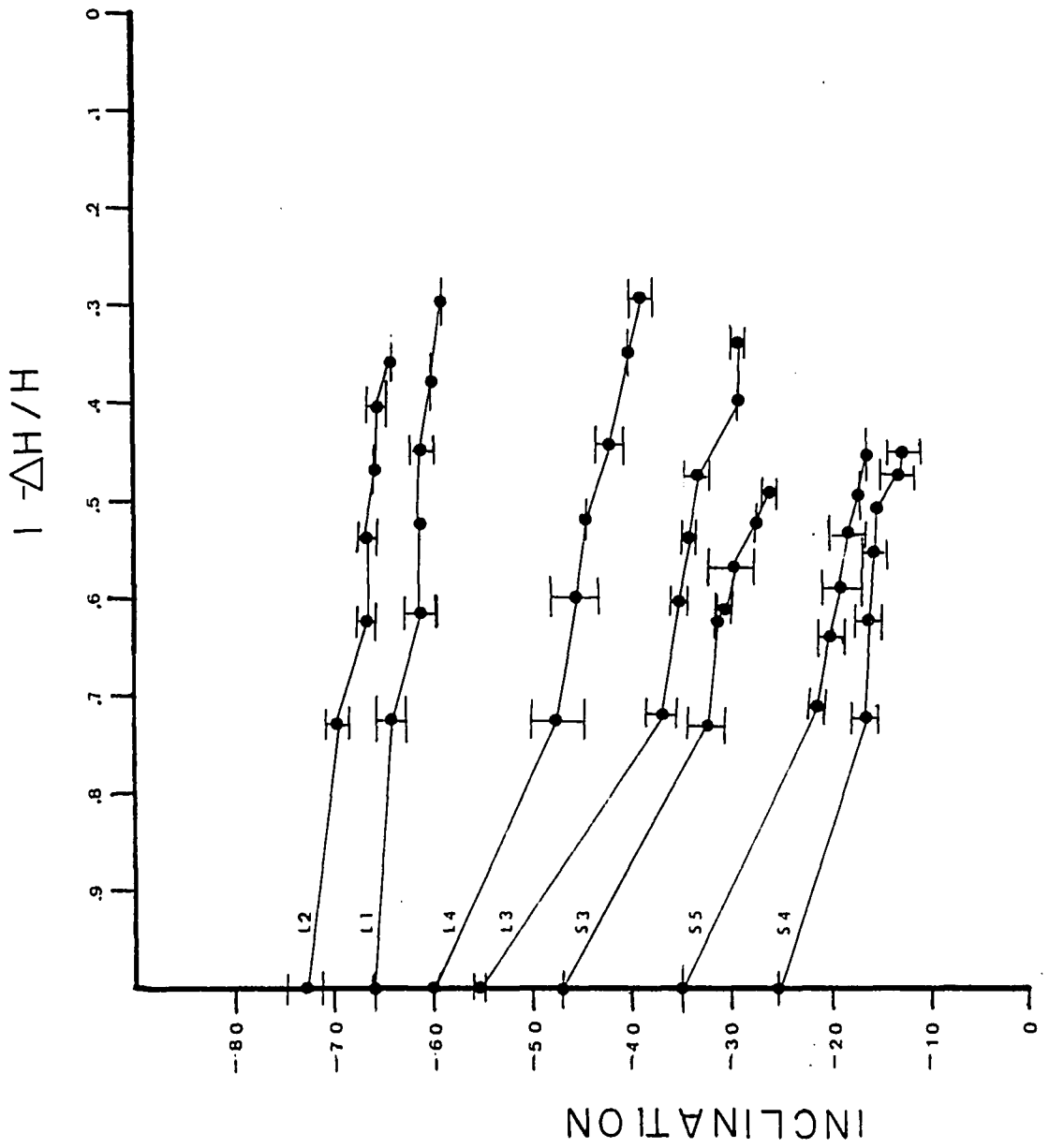
In comparison, when Hamano (1980) performed his compaction analyses, his samples, which were slowly compacted to a pressure equalling the initial load of this experiment, did not show large deviations from the applied magnetic field. This is probably due to a much slower application of the low pressures.

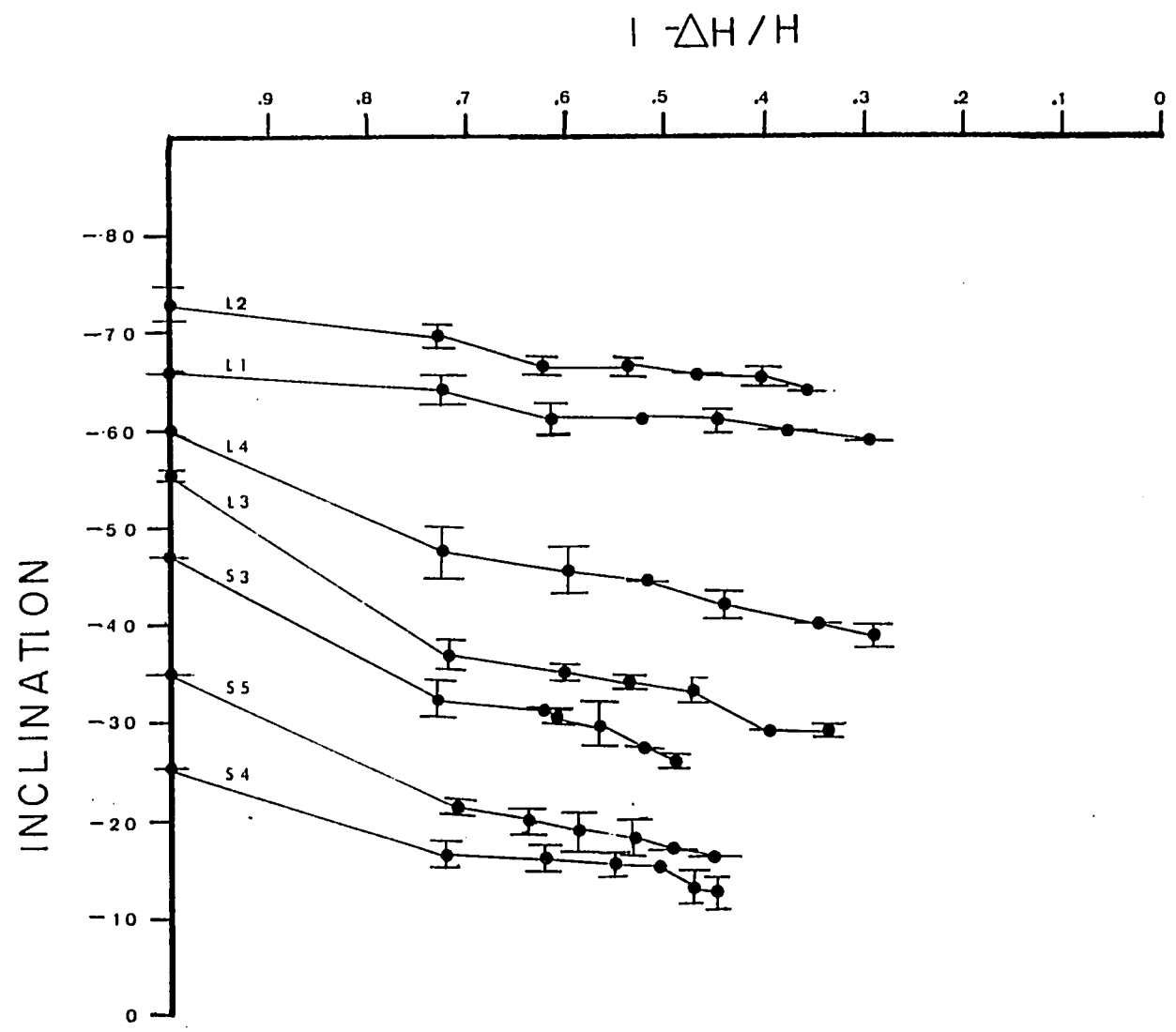
As consolidation continues, the change of the inclination is more gentle and linear. This linear change in the inclination suggests that the change in the remanence vector is directly related to the amount of volume change.

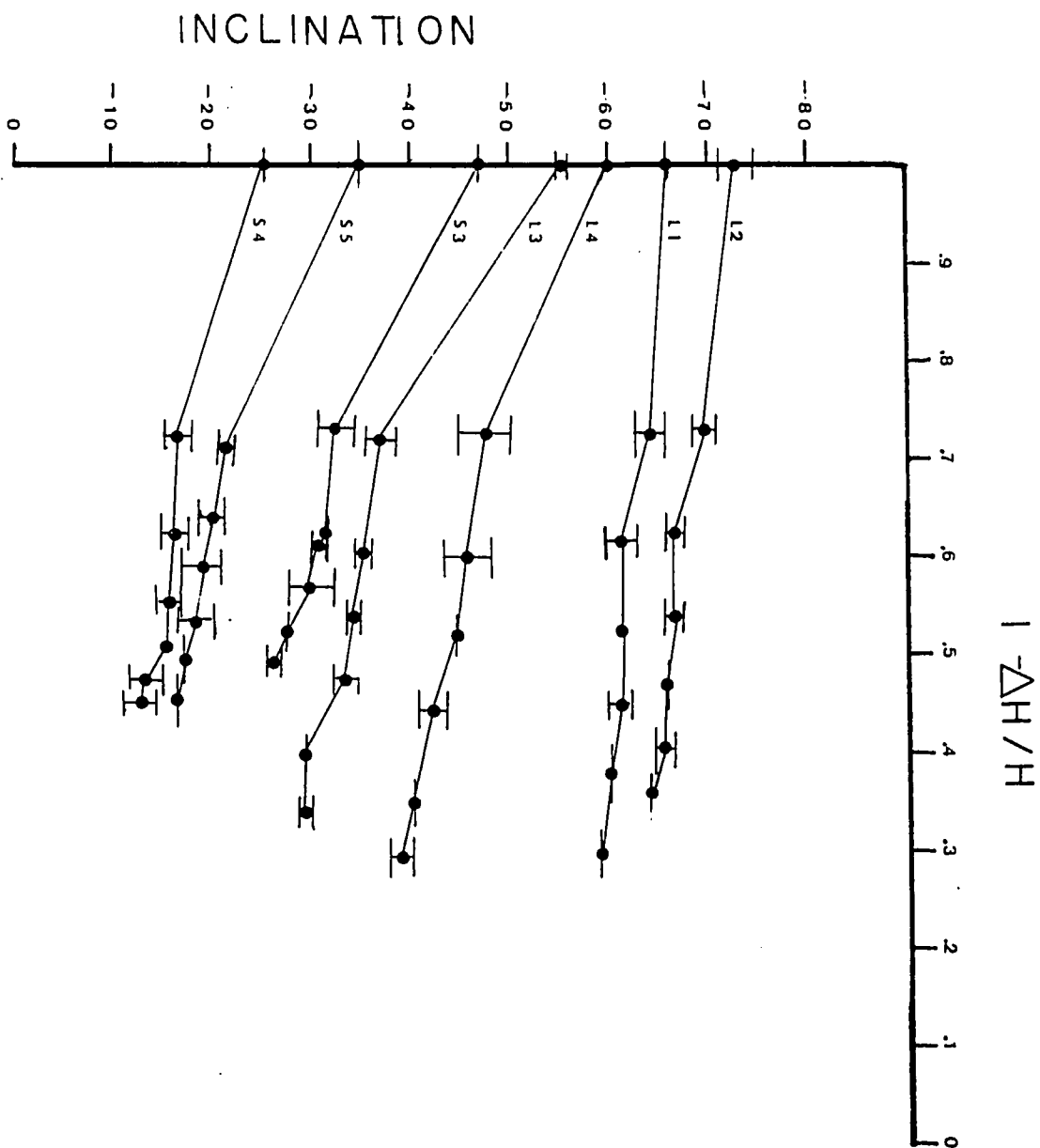
Samples S3, S4, and S5 had compacted in such a way that after the third load was applied, the amount of rebound was equal to or greater than the change in height resulting

Figure 8 - Inclination (degrees) vs. $1-\Delta H/H$ (synthetic sediment)

From top to bottom, the samples are L2, L1, L4, L3, S3, S5, and S4. Note that the L-series of samples consolidated more than the S-series. However, the pattern of change is similar. There is an initial jump as the first load is applied. The trend is then linear with respect to the volume change. These values do not take rebound into account.







from consolidation. Figure 8 is a graph of the inclination vs. $1-\Delta H/H$ for these three samples. Included on the graph are rebound and theoretical points calculated from the Blow and Hamilton (1978) model.

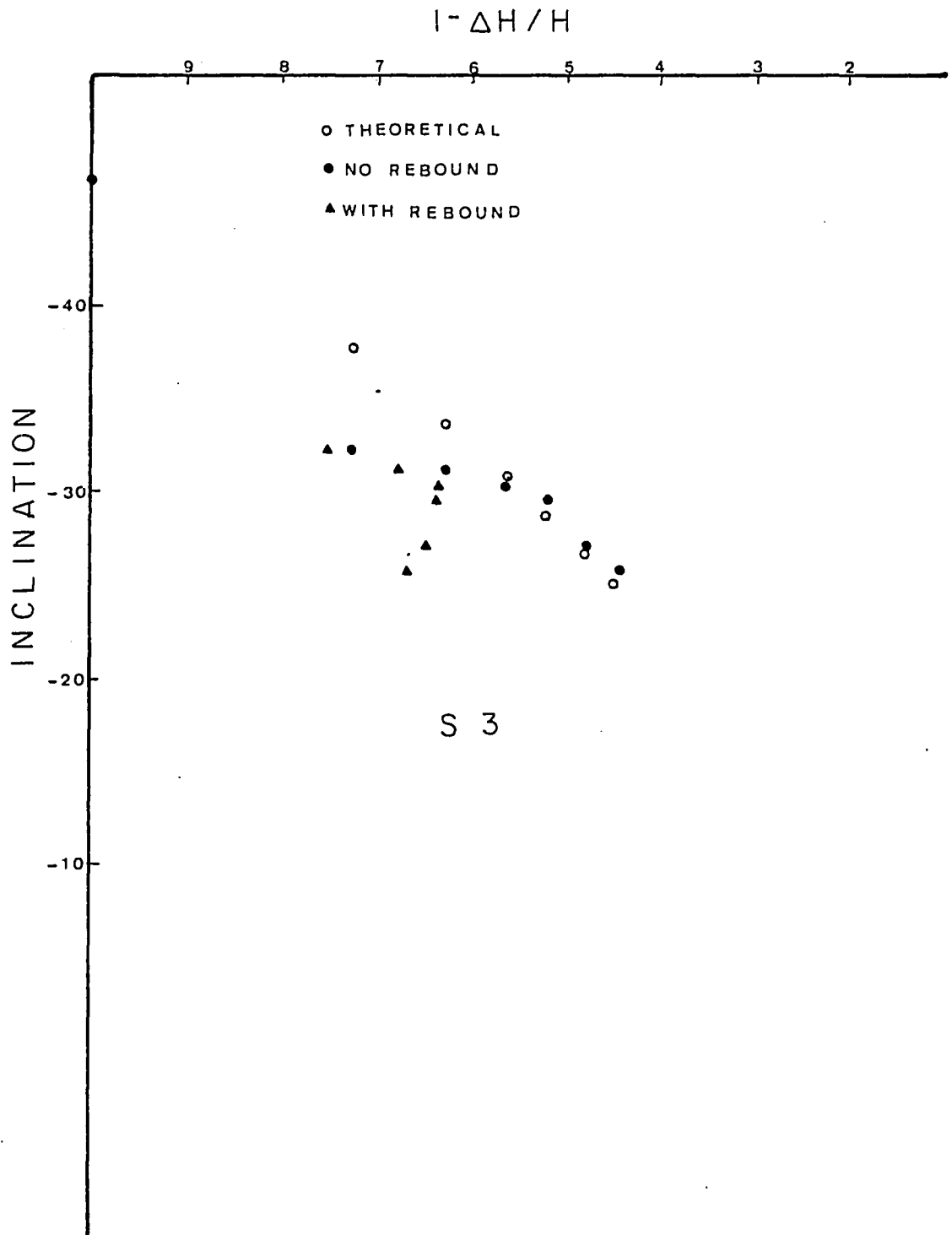
If the inclination were solely a function of the change in sample height (or volume), then rebound would result in changes in inclination to the same degree as compaction. This is not seen in these plots. The inclination is always shallower, even in samples where the amount of rebound was actually greater than the amount of compaction. Thus compaction dominates the system and rebound plays a minor role in determining what the final inclination will be.

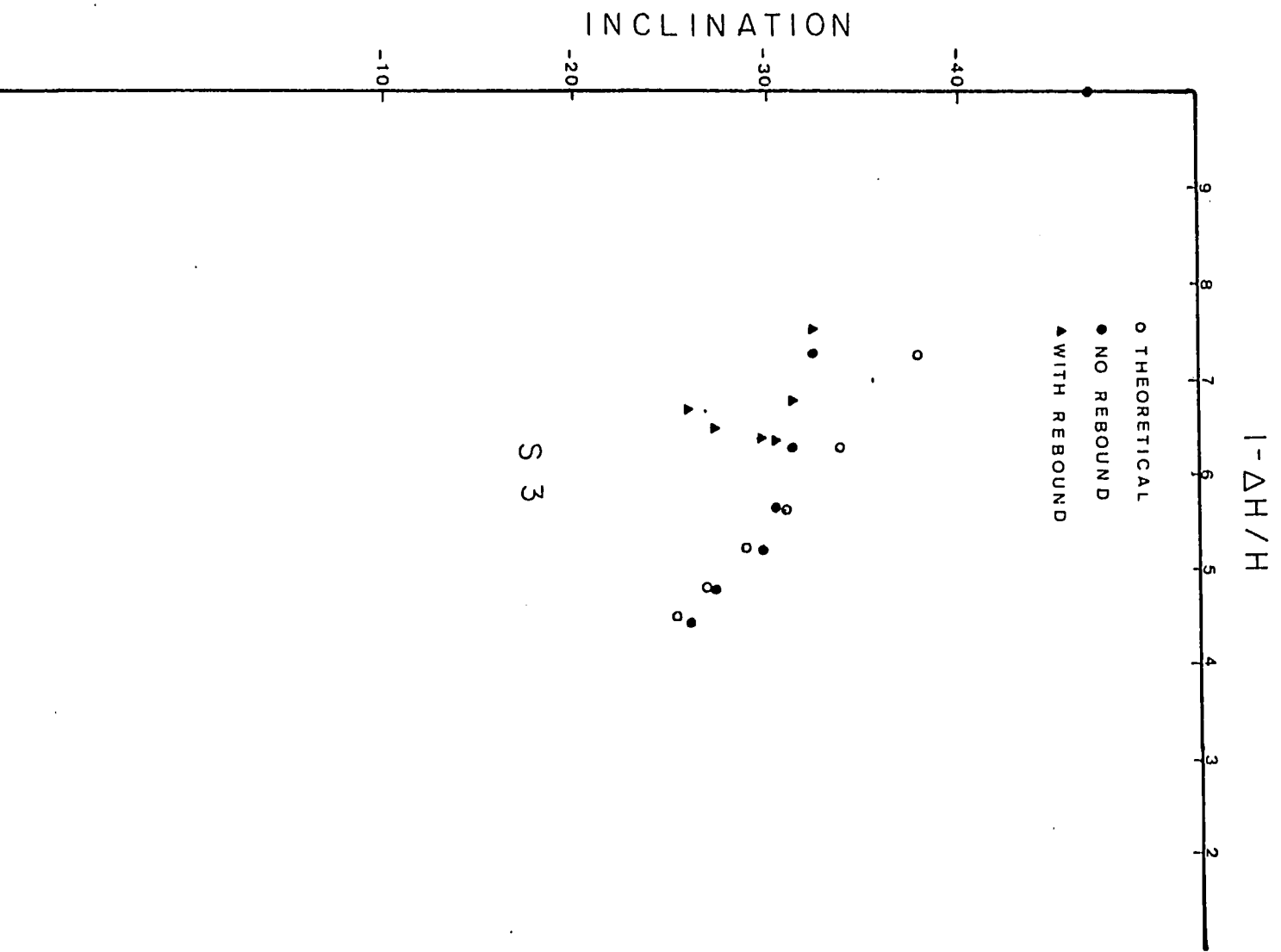
The data points calculated from the Blow and Hamilton (1980) model do not follow the same path as the data points collected in this experiment. For samples S3 and S4, the theoretical points intersect the data at 1/2 the original volume, and for sample S5, they do not intersect the graph. Therefore, it is seen that the Blow and Hamilton model does not represent the compaction effects shown in this data.

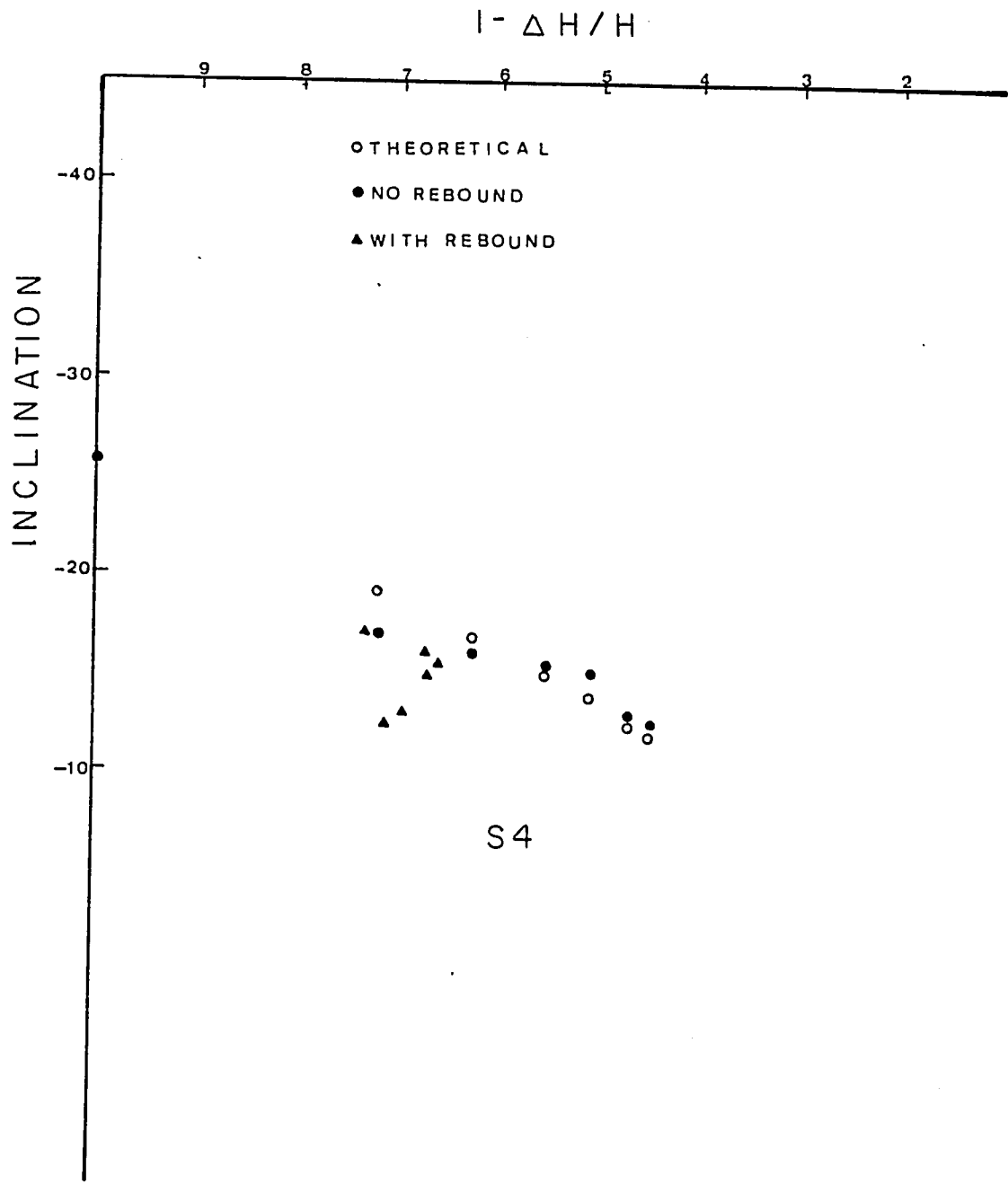
Figure 9 is a graph of declination vs. $1-\Delta H/H$. With the possible exception of one sample (L1), and a jump that occurs when the first load is applied to all samples, the declination appears to remain constant throughout the analyses.

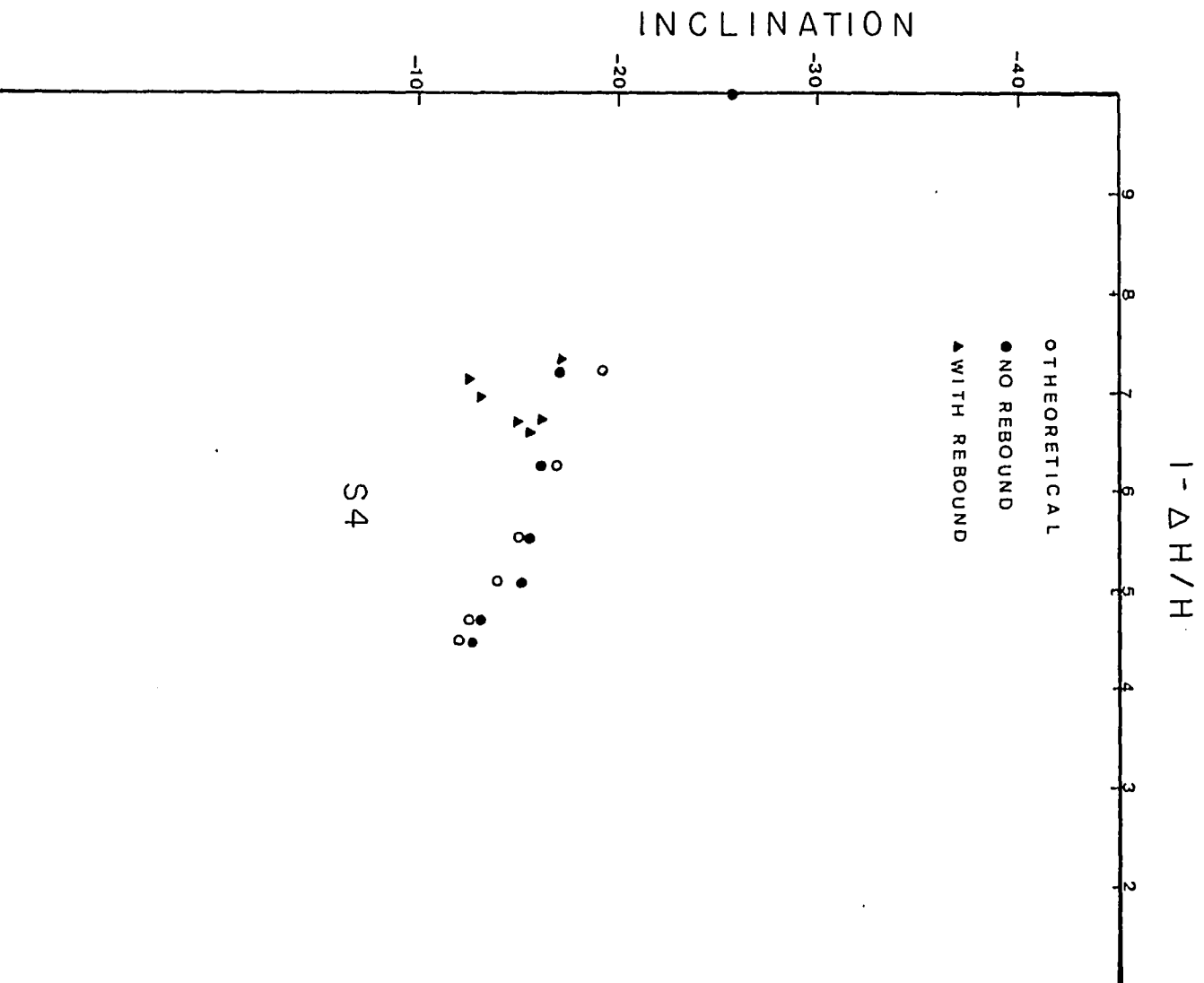
Figure 9 - Inclination (degrees), Theoretical Inclination, and Inclination Corrected for Rebound vs. $1-\Delta H/H$ for Samples S3 (A), S4 (B), and S5(C).

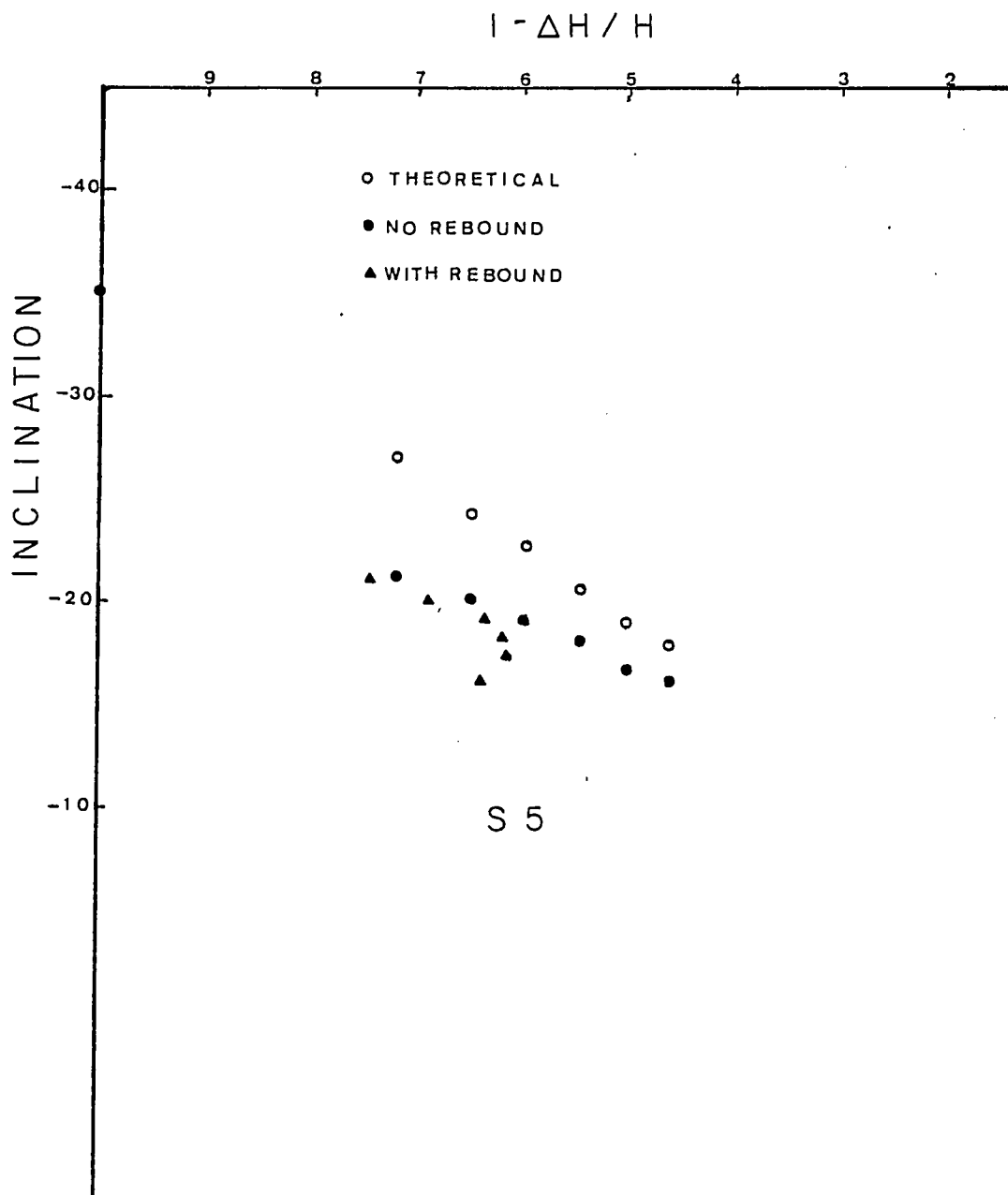
The theoretical points were calculated using the model of Blow and Hamilton (1980). If the compaction effect were solely a function of volume change, then where the rebound equalled compaction, the inclination should remain the same, and where rebound was greater than compaction, the inclination should become steeper. This is not seen. The Blow and Hamilton (1980) data points do not follow the trend of data in this experiment. This suggests that: 1) the Blow and Hamilton model can not be used to explain these compaction results, and 2) compaction will determine what the final inclination will be, with rebound having little significance.











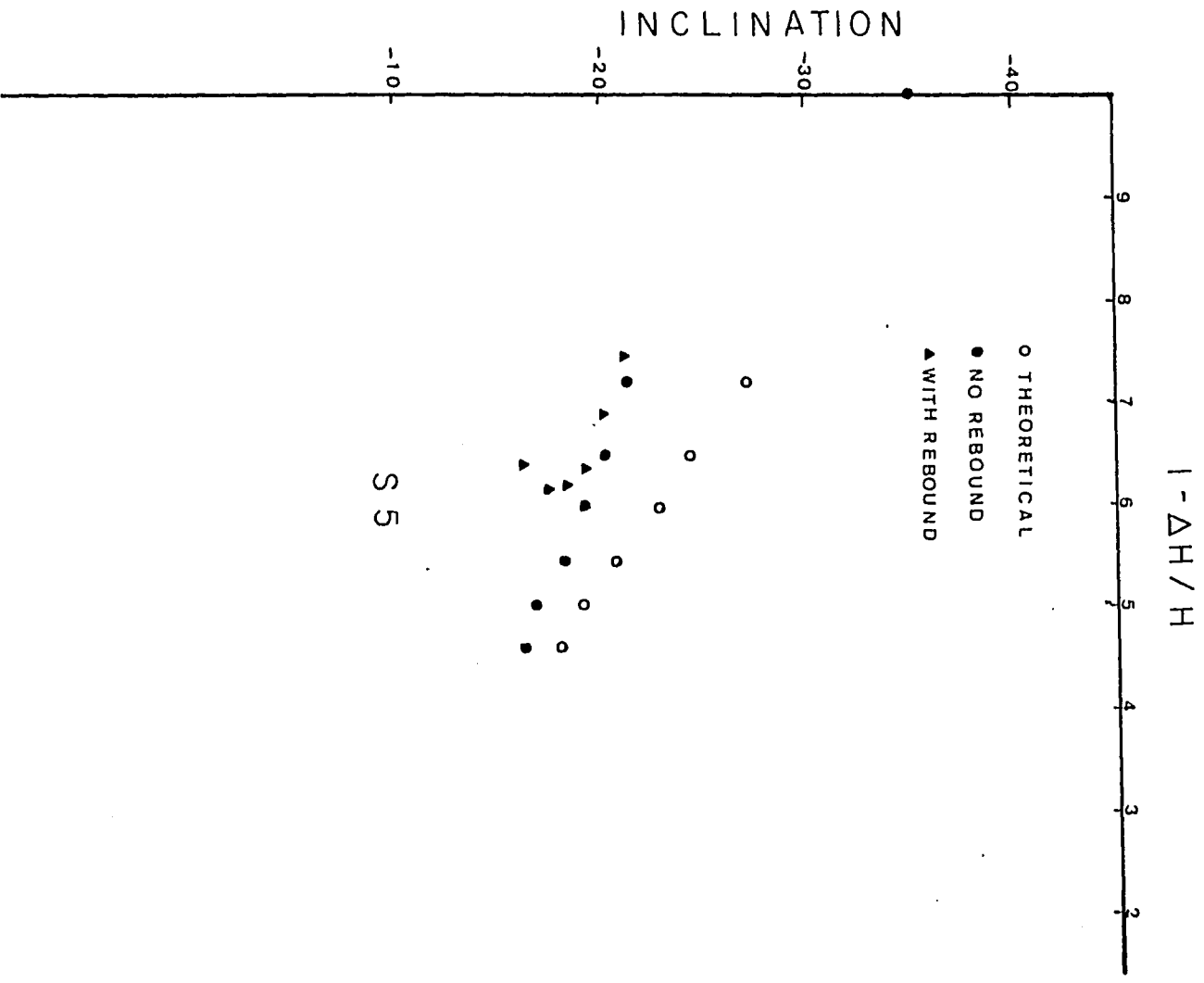
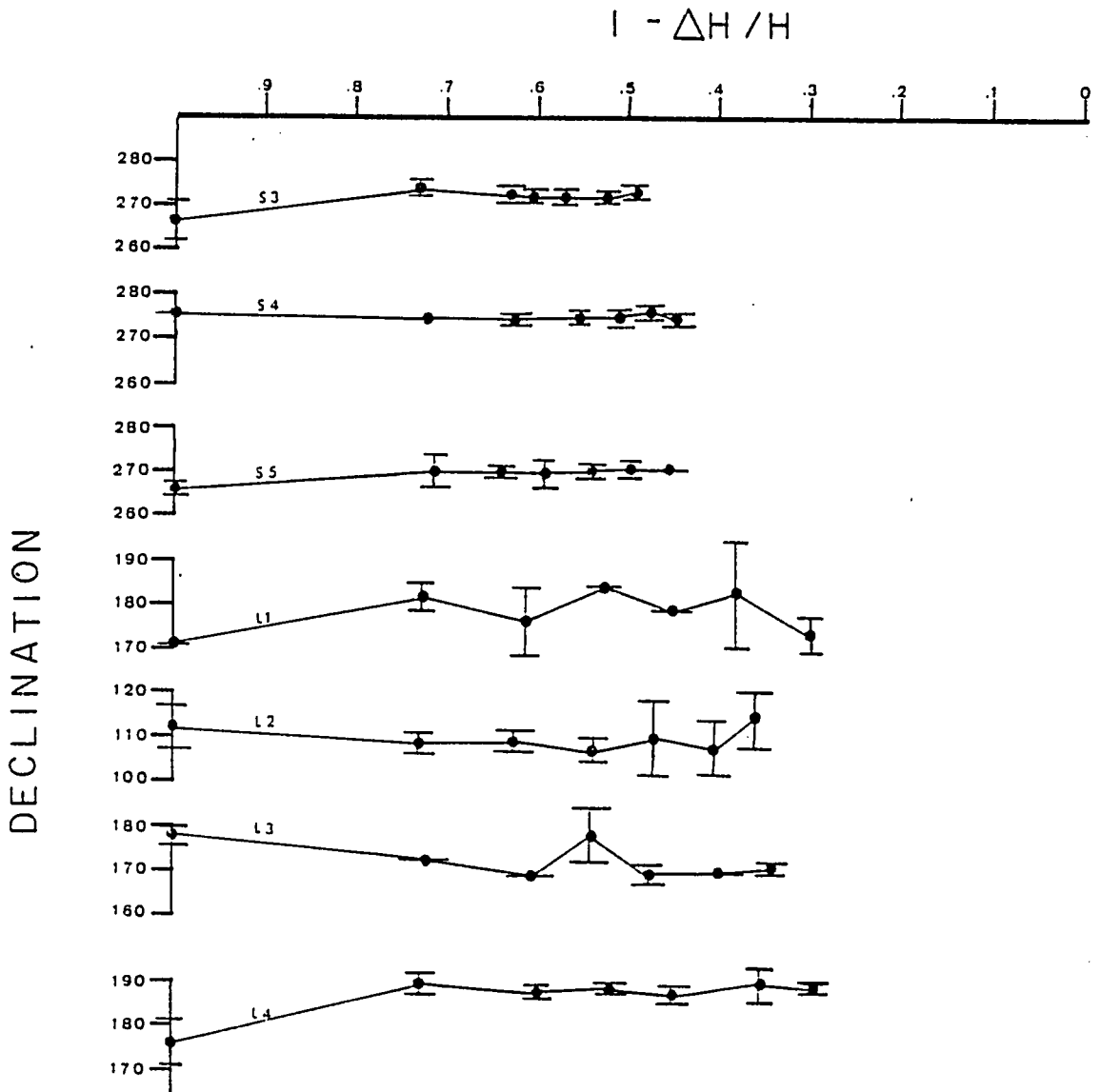
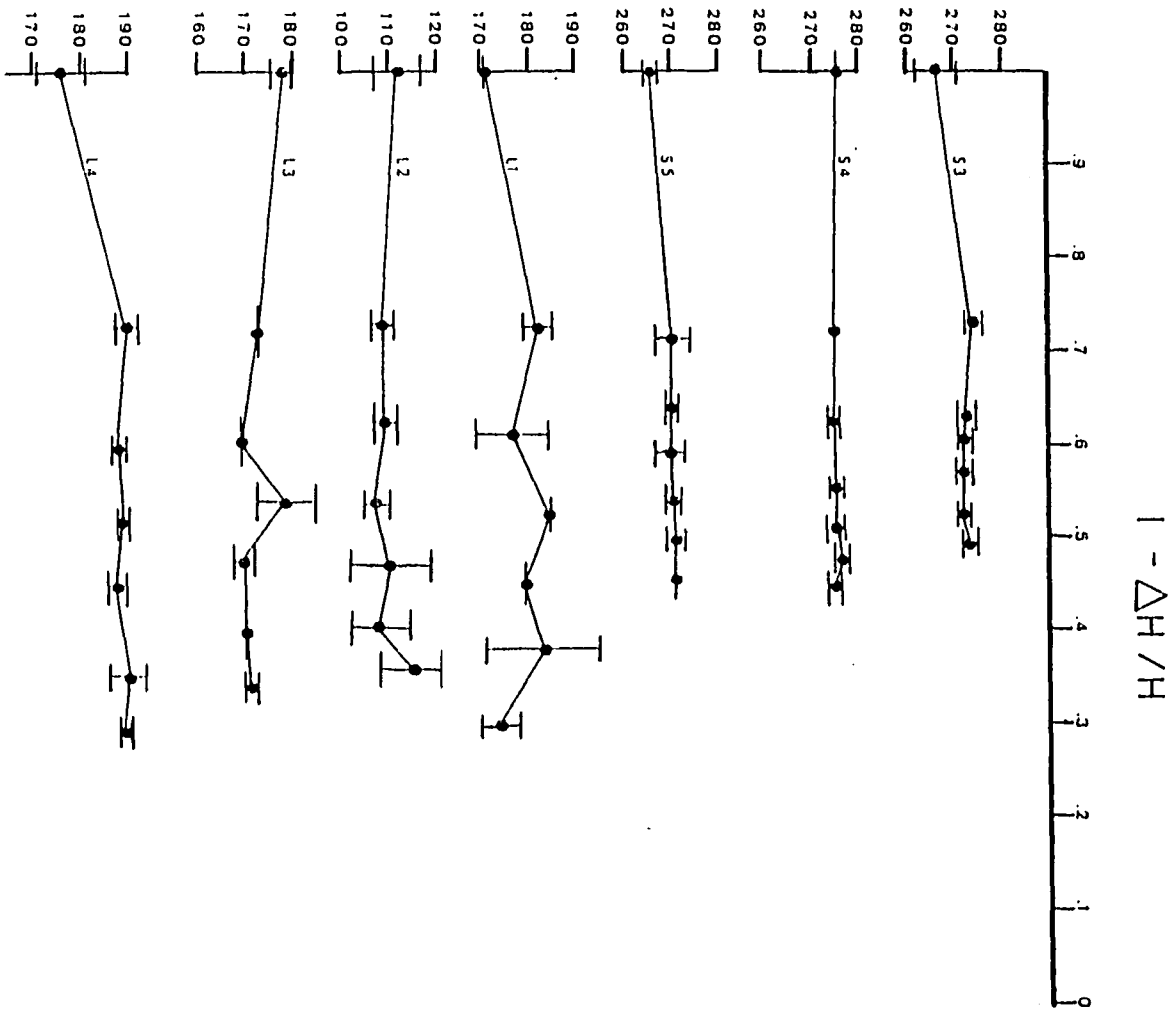


Figure 10--Declination (degrees) vs. $1-\Delta H/H$ (synthetic sediment).

From top to bottom, the samples are S3, S4, S5, L1, L2, L3, and L4. Except for the initial jump associated with the first load, the declination appears constant. Although some of the points appear to vary, the amount of error associated with these points suggest that there is no significant change.



DECLINATION



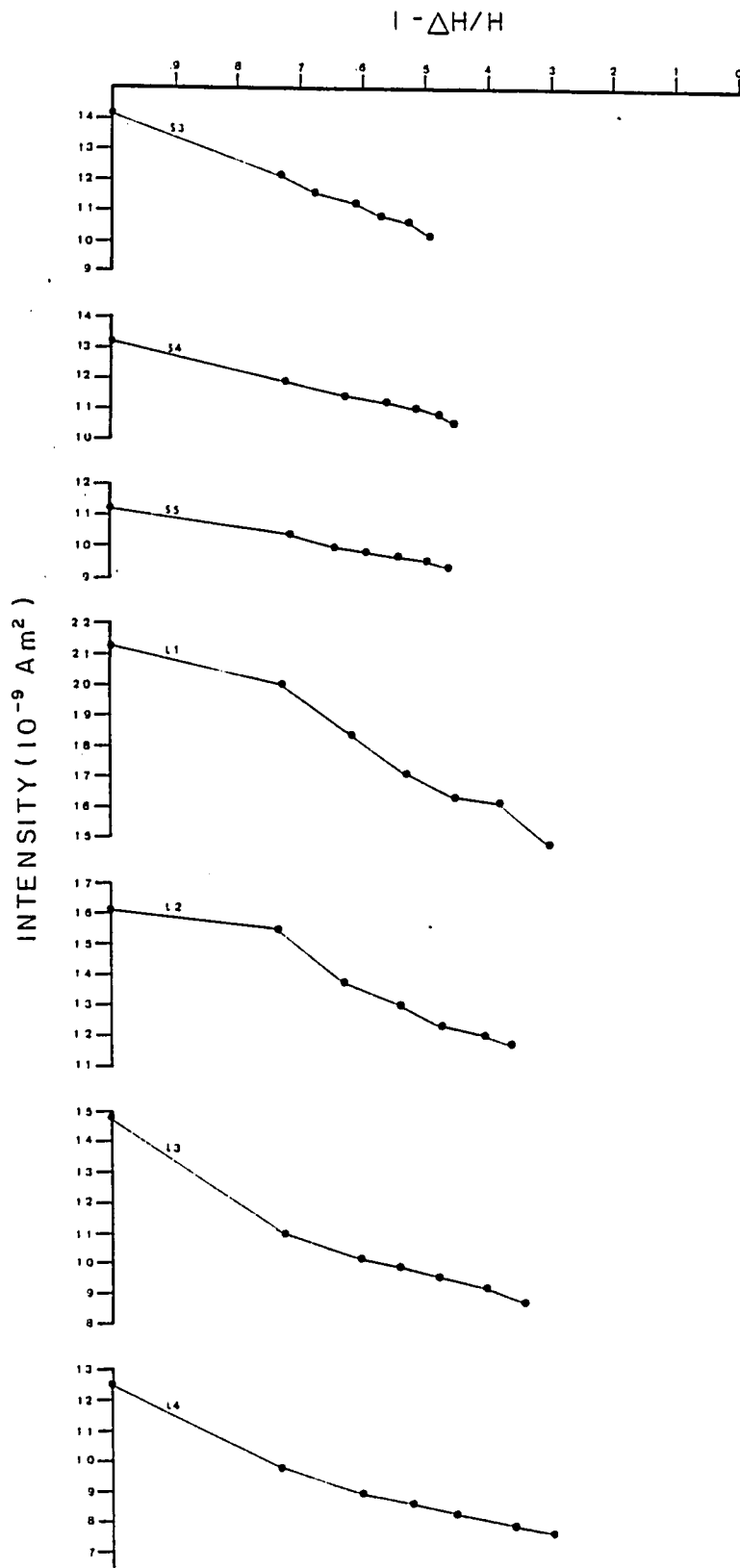
When averaged over 2,000 years, the earth's magnetic field approximates the axial geocentric dipole (Opdyke and Henry, 1976) and the magnetic declination always points to the north pole (McElhinny, 1973). The declination has been used to orient cores (Stow, 1978). The data collected with this experiment suggest that compaction is not an important process to consider when working with the magnetic declination.

Figure 10 is a graph of magnetic intensity vs. $1-\Delta H/H$. This shows a continuing decrease in magnetic intensity as consolidation proceeds. A similar phenomenon was seen with samples analyzed by Henshaw and Merrill (1976) when their samples were allowed to dry over time, and Hamano (1980) noted a decrease in intensity as the initial void ratio changes. The reason for this is not known. The decrease in intensity is apparently related to water content and the associated change in grain orientation.

Figures 12 to 15 are graphs of the magnetic data vs. the estimated percentage of water and depth. The general trends of the remanence data is similar to that of the graphs of remanance vs. $1-\Delta H/H$ because the percentage water is considered to be linearly related to the change in sample volume in this experiment.

Figure 11 - Intensity (10^{-9} Am²) vs. $1-\Delta H/H$ (synthetic sediment).

The samples are in the same order as Figure 9. In all cases, the intensity decreases as consolidation proceeds. This suggests that magnetic grains move closer together and cancel each other as compaction continues.



INTENSITY (10^{-9} A m^2)

$H/\nabla H - 1$

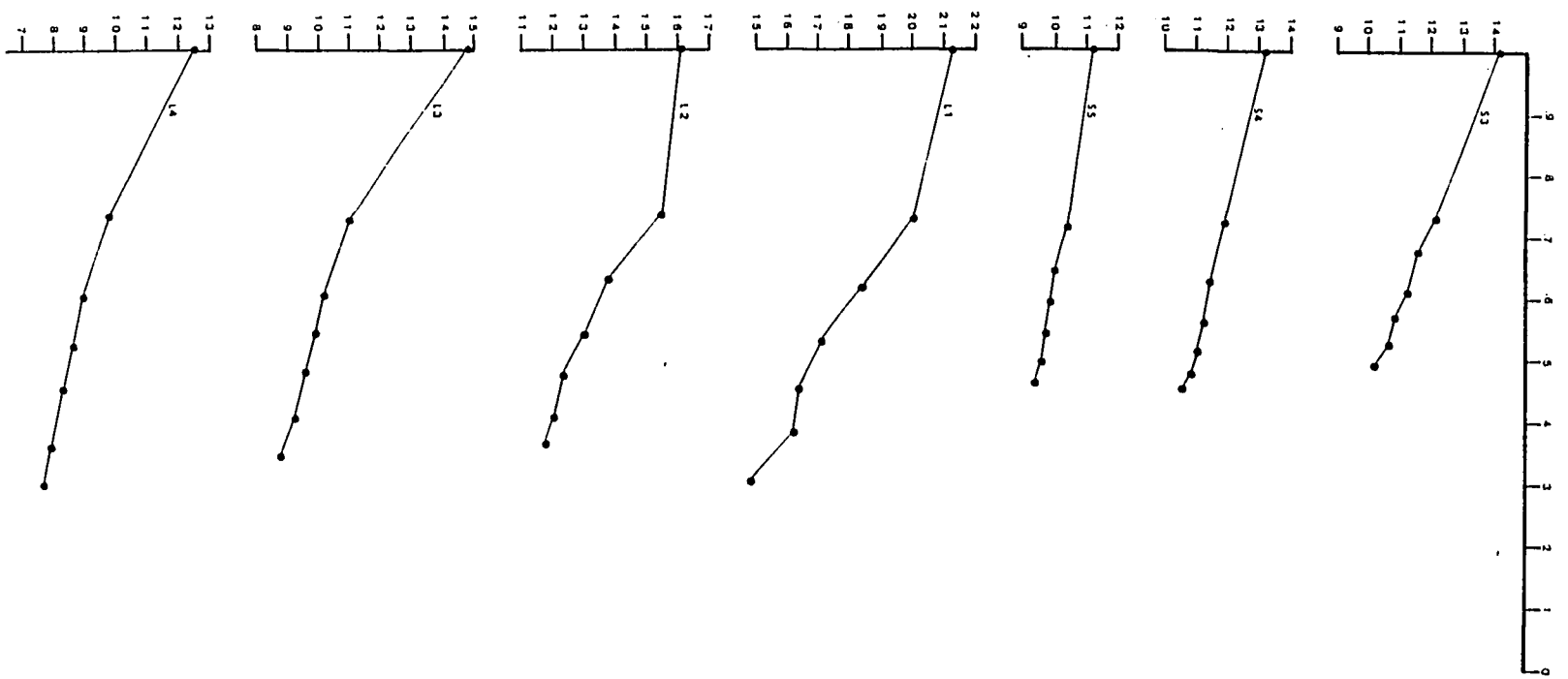
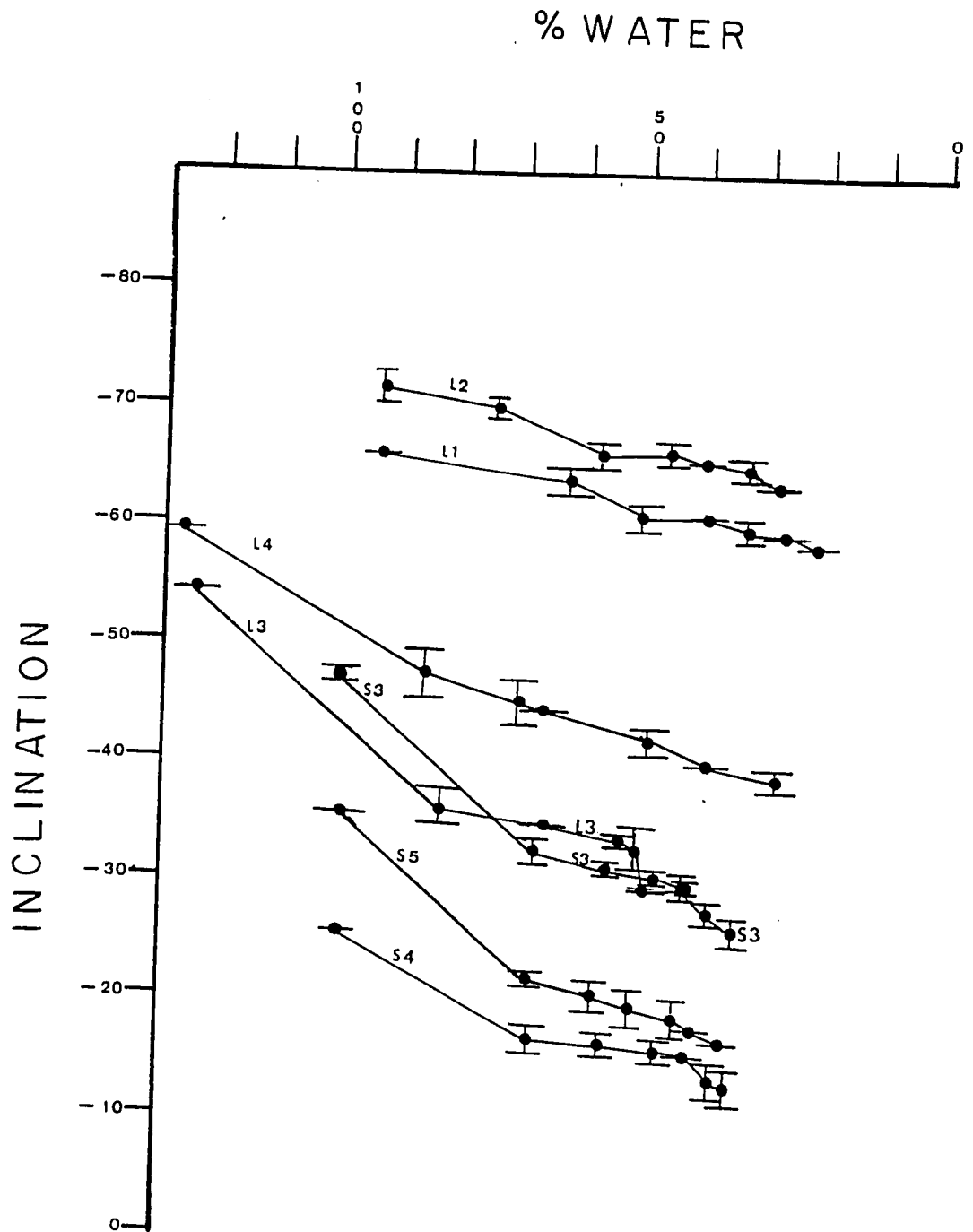
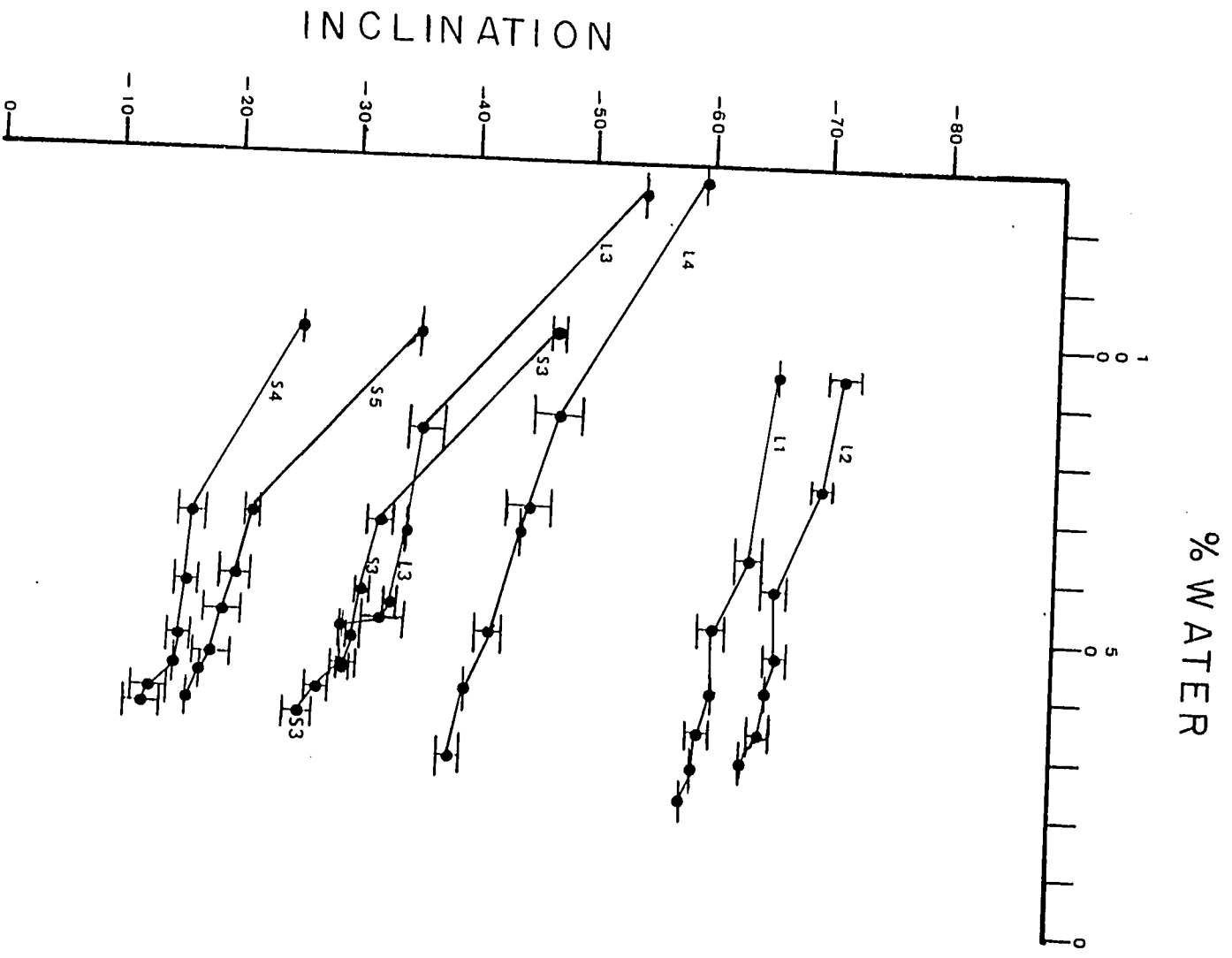


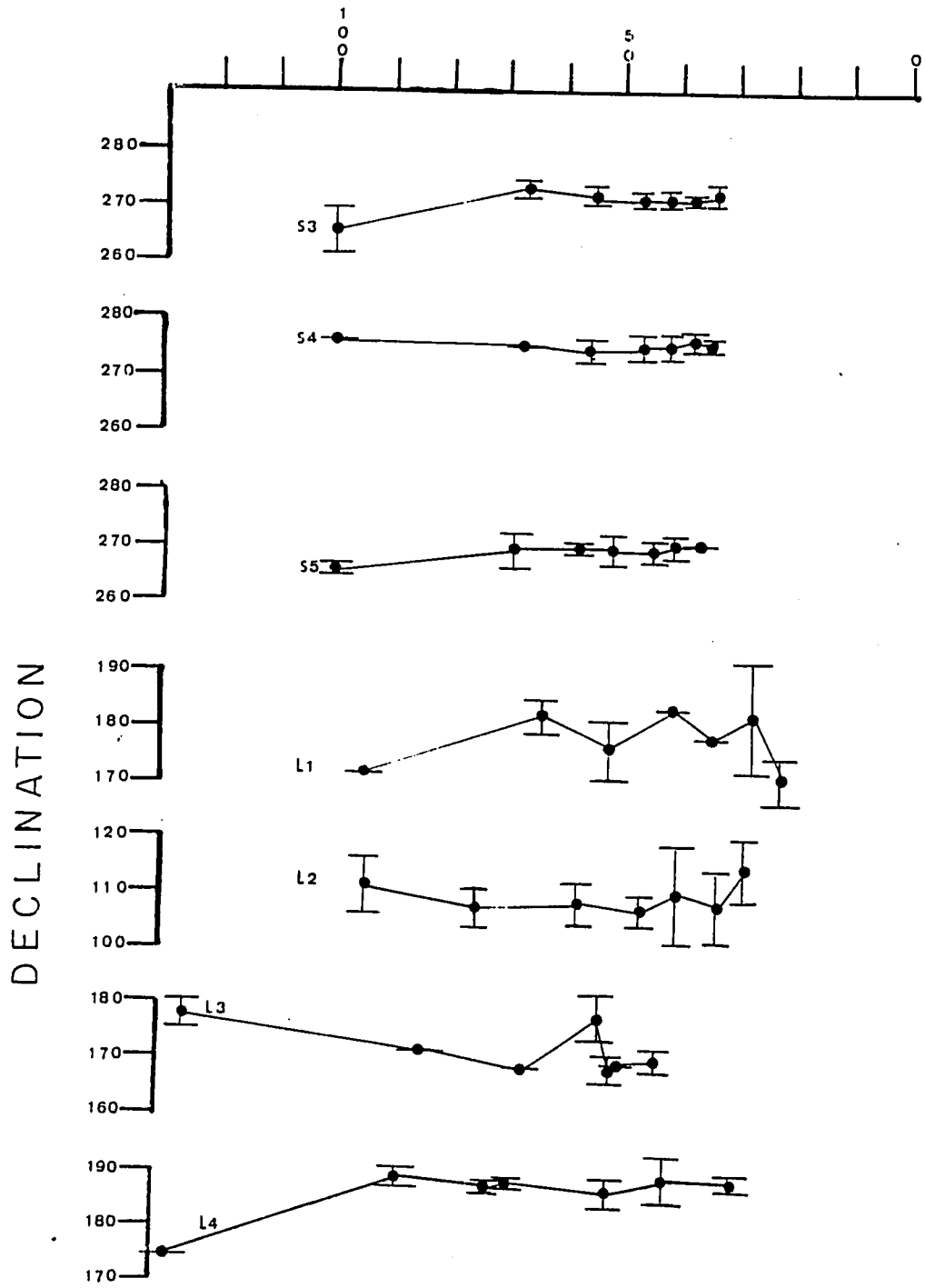
Figure 12 - Inclination (degrees) Declination (degrees)
and intensity (10^{-9}Am^2) vs. %Water (synthetic
sediment).

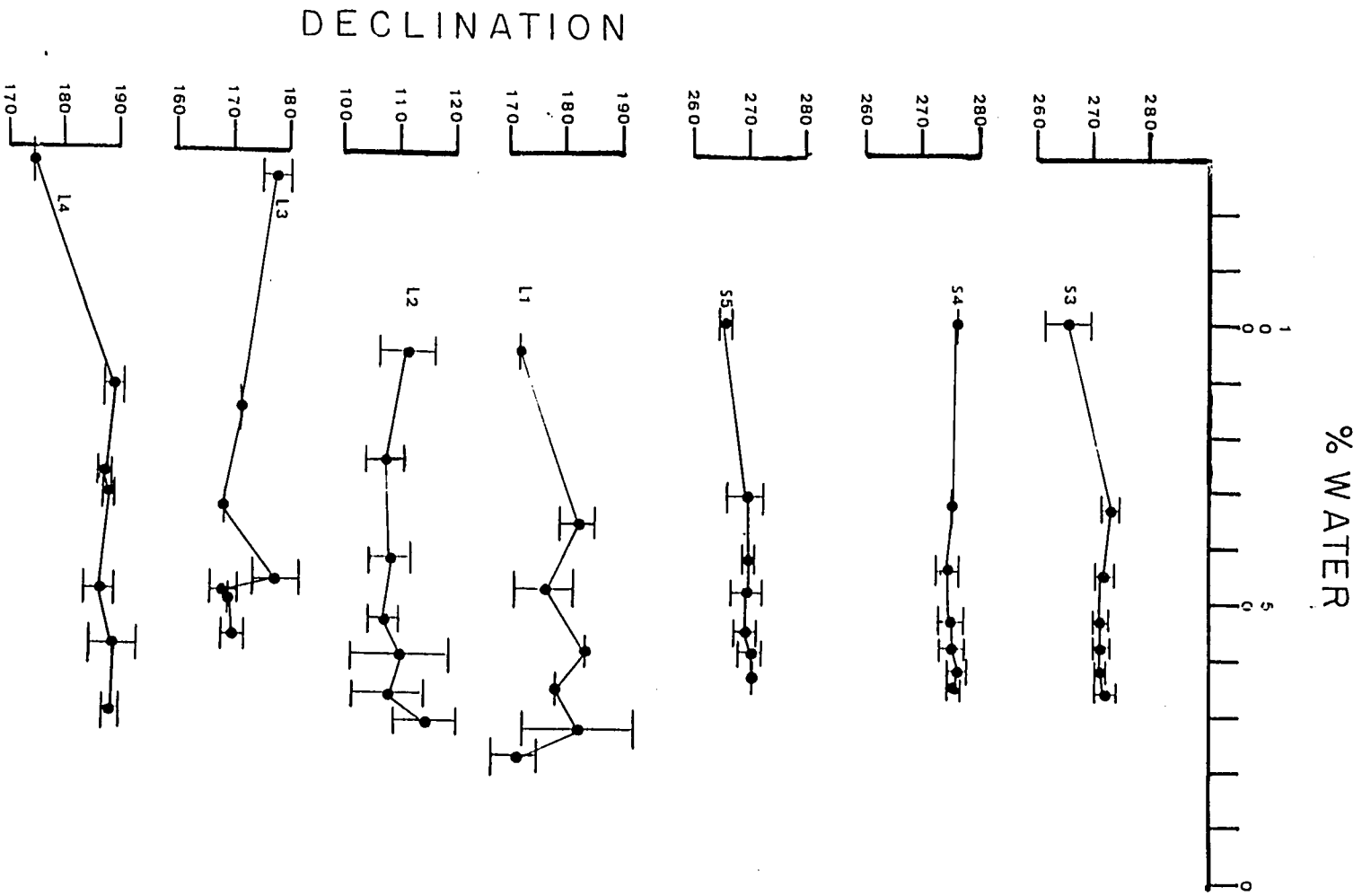
The change in water content is considered to be a linear
function to the sample height. These graphs show similar
trends to Figures 7, 9, and 10.

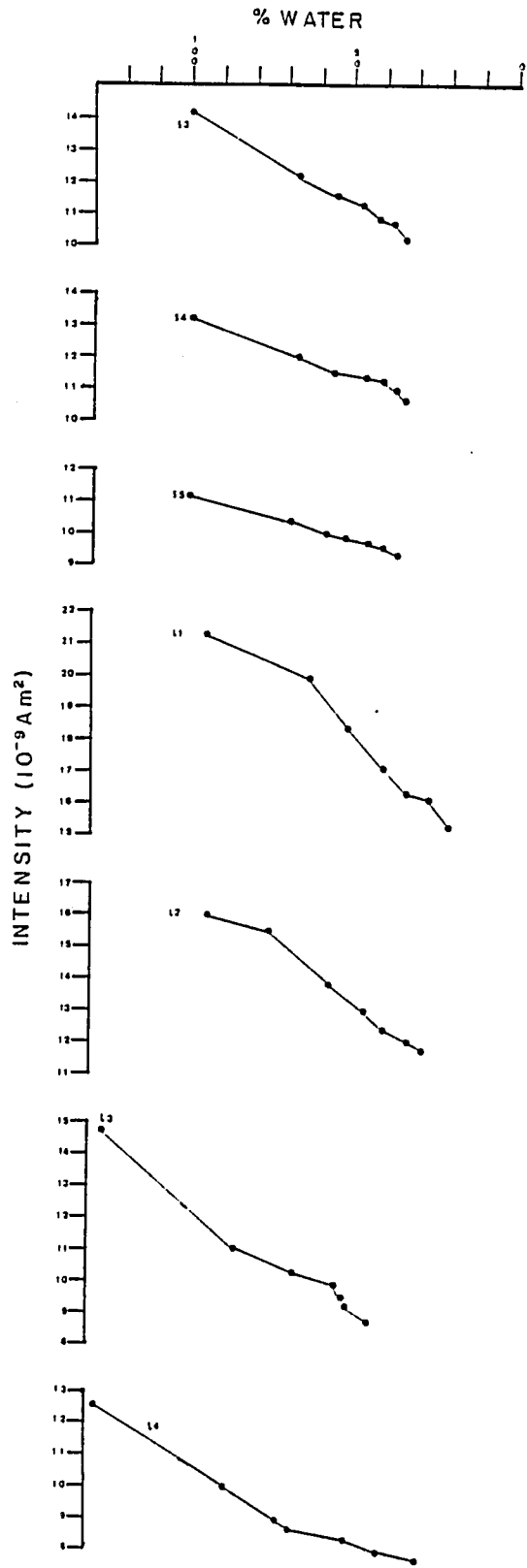




% WATER







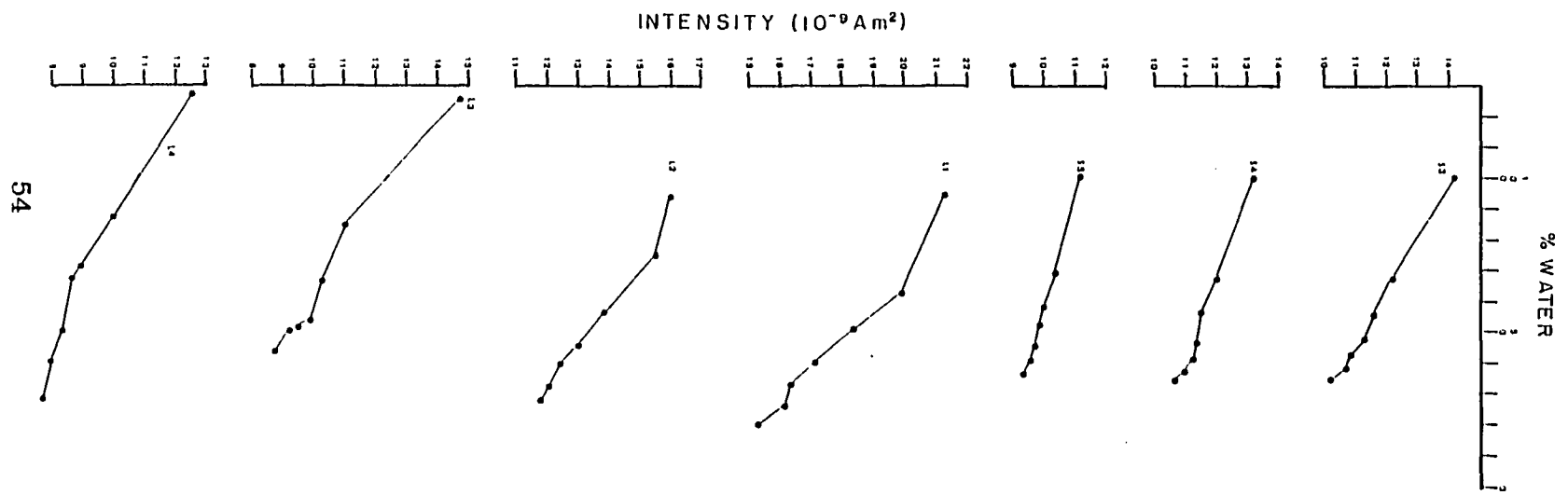
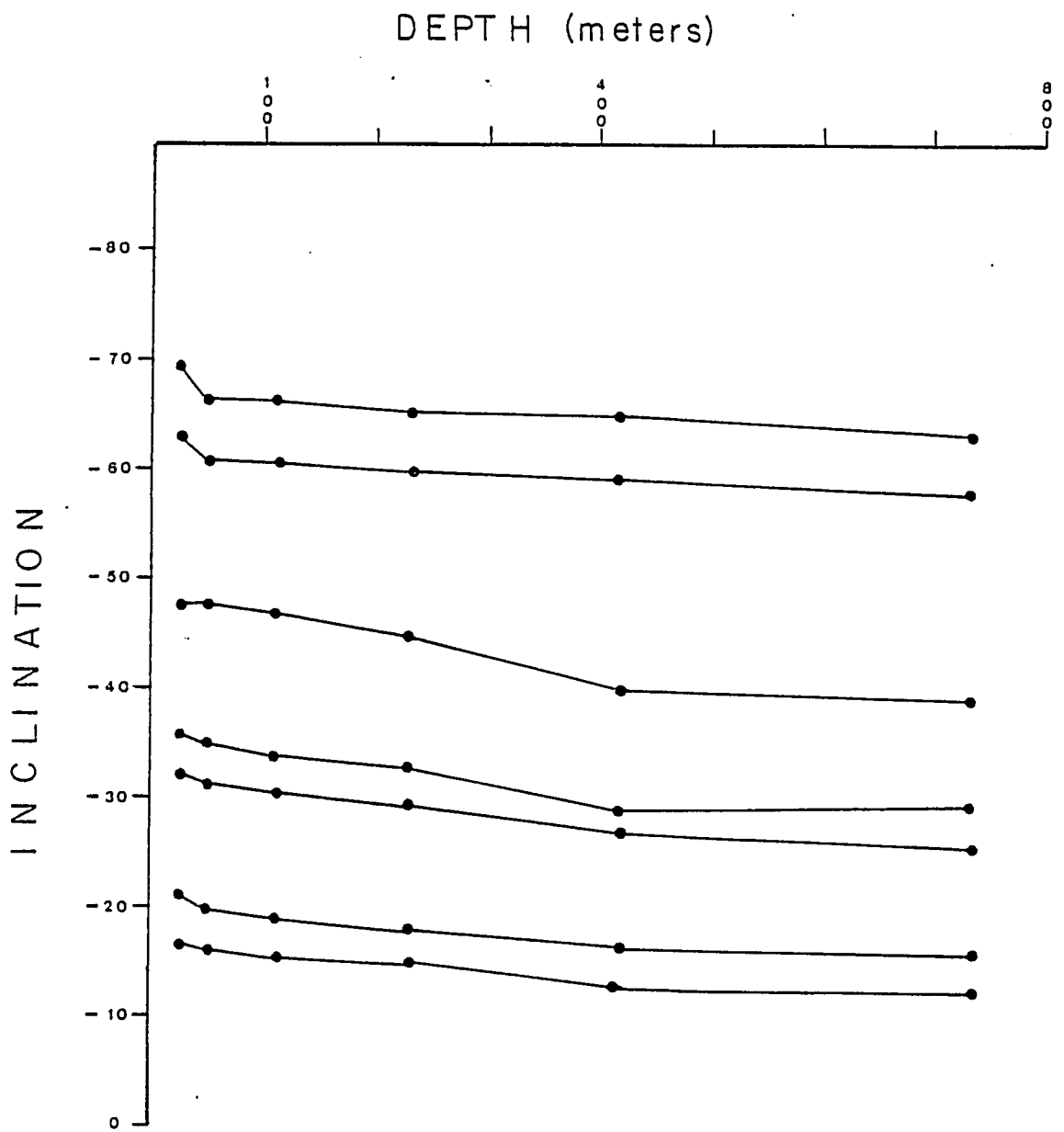


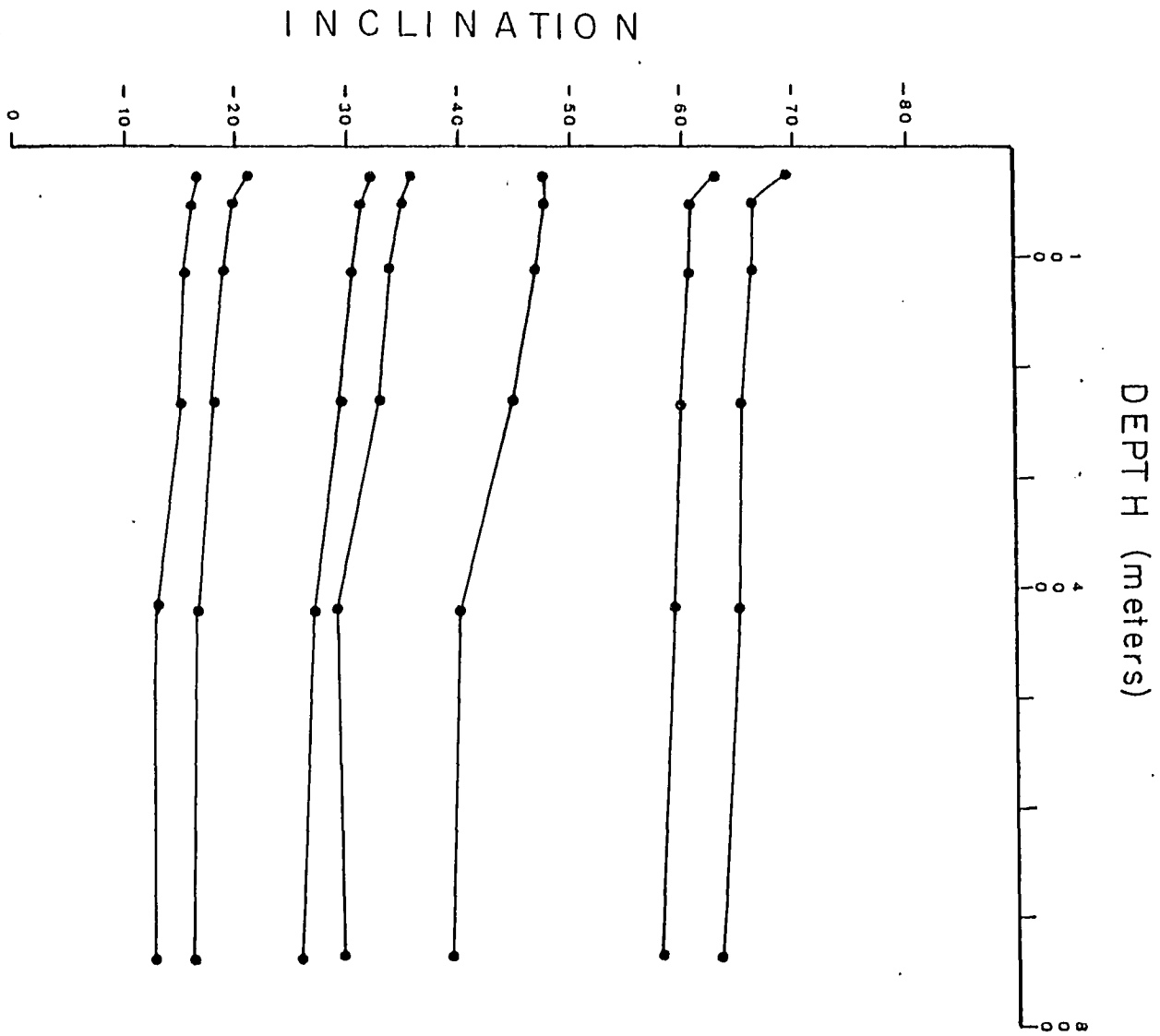
Figure 13 - Inclination (degrees) vs. Depth of Burial
(meters) (synthetic sediment).

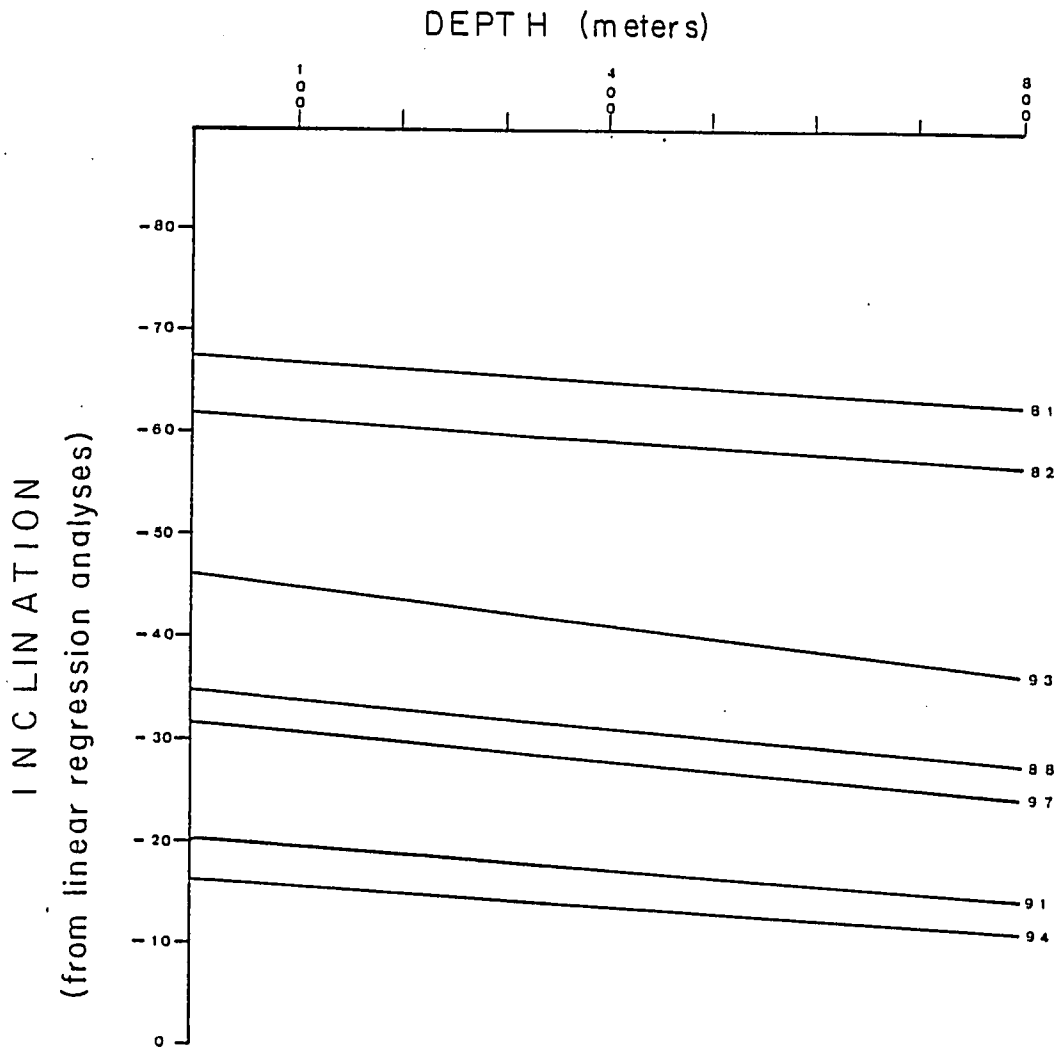
A family of curves is developed that can be used to correct for the effects of consolidation on the remanent magnetism of sediments. Graph A shows the data collected during the experiment, and Graph B is the result of linear regression analyses performed on the data sets. The numbers next to each line are the correlation coefficients. To correct for compaction, one needs to find the point corresponding to the depth of burial and the inclination, then follow the lines to the origin. This graph is representative for shaly deposits, but will not be representative for other types of sediments.

When values for the inclination are drawn on the same graph vs. depth, a family of curves develop that appear linear. Linear regression analyses were performed on these data to find the best fit line for each sample. This is shown in Figure 13b. Lines were drawn to an equivalent depth of 800 meters. From graphs such as these, it may be possible to estimate the original inclination. From knowledge of the depth of burial of a sample, and the inclination of the sample, one can simply find the point on the graph corresponding to those values and retrace it to the origin (zero depth).

When magnetic intensity is plotted vs. depth (Figure 14), the curves appear to be hyperbolic from the origin. It appears to flatten out as depths become very large. This suggests that the further one goes down core, the intensity will undergo little change. Thus, the magnetic intensity should never equal zero by compaction alone. The data also suggests that perhaps the majority of the remanence change will occur in the first couple of hundred meters of burial. Kent and Spariosou (1982) reported on an approximately 200 meter hydraulic piston core at DSDP Site 502, in the Carribean. Their data suggested that there may be compaction processes affecting the remanence of the core, for the mean remanent inclination shallowed with depth. However, they did not conclude that the shallowing was compaction







INCLINATION
(from linear regression analyses)

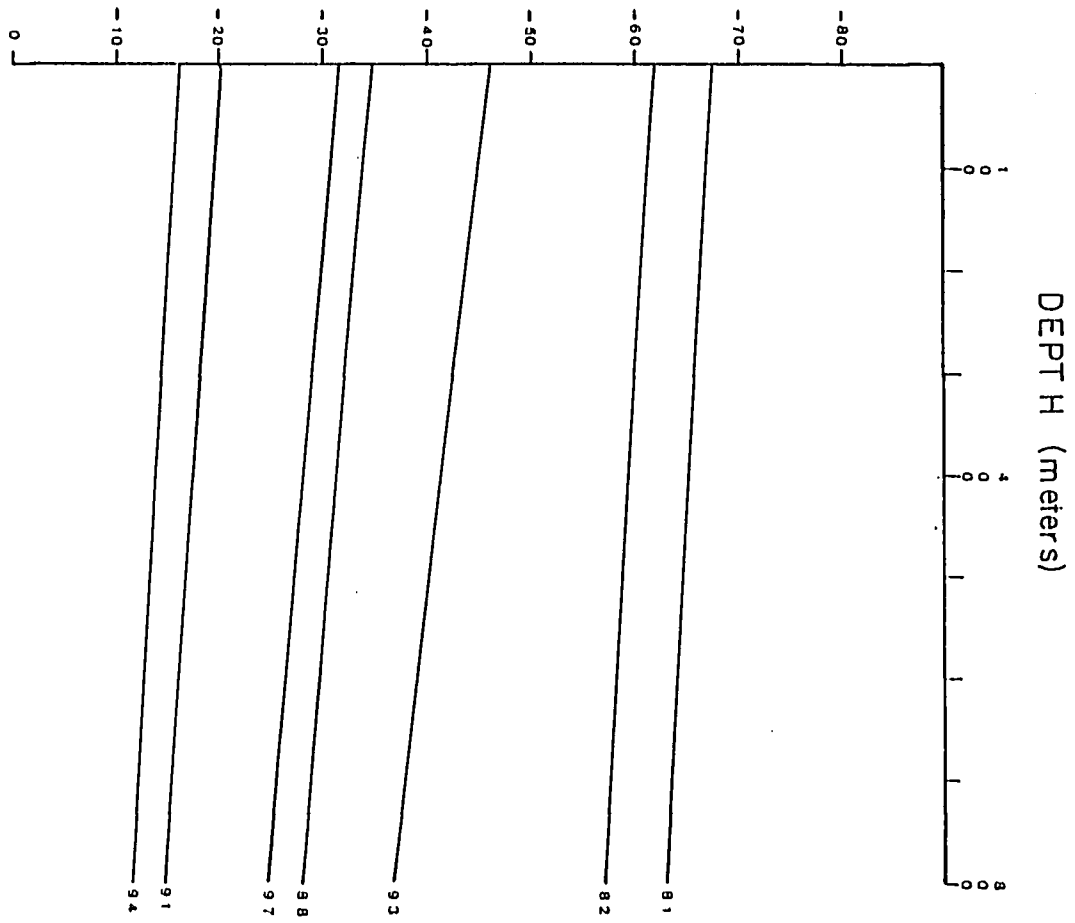
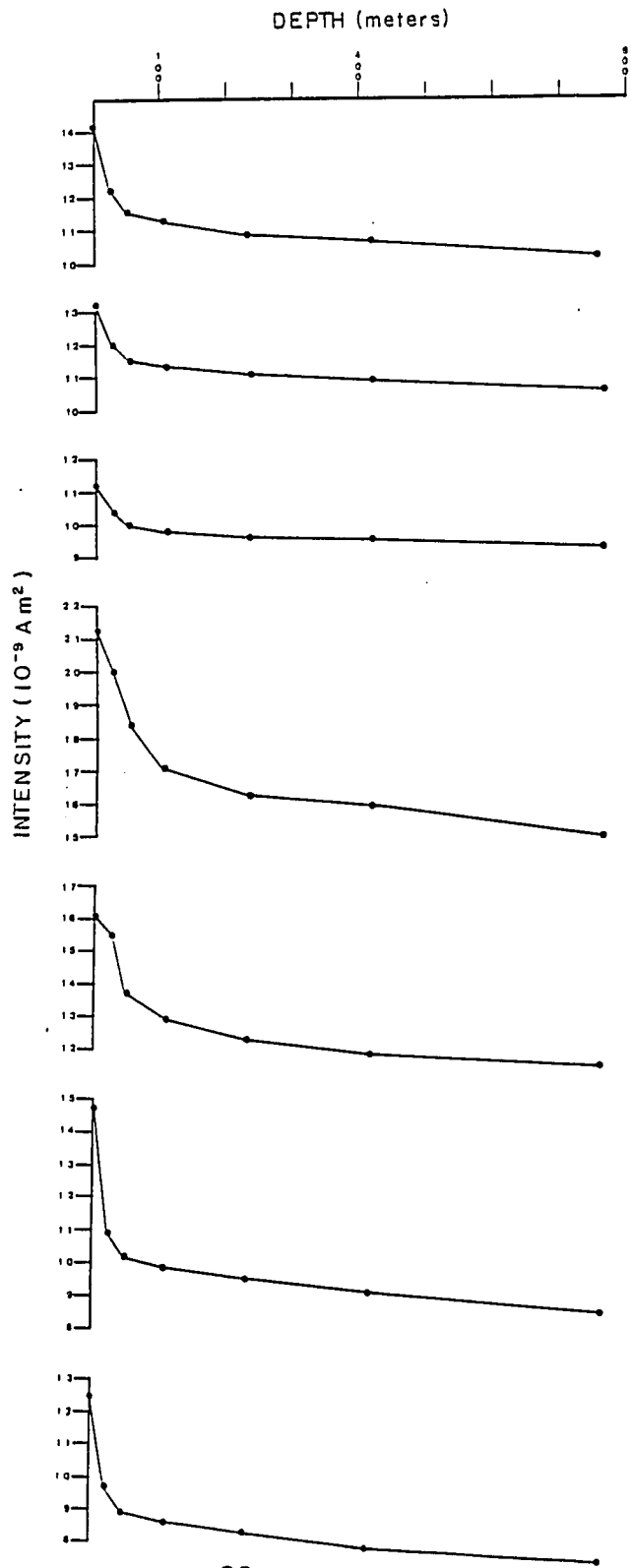
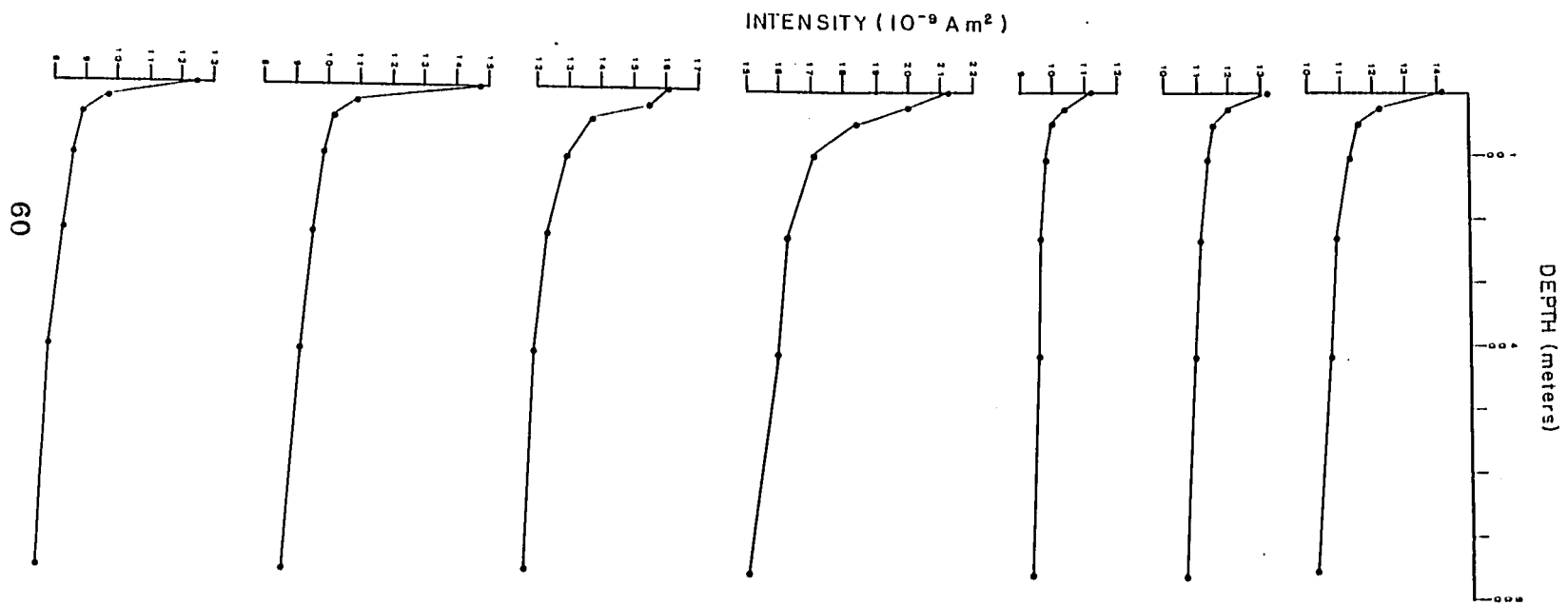


Figure 14 - Intensity (10^{-9} Am^2) vs. Depth of Burial
(meters) (synthetic sediment).

As the depth increases, the amount of change in intensity decreases. Most of the change occurs within the first 300 meters.





related (Spariosou, personal communication). Hopefully, as more data from hydraulic cores is published, more compaction effects will be seen.

Figure 15 is a graph of declination vs depth of burial. Figure 9 (declination vs. $1-\Delta H/H$) suggests that declination does not change during compaction. Hence, no change is seen with respect to depth.

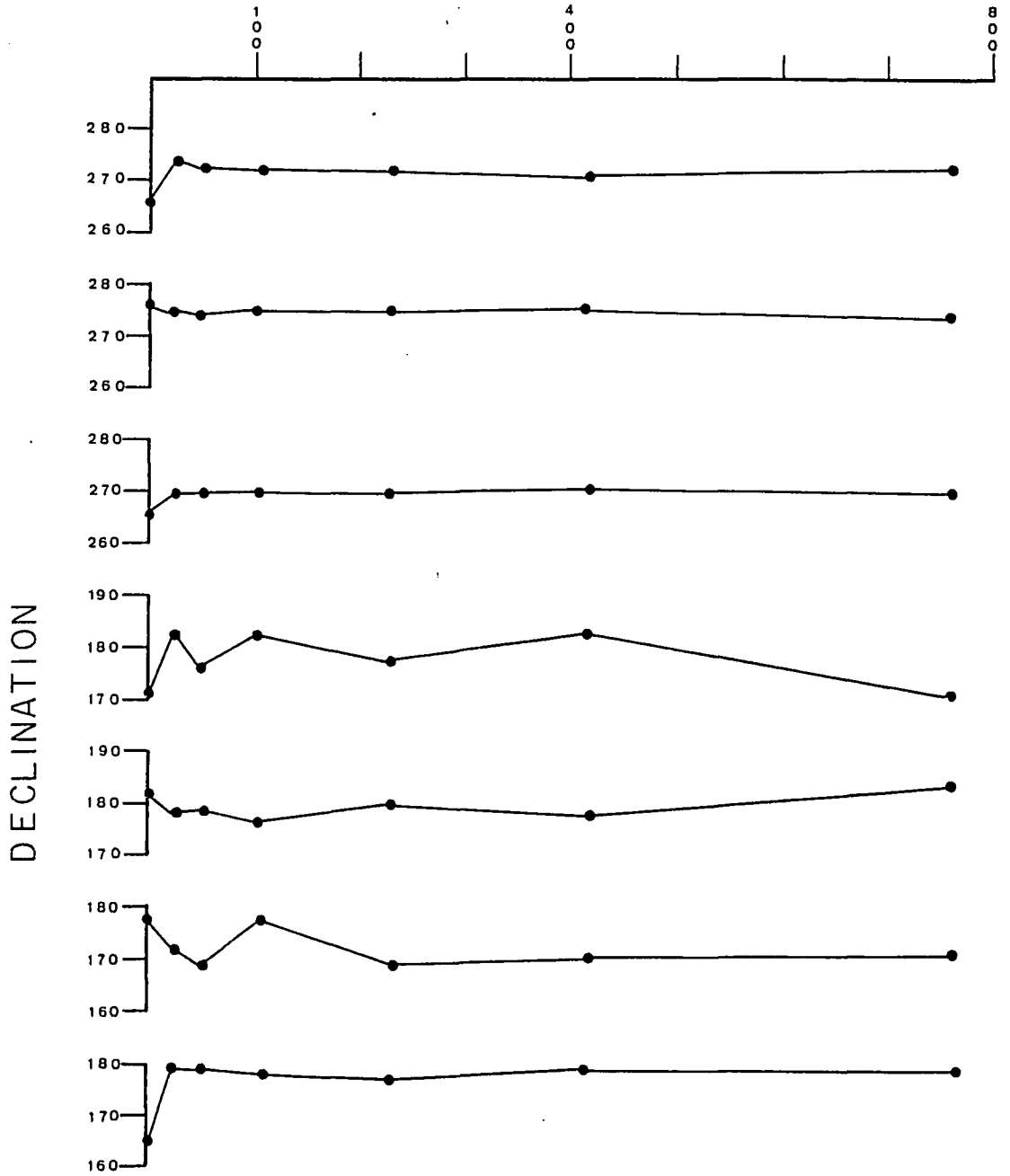
Figure 16 is two graphs of change in inclination vs. initial inclination (initial inclination is the value of the inclination after the first load). Graph A was taken directly from the experimental analyses, while graph B was taken from the linear regression analyses. These show a steady increase until the initial inclination approaches 45° . These two data points greater than 45° do not fall into a pattern suggestive of a smooth decrease. The same amount of change was expected to occur on both sides of 45° . However, the fact that two values of initial inclination larger than 45° have ΔI 's less than the ΔI at 45° supports the hypothesis that the greatest change in inclination is at 45° .

Tucker (1980) suggested that compaction may only affect low coercivity, larger magnetic grains while leaving untouched the high coercivity, smaller magnetic grains. To test this hypothesis, three samples (L1, L2, and L4) were

Figure 15 - Declination (degrees) vs. Depth of Burial
(meters) (synthetic sediment)

The declination essentially remains constant with depth.

DEPTH (meters)



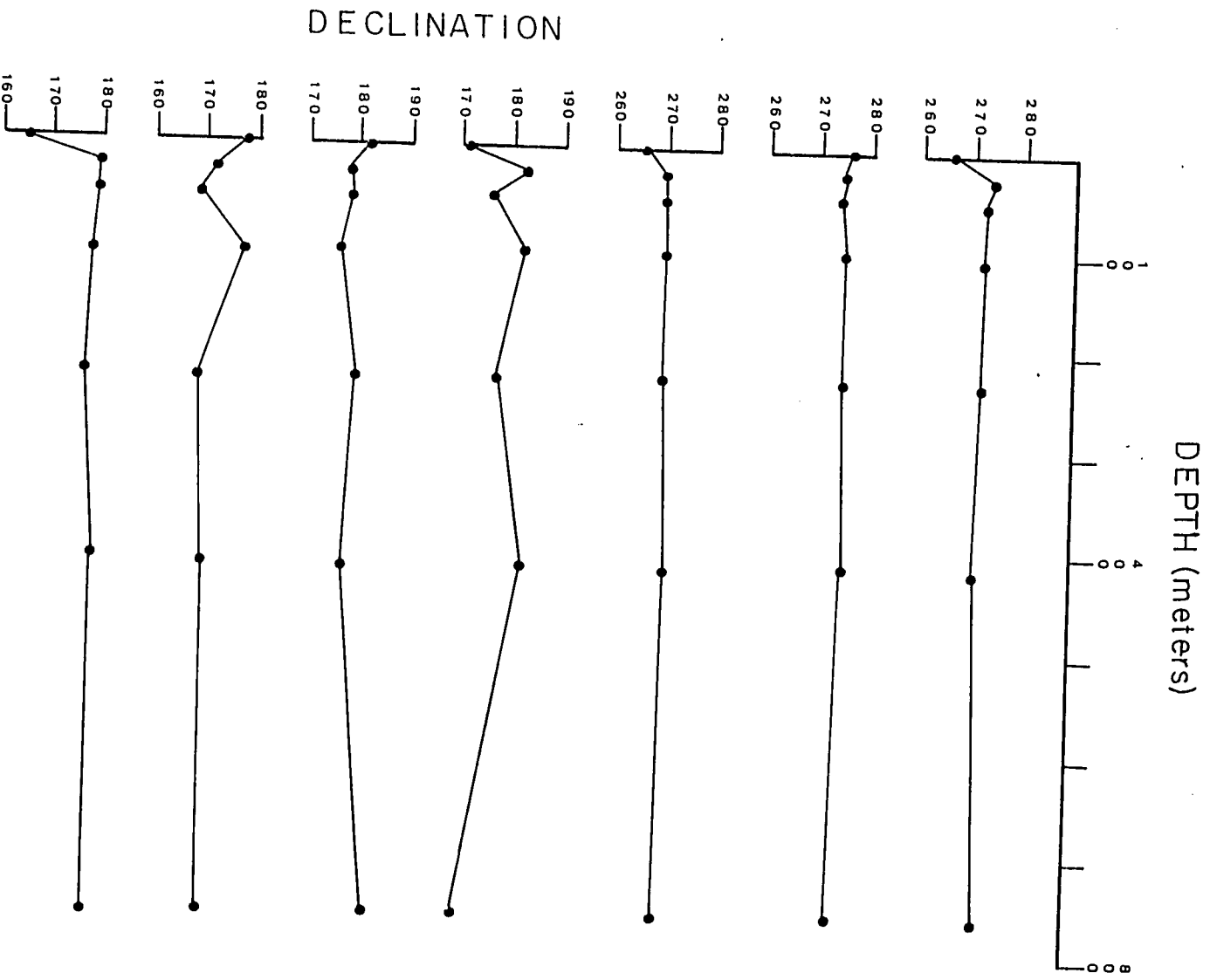
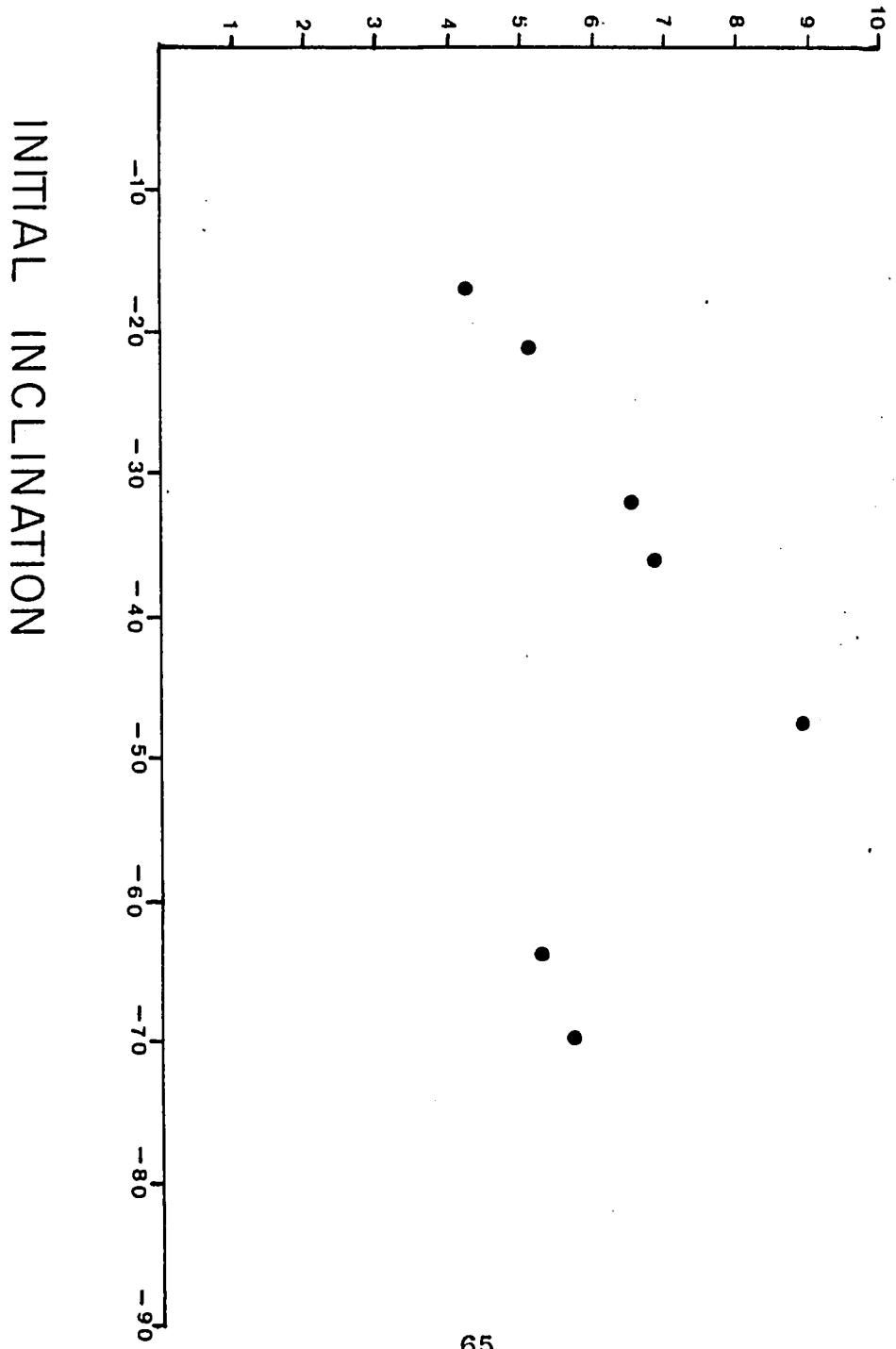


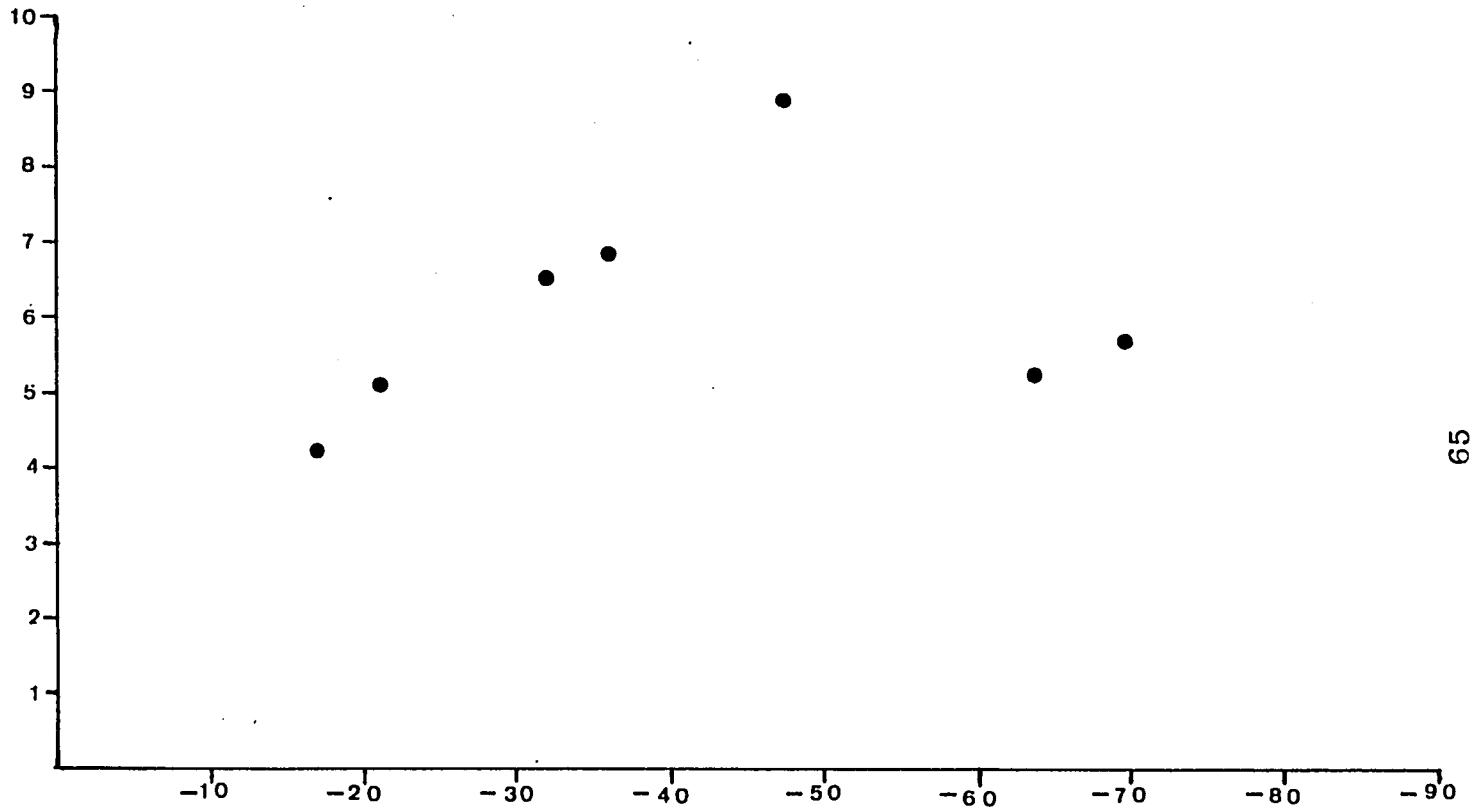
Figure 16 - Change in Inclination (degrees) vs. Initial
Inclination (degrees) (synthetic sediment).

As mentioned in the text, the initial inclination is taken to be the value obtained after the first load was reached. The graphs appear to peak at $\sim 45^\circ$. This suggests that the largest change in inclination would occur with an initial inclination of $\sim 45^\circ$. Graph A shows the data from the compaction analyses, and Graph B the data derived from the linear regression analyses (Figure 13). Both show similar trends. It was hoped that a mirroring of the data points on both sides of 45° would occur. However, the two points at initial inclinations greater than 45° do not show this.

CHANGE in INCLINATION

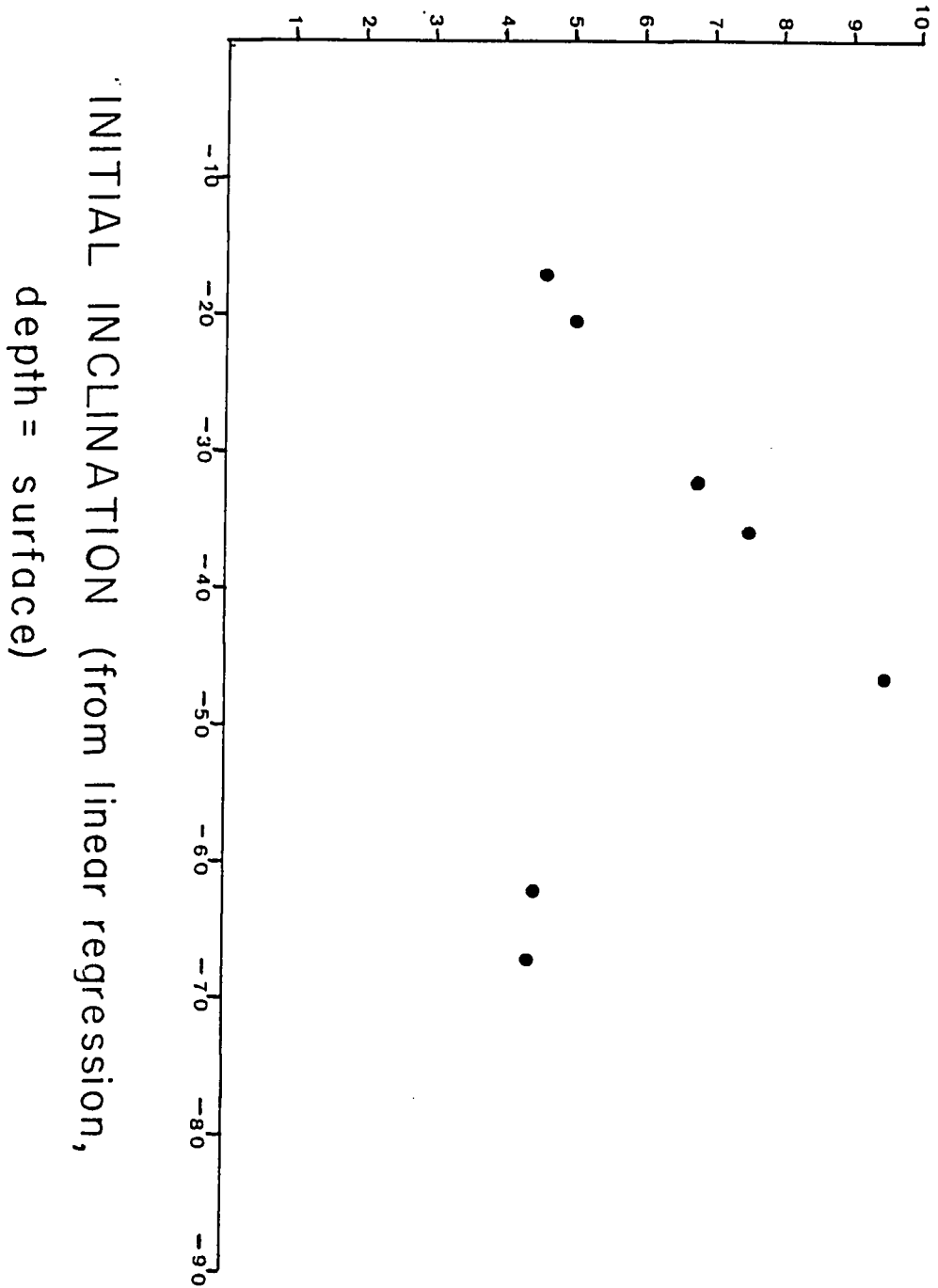


CHANGE in INCLINATION

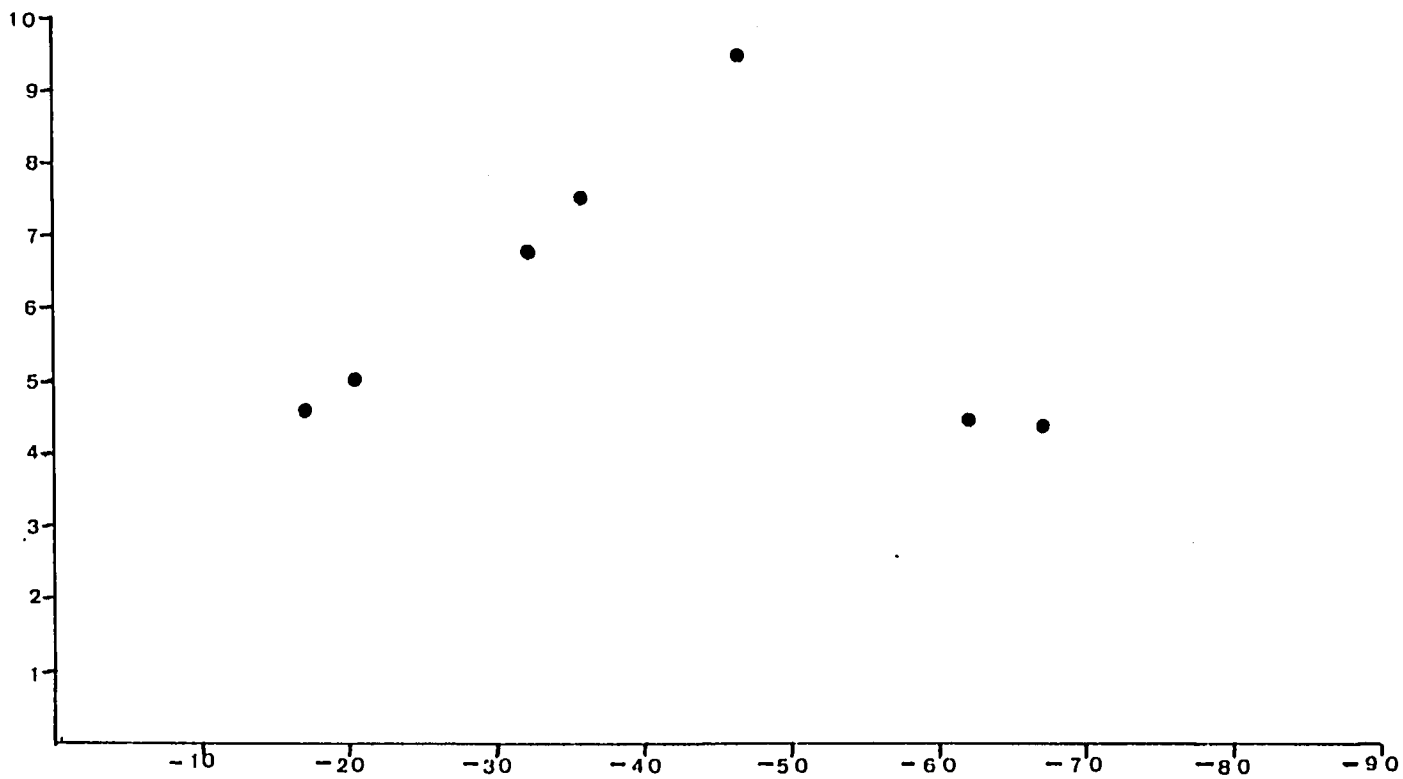


INITIAL INCLINATION

CHANGE in INCLINATION
(depth = 800 meters)



CHANGE in INCLINATION
(depth = 800 meters)



INITIAL INCLINATION (from linear regression,
depth = surface)

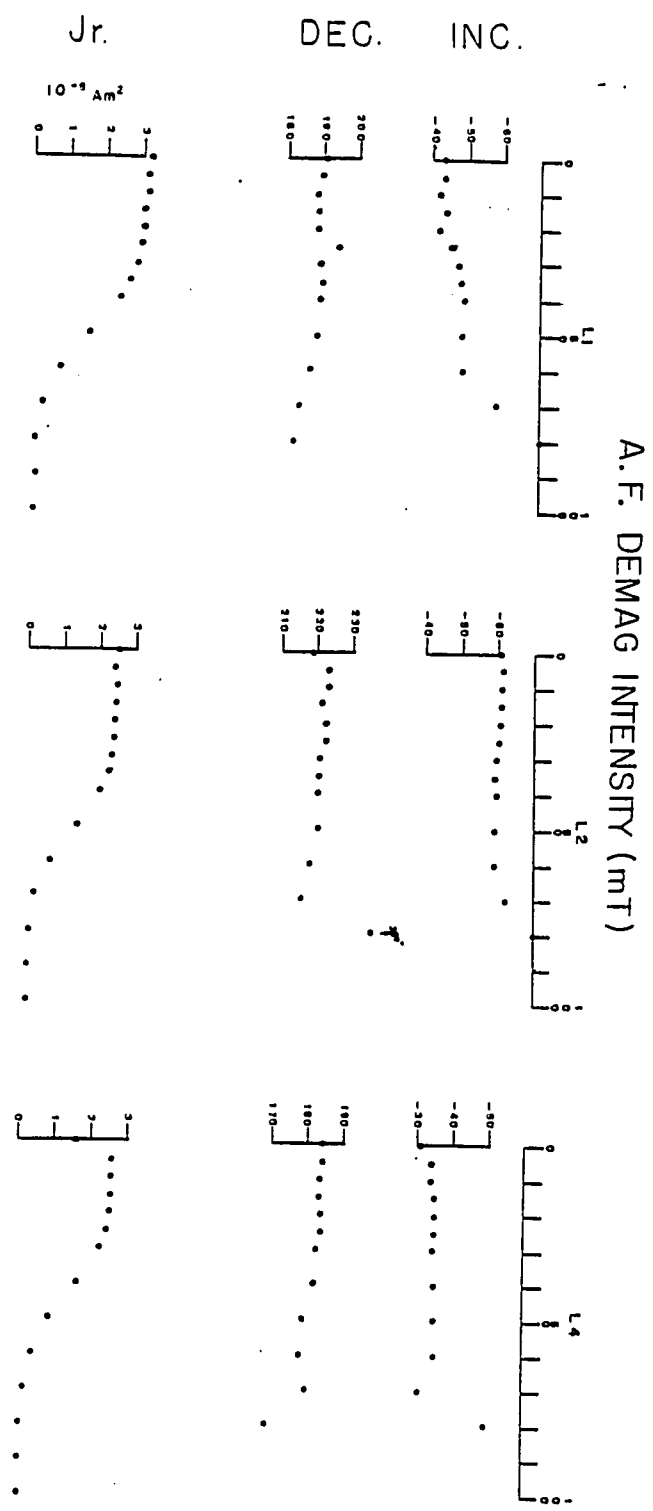
demagnetized by alternating field demagnetization (AFD). If the higher coercivity grains were not affected, one would expect the magnetic inclinations to become steeper during progressive steps in demagnetization as the remanence resulting from the lower coercivity grains is removed at lower fields.

Figure 17 is the graph of the results. Samples L2 and L4 show no significant change in magnetic inclination until an AFD field of 60 mT. After 60 mT, the data becomes scattered as the samples' intensities are less than half the original intensity. This suggests that noise from the sample at such high demagnetization fields results in the loss of the original signal.

In the case for sample L1 the inclination steadily steepens throughout the demagnetization procedure while the declination shows no significant change. This supports the idea of Tucker (1980) that, at least for this sample, the small, high coercivity grains are untouched by compaction.

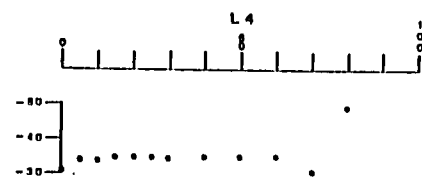
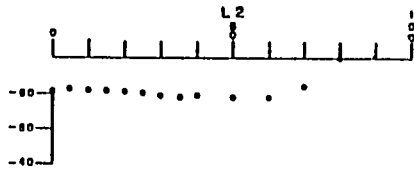
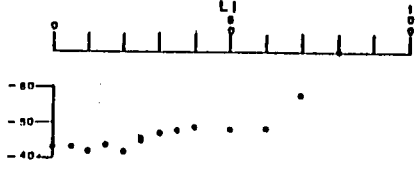
Figure 17 - Demagnetization Curves for Samples L1, L2, and L4.

Samples L2 and L4 have magnetic inclinations that show no significant change until after 60 mT. After this point, the data becomes scattered as the intensity drops to 1/2 the original intensity. The noise from the sample at such high demagnetization fields results in the loss of the original signal. However, for sample L1, the inclination steadily steepens while the declination shows no significant change. This supports the idea of Tucker (1980), that the small high coercivity grains are untouched by compaction.



A.F. DEMAG INTENSITY (mT)

INC.

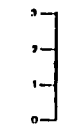
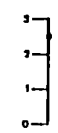
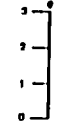


DEC.



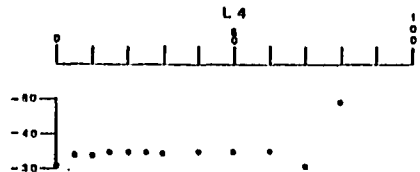
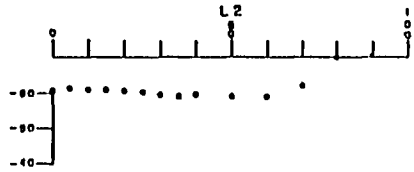
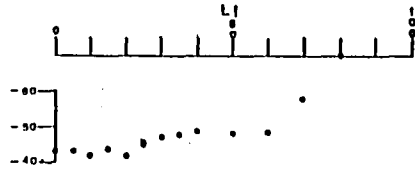
Jr.

10^{-4} Am^2

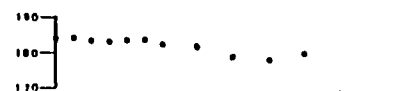
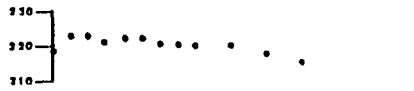
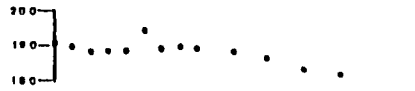


A. F. DEMAG INTENSITY (mT)

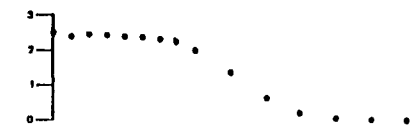
INC.



DEC.



Jr.



Marine Sediment

The marine samples (M4, M5, and Mc) show a different pattern of magnetic change than the synthetic material. Figure 18 compares the results of samples M4 and M5.

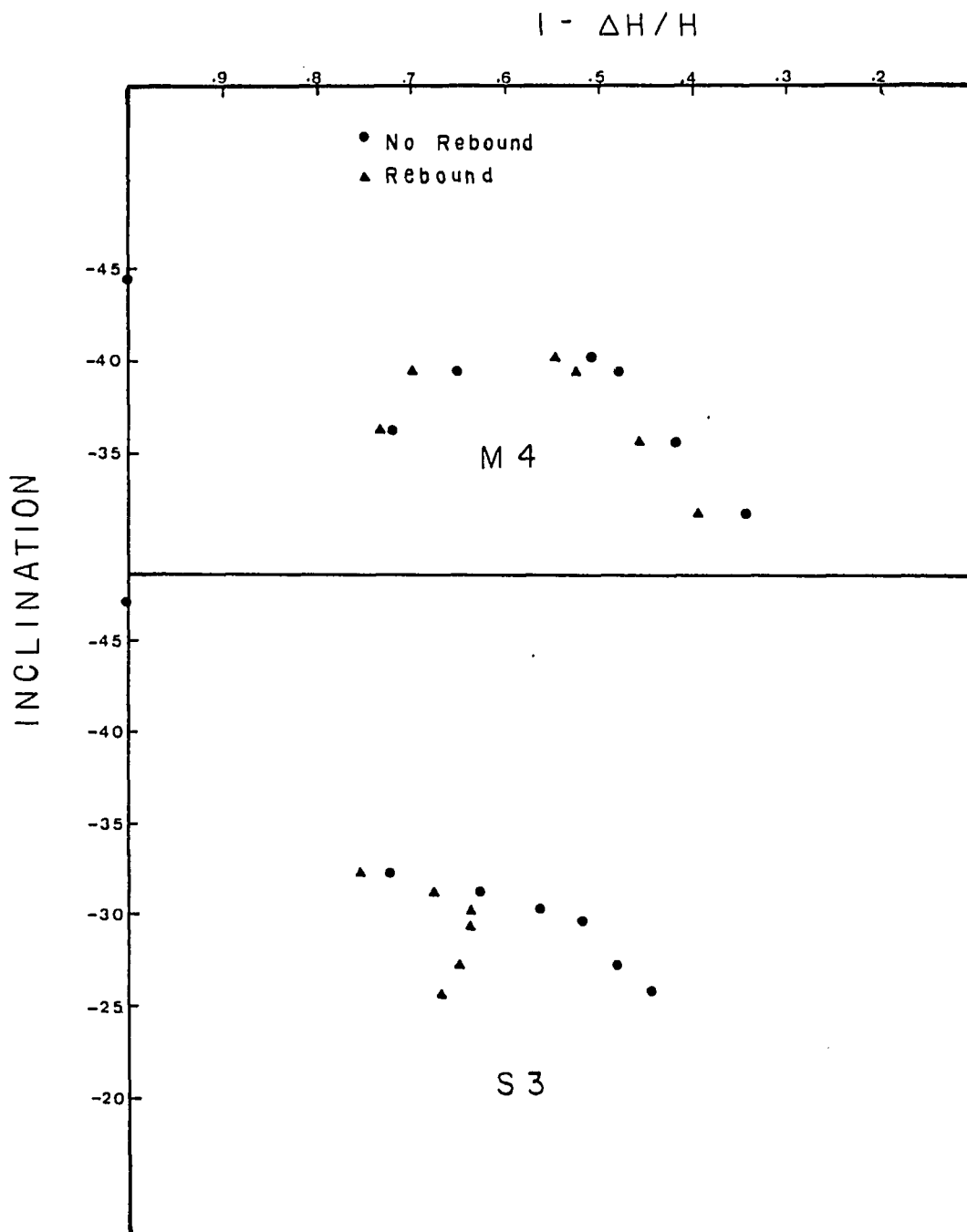
Sample M5 is included with the data, but is not considered characteristic of the marine sediment. During this analysis, the intake valve of the consolidometer became clogged with rust from the pipes supplying air to the machine. Because of this, the consolidometer was unstable throughout the procedure. This unfortunately, was not discovered until well into the experiment. Instead of repeating this analysis, the Mc series were run. The Mc series is the results of six (6) samples (M6 to M11) analyzed by not stopping compaction until a desired load was attained. Figure 19 is the graphical representation of the magnetic data vs. $1-\Delta H/H$.

Sample M4 has the initial jump in inclination as seen in the synthetic sample. However, after the second load was applied, the inclination became steeper and constant until after the fifth load, it became shallow again.

The magnetic declination was erratic, with large errors showing no stability. The intensity, however, did decrease with consolidation in similar fashion to the synthetic material.

Figure 18 - Inclination (degrees) vs. $1-\Delta H/H$ for Samples S3 and M4.

These two samples were initially magnetized near 45° , and are used to contrast the change in inclination of each. Whereas the synthetic sediment continuously shallows, the marine sediment shallows, then steepens, then shallows again. The theoretical points are the same for both data. The rebound data shows that the synthetic sediment rebounded more than the marine.



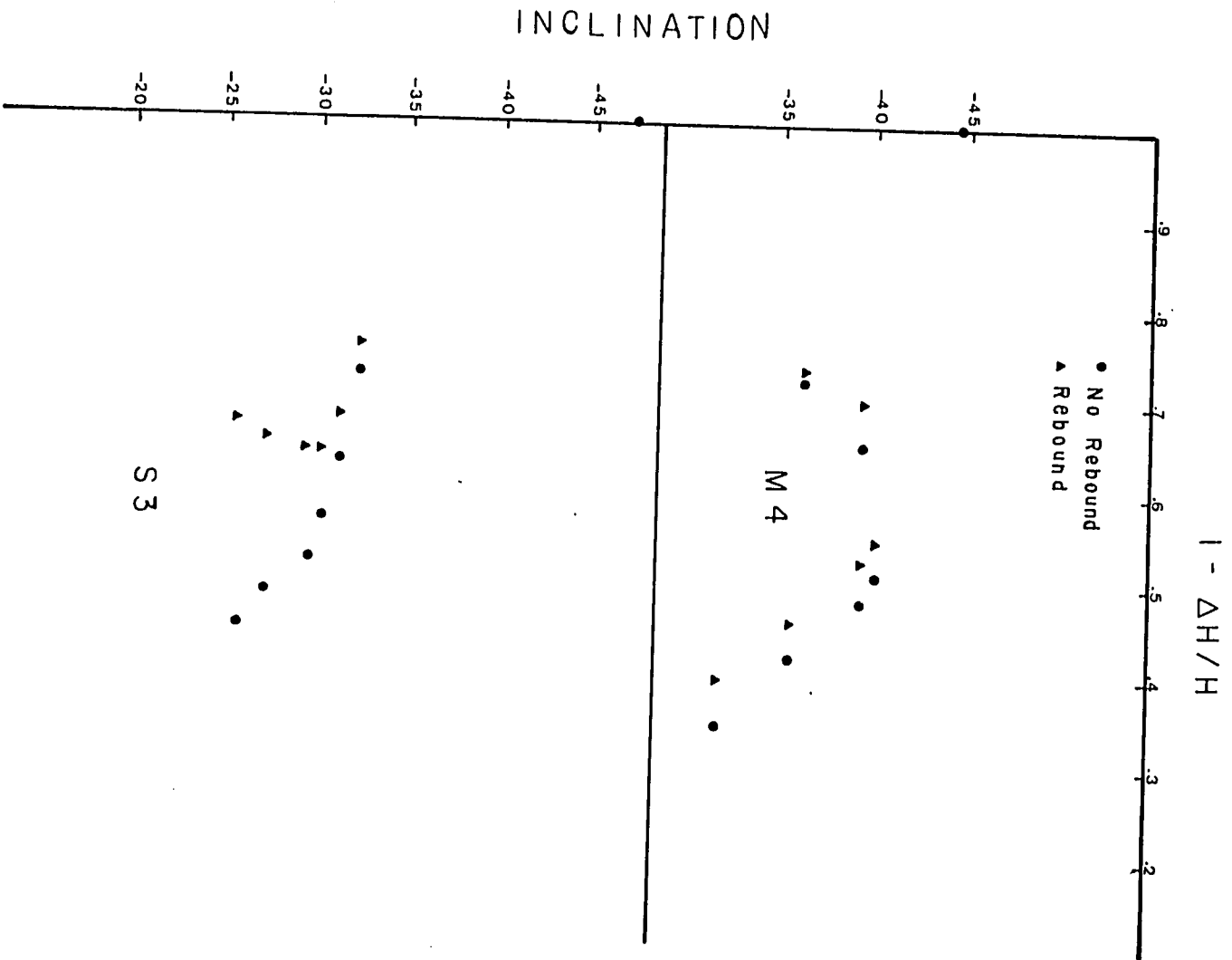
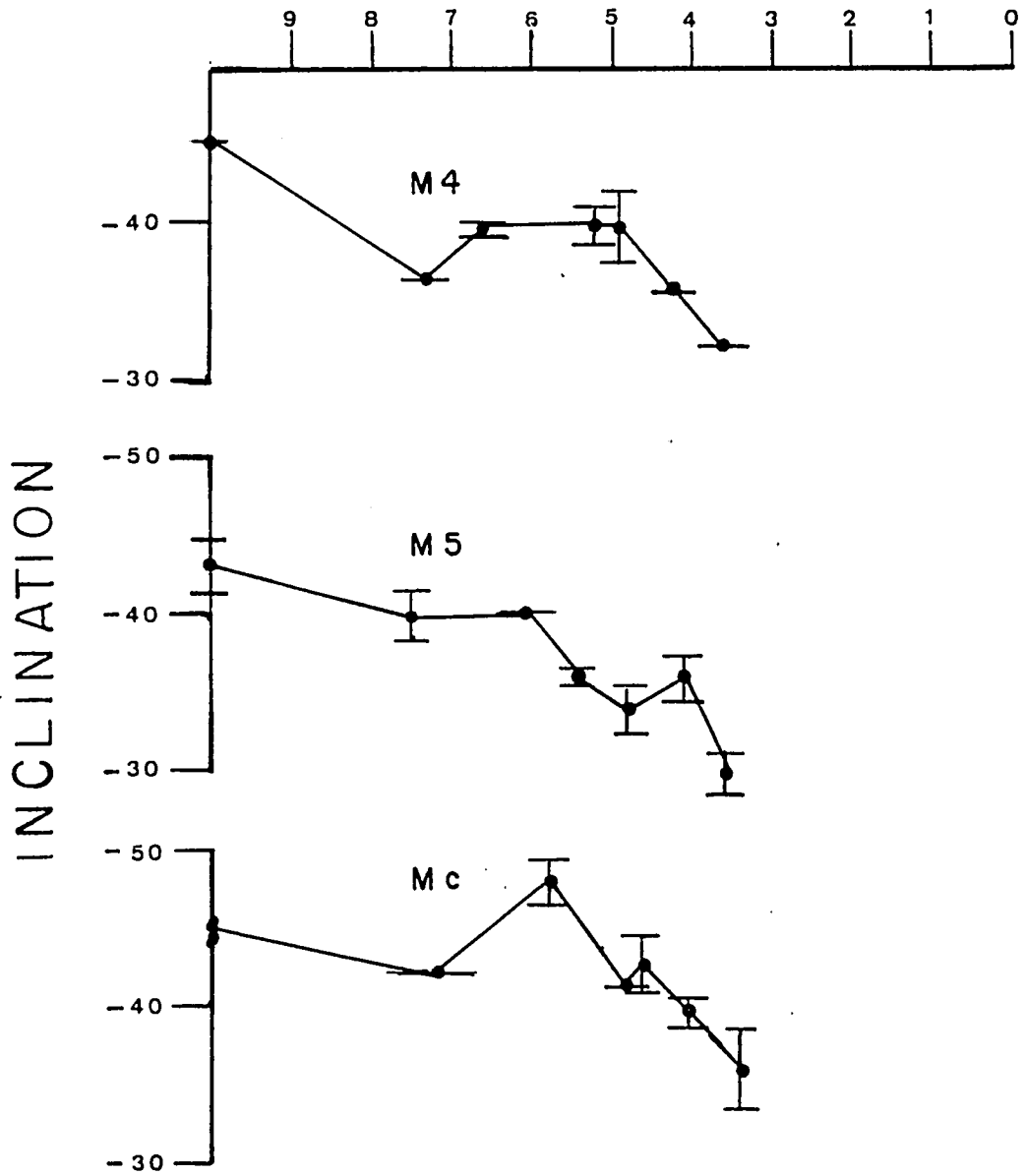


Figure 19 - Inclination (degrees), Declination (degrees) and Intensity (10^{-10}Am^2) vs. $1 - \Delta H/H$ (marine sediment).

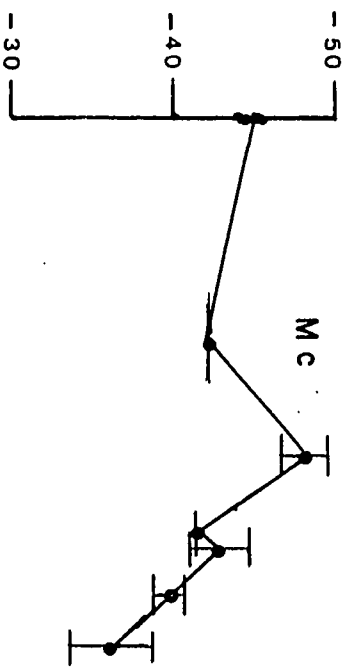
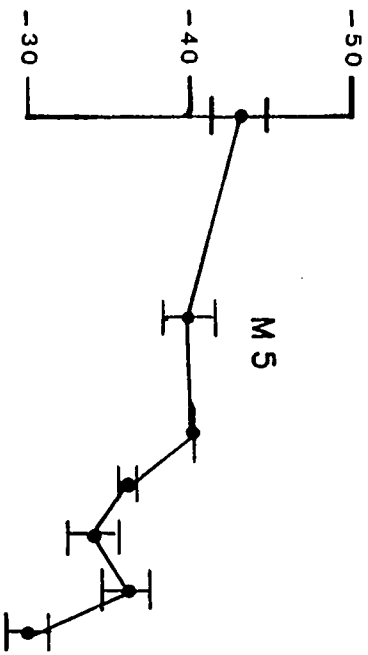
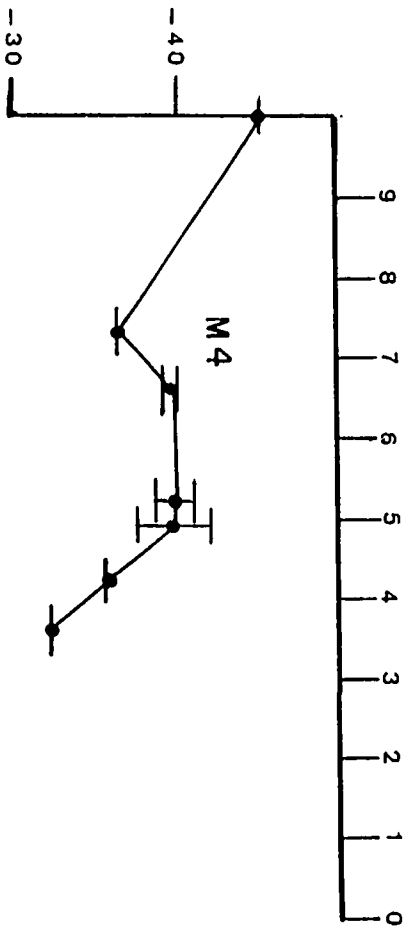
Sample M5 is not considered to properly represent the marine sediment because of problems with the consolidometer during analysis. Samples M4 and Mc show similar trends of change in inclination as consolidation occurs. Although there is an increase in inclination after the second load is applied to the Mc samples, there is no corresponding data point for the M4 sample. However, the trend of the M4 sample is to steepen, and, perhaps, if M4 had continued to compact on the second load, a similar data point would have been seen. Both procedures, therefore may be consistent. The declination appears to vary and is erratic. However, the large amount of error associated with the data points suggest that it is constant like the synthetic sediment.

The intensity decreases during consolidation in similar manner to the synthetic samples suggesting that similar processes occur in both sediments that give rise to the decreasing intensity. Because the initial differences in declination and intensity of the individual Mc samples, they are not included in the Figures. The Mc samples M6 to M12 which were analyzed by compacting until the desired load was reached.

$$1 - \Delta H / H$$

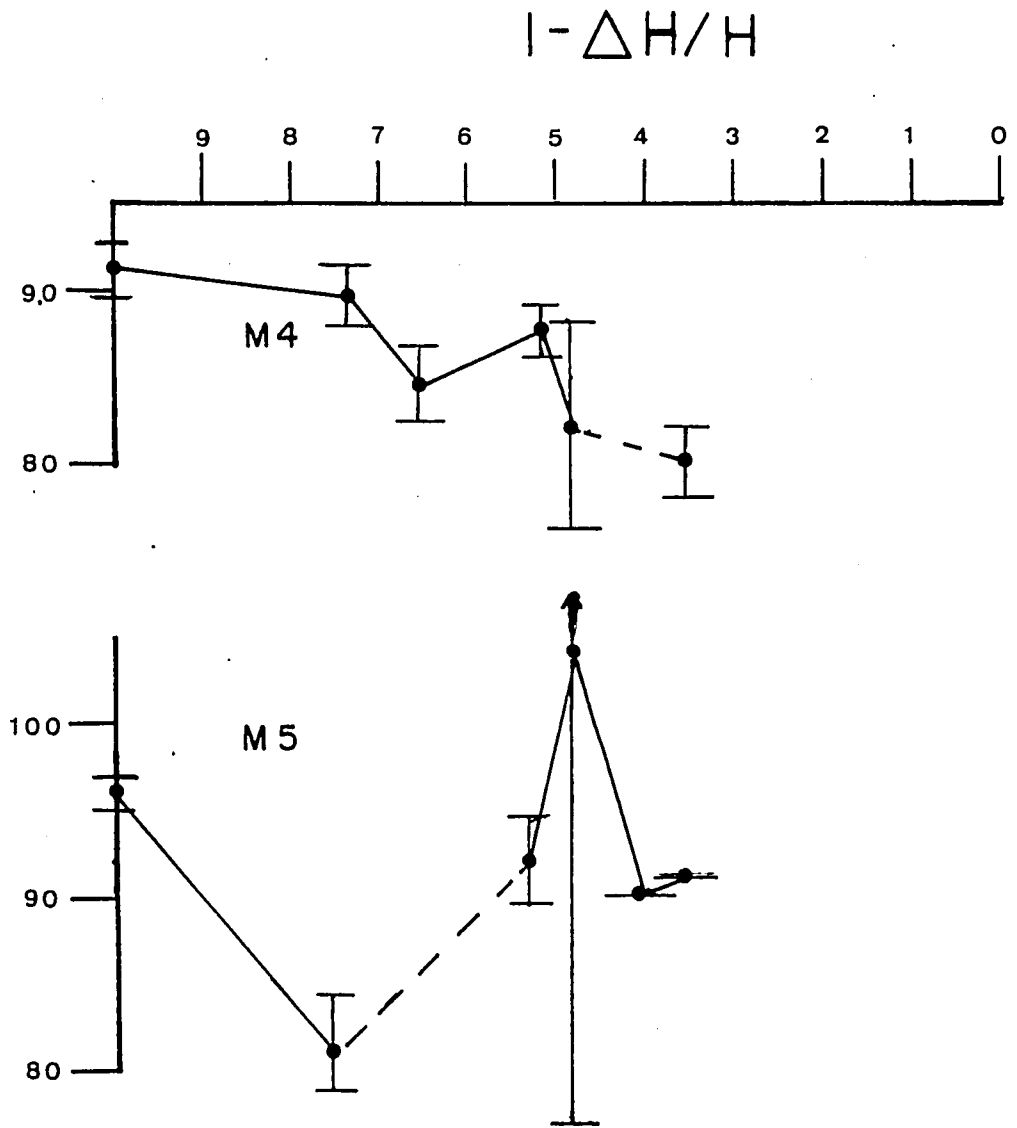


$1 - \Delta H/H$

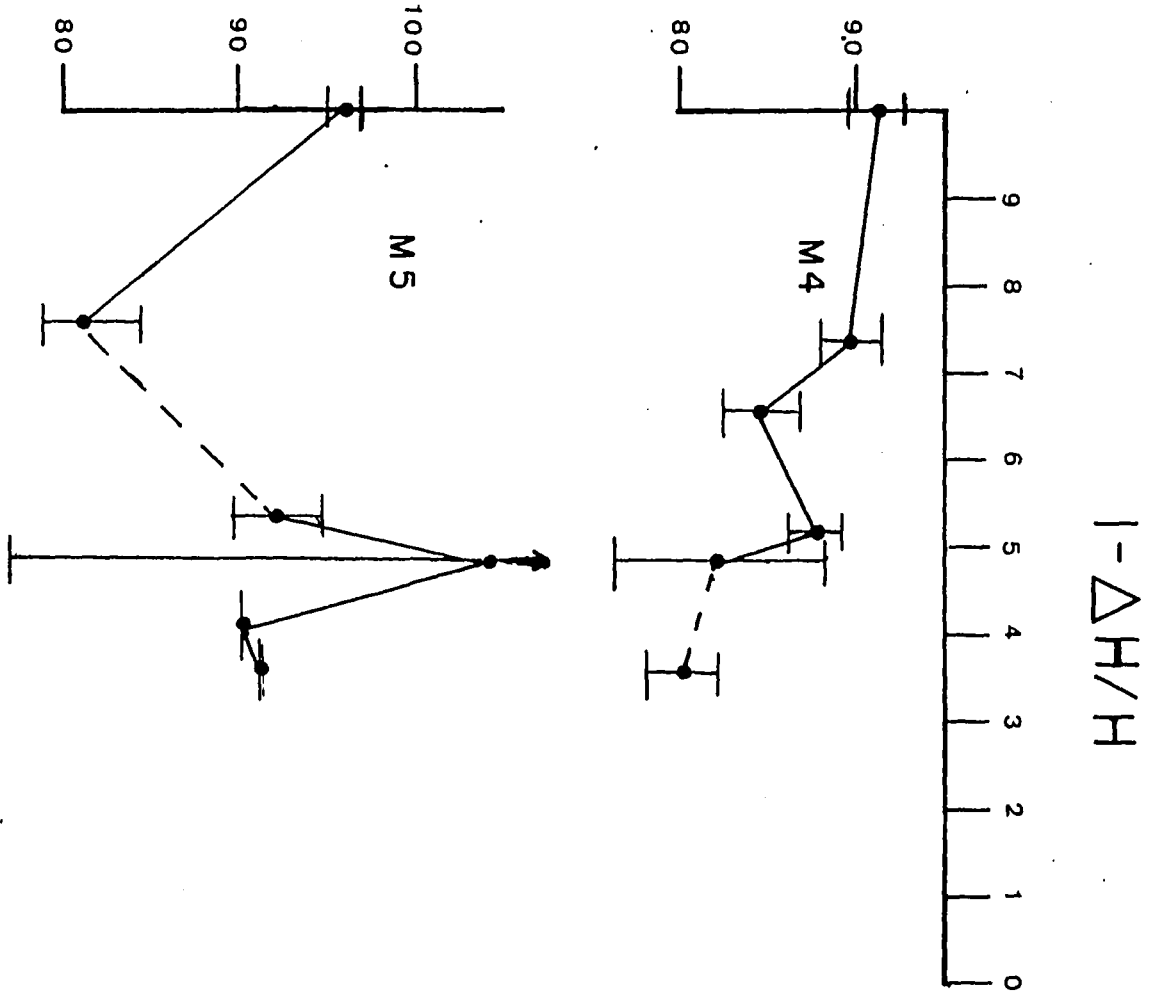


INCLINATION

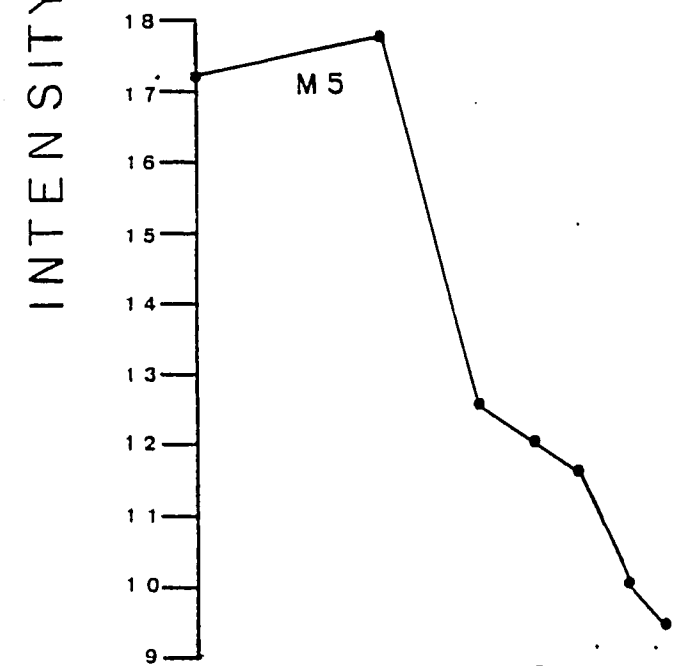
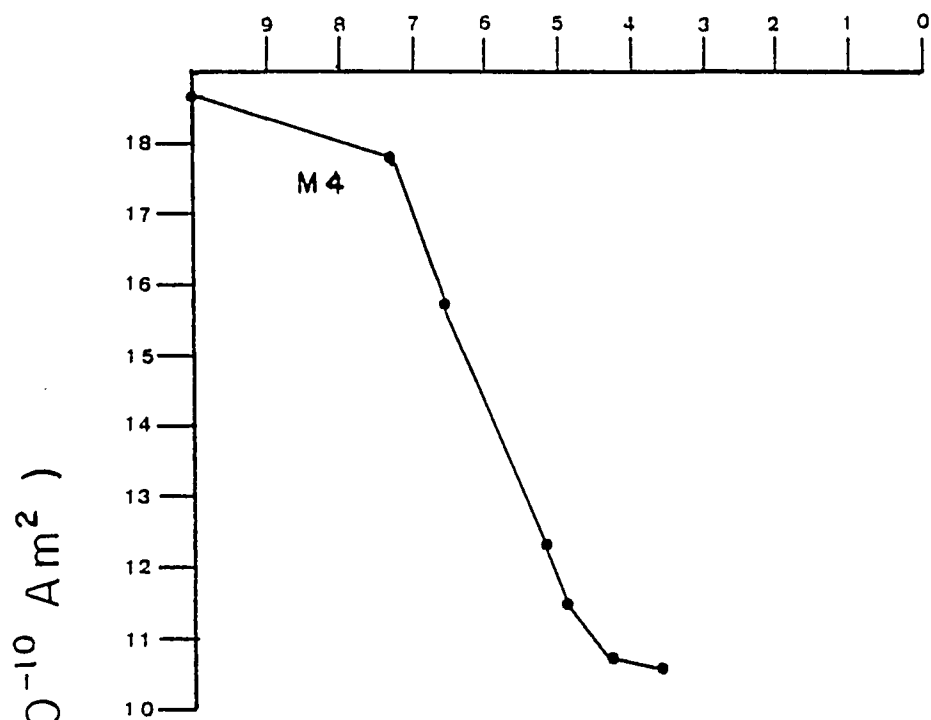
DECLINATION



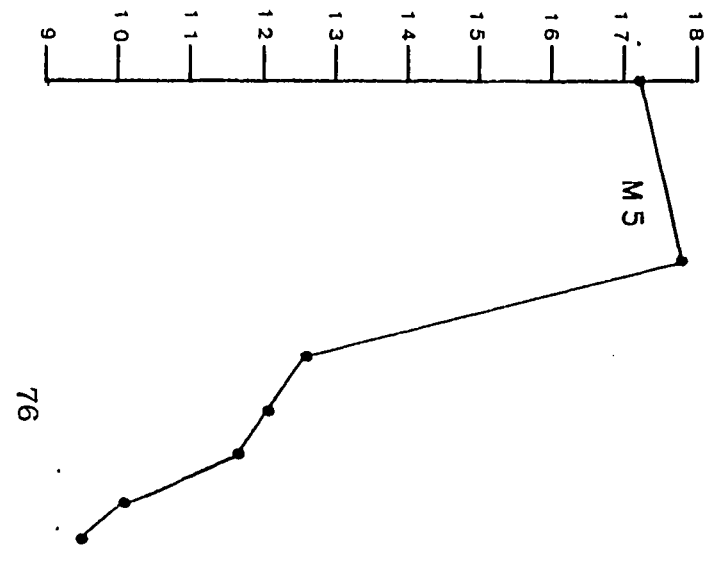
DECLINATION



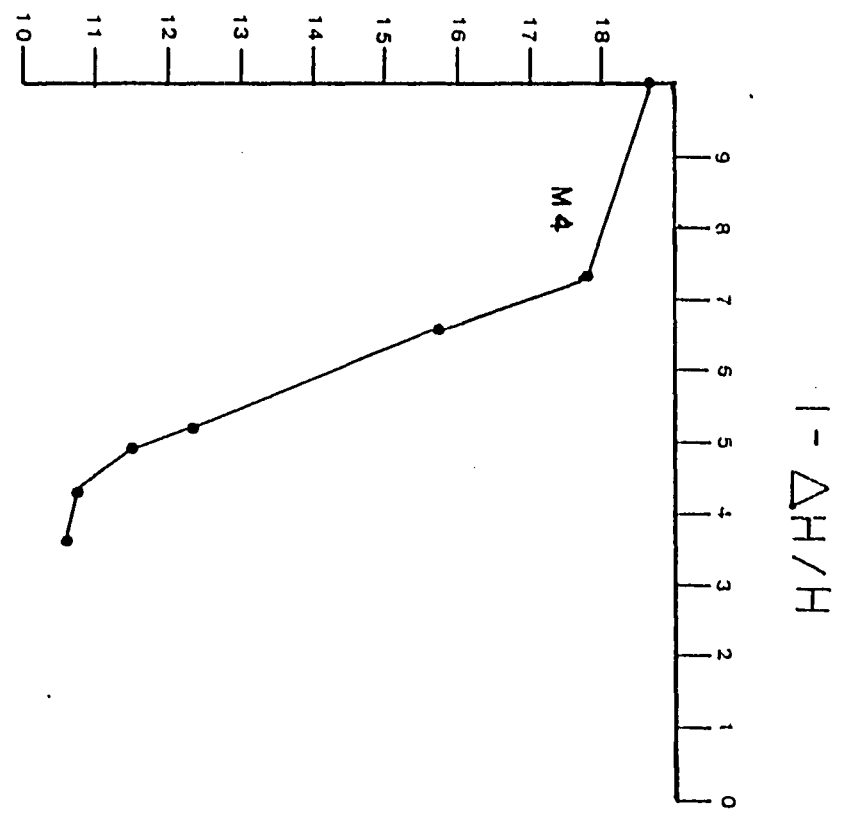
$$1 - \Delta H / H$$



INTENSITY (10^{-10} Am^2)



76



$1 - \Delta H/H$

The change in magnetic inclination associated with the Mc samples is similar to the change associated with the M4 sample. There is the initial jump in inclination, followed by a steepening when the second load is applied. After the fourth load is applied the subsequent inclination values are shallower as compaction continues.

An increase in inclination is seen in the values for the sample compacted to the second load that is not seen in the M4 sample. However, where the spike is seen there is no corresponding data for the M4 sample. It is difficult to conclude that if the M4 sample had compacted to the same degree as the Mc sample on the second load that the subsequent inclination would be steeper than what is seen. The trend of steepening inclination when the second load is applied is seen with M4. Thus there is at least a suggestion that the same point would have been reached by M4 if it had been compacted to the same degree as Mc on the second load.

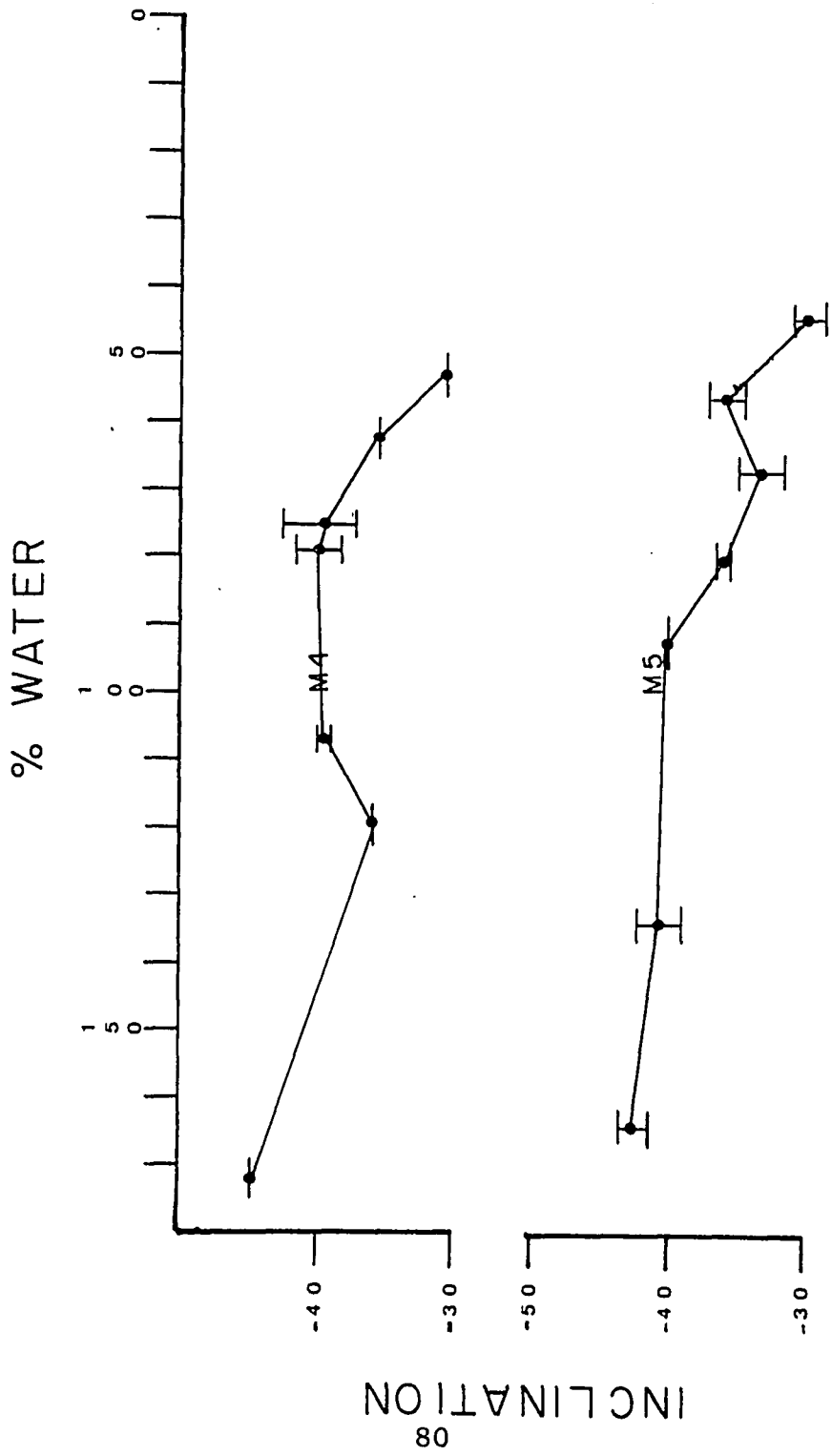
For the marine sediment, the manner in which the sample is compacted (stepwise with removal from the consolidometer between loads to stepwise with no removal until a particular load was attained) does not appear to affect the remanent magnetism. Only the fact that the sediment was consolidated appears to result in the apparent change in remanent magnetism.

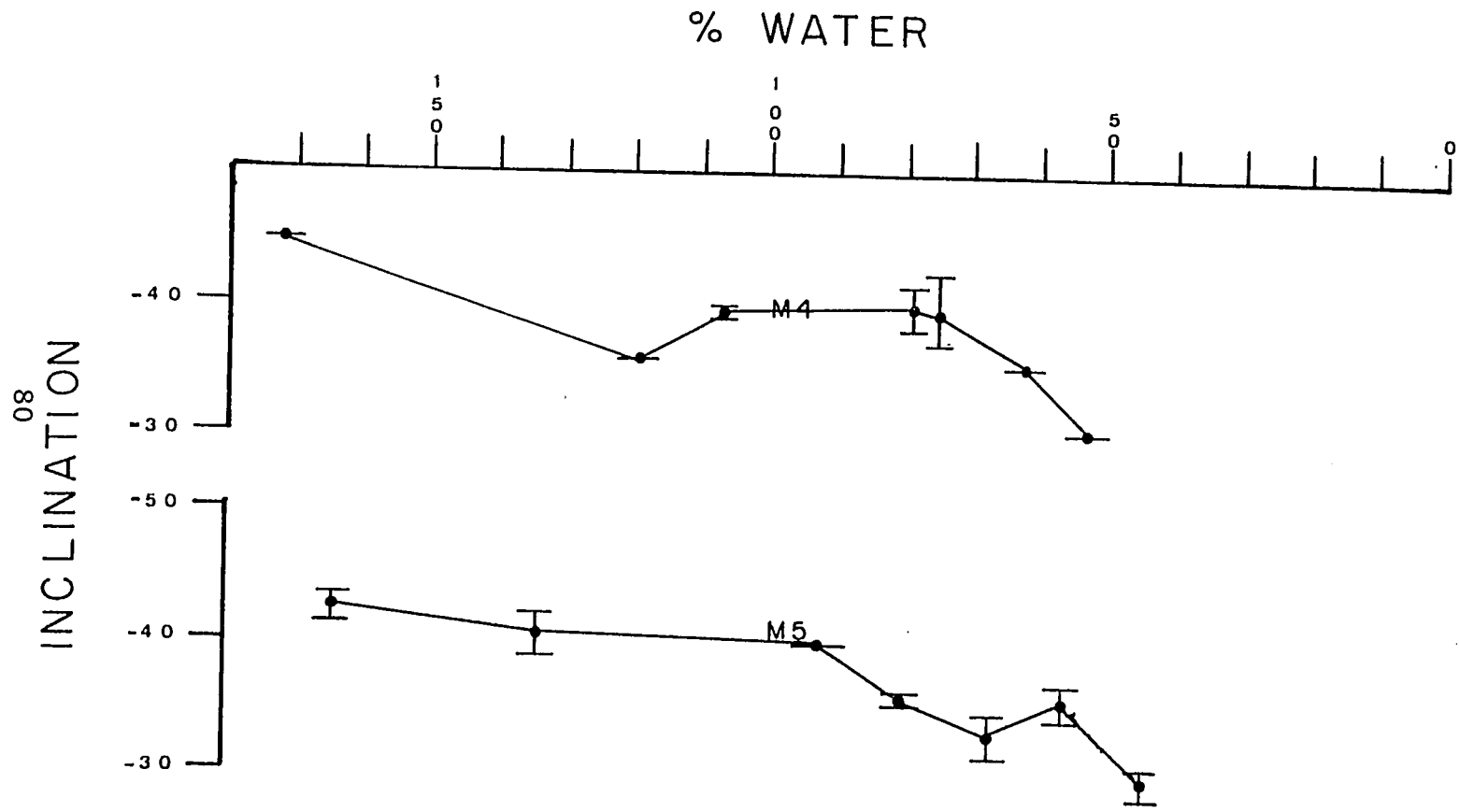
Figure 20 shows the magnetic data vs. % water. Because the % water is considered to be linearly related to the change in height, Figure 20 shows the same basic trend as Figure 19.

Figure 21 shows the magnetic data vs. depth of burial.

Figure 20 - Inclination (degrees), Declination (degrees),
and Intensity (10^{-10} Am²) vs. % Water
(marine sediment).

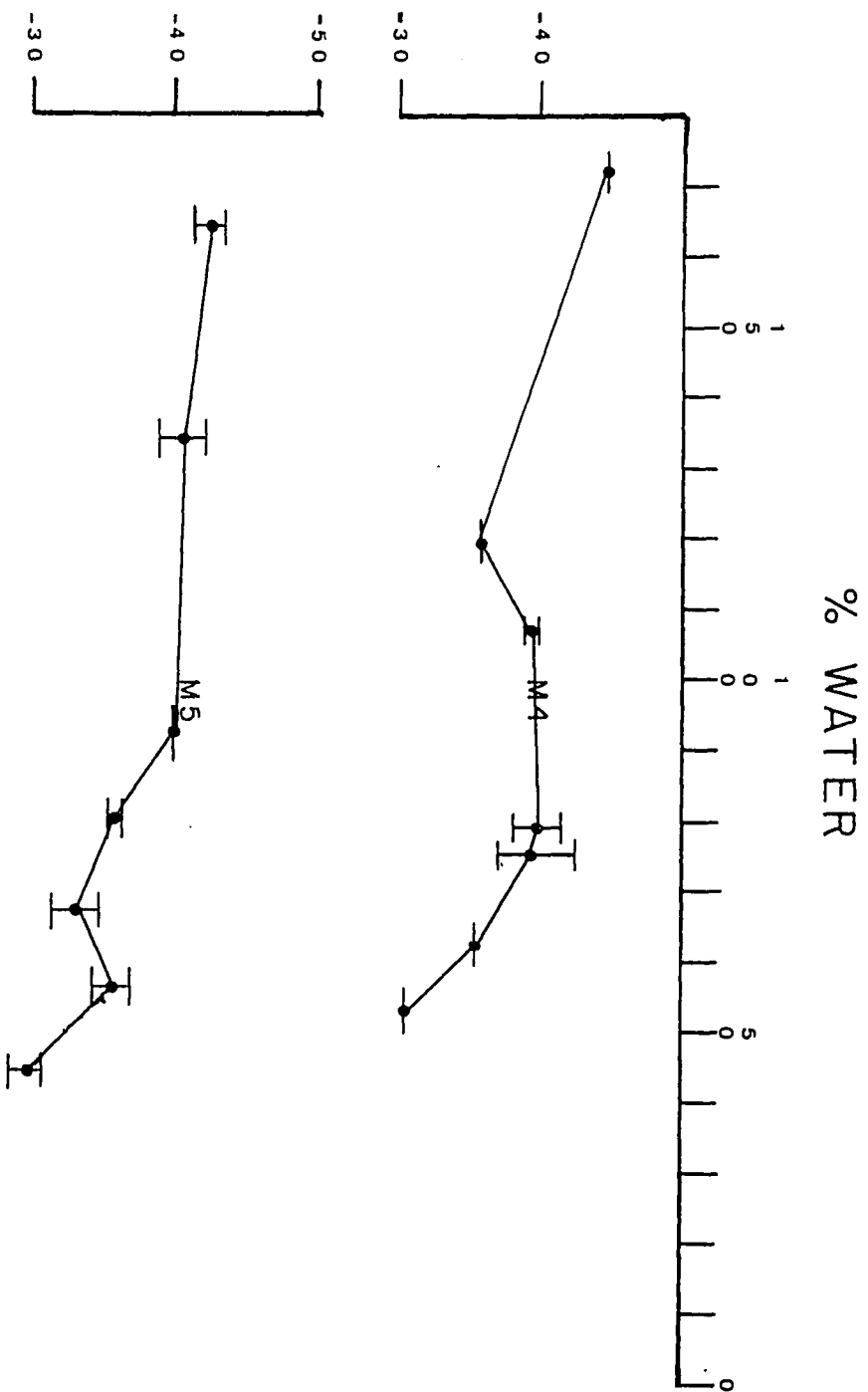
These show similar trends as Figure 19 because of the
linear relationship between sample height and % water.

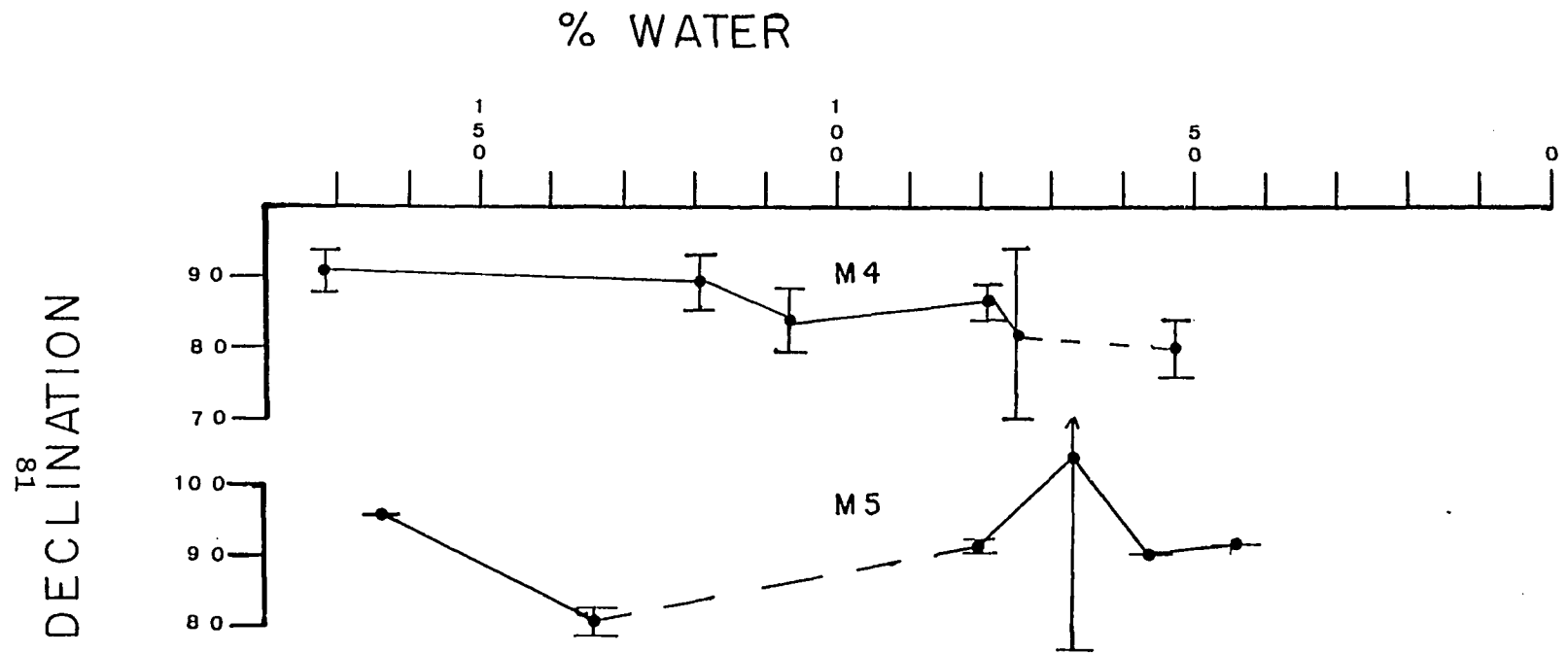




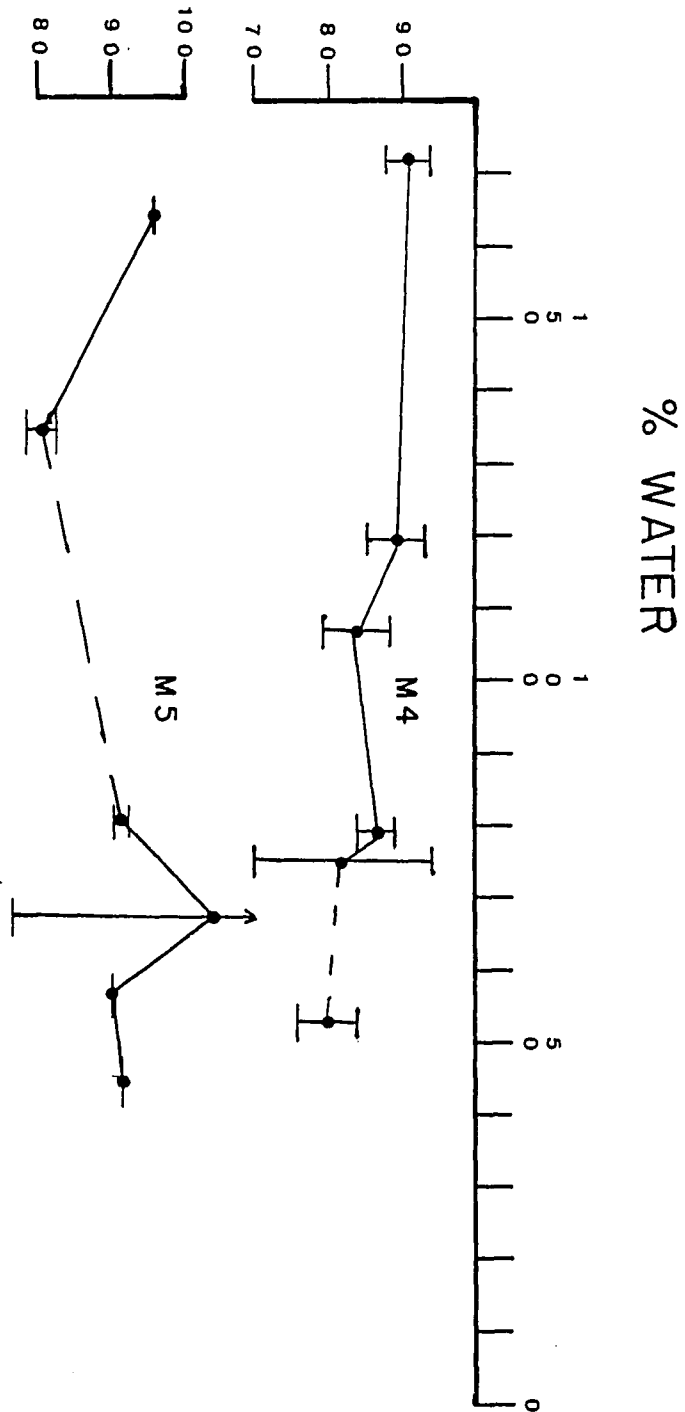
08

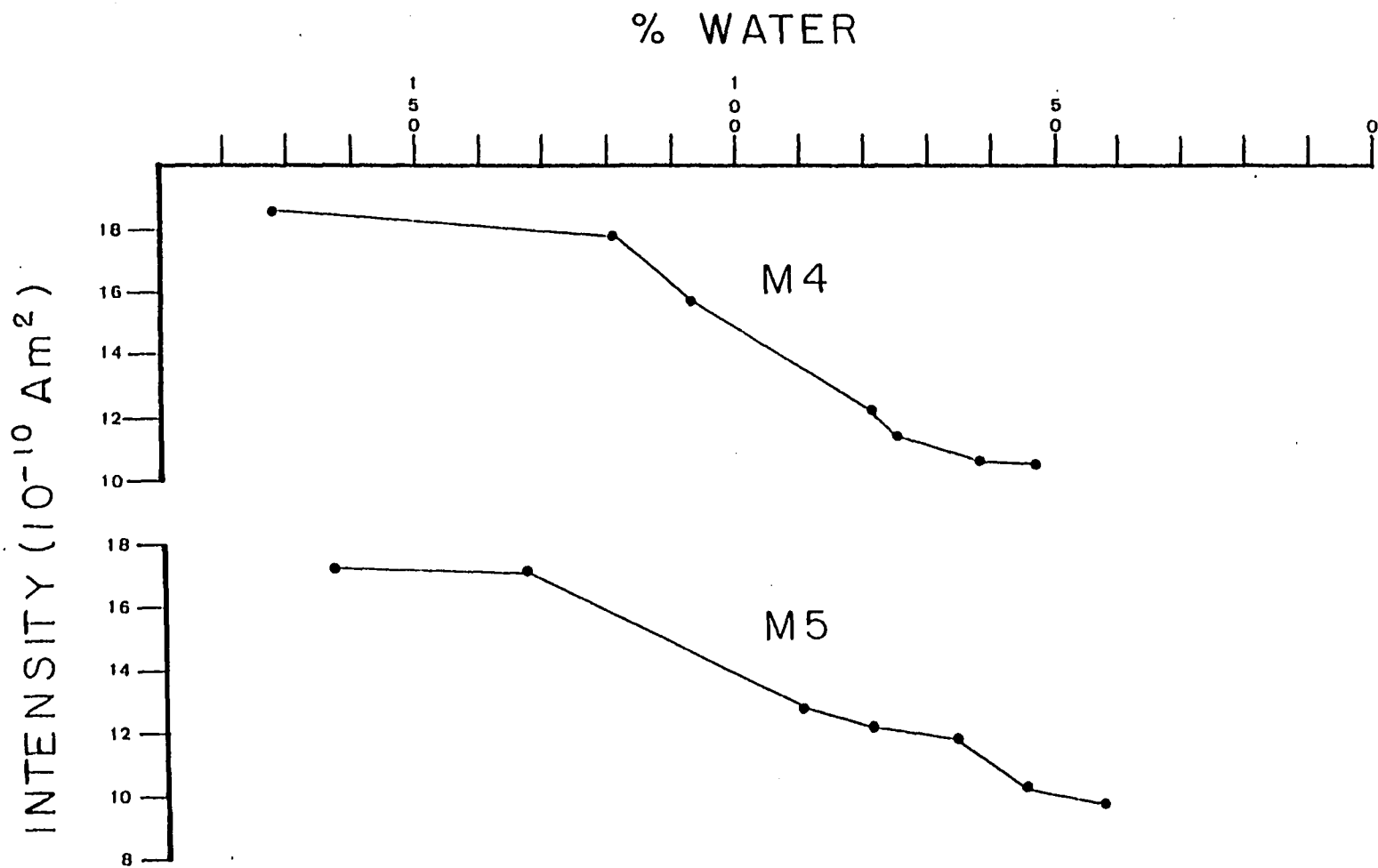
INCLINATION





DECLINATION





INTENSITY (10^{-10} Am²)

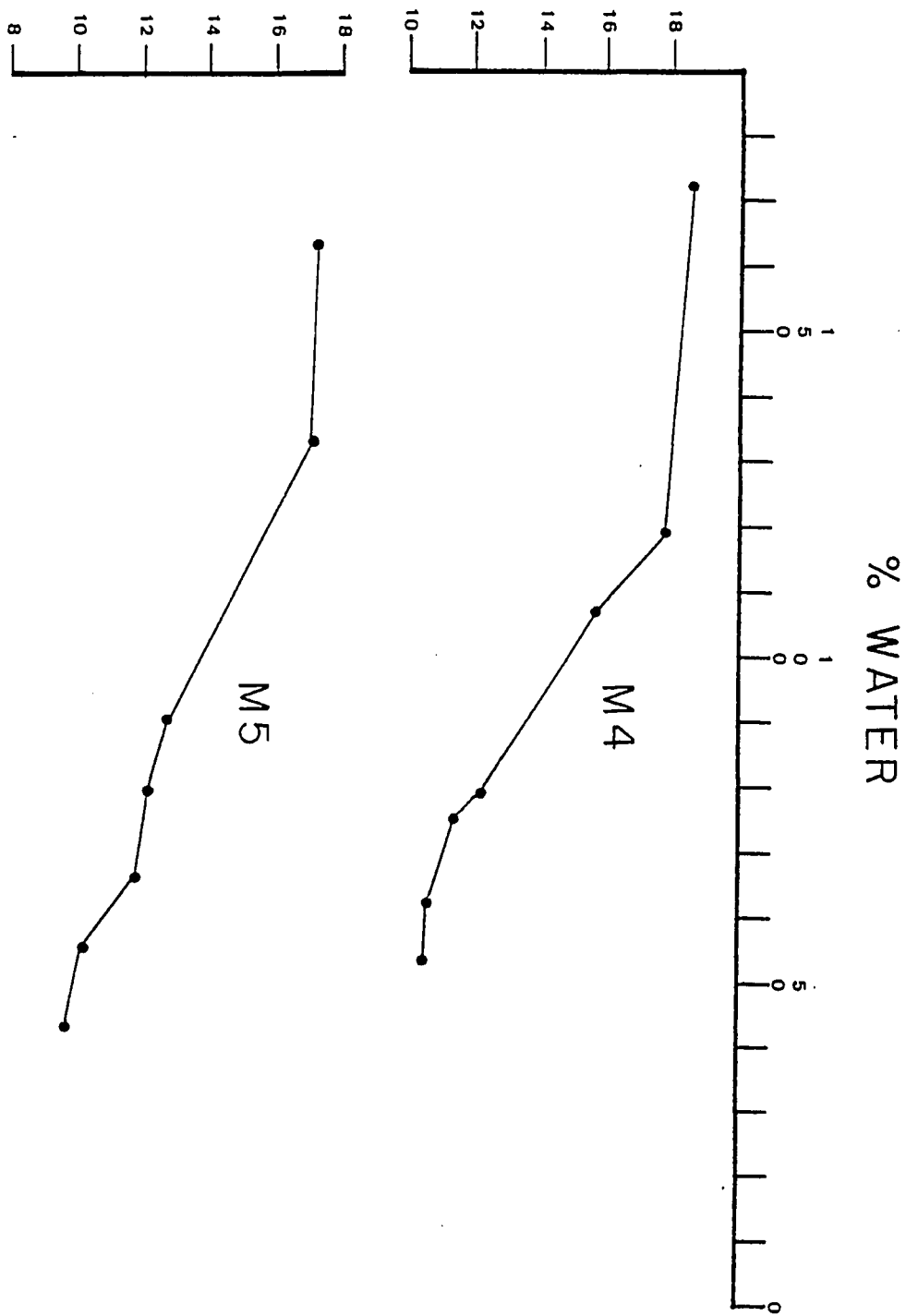
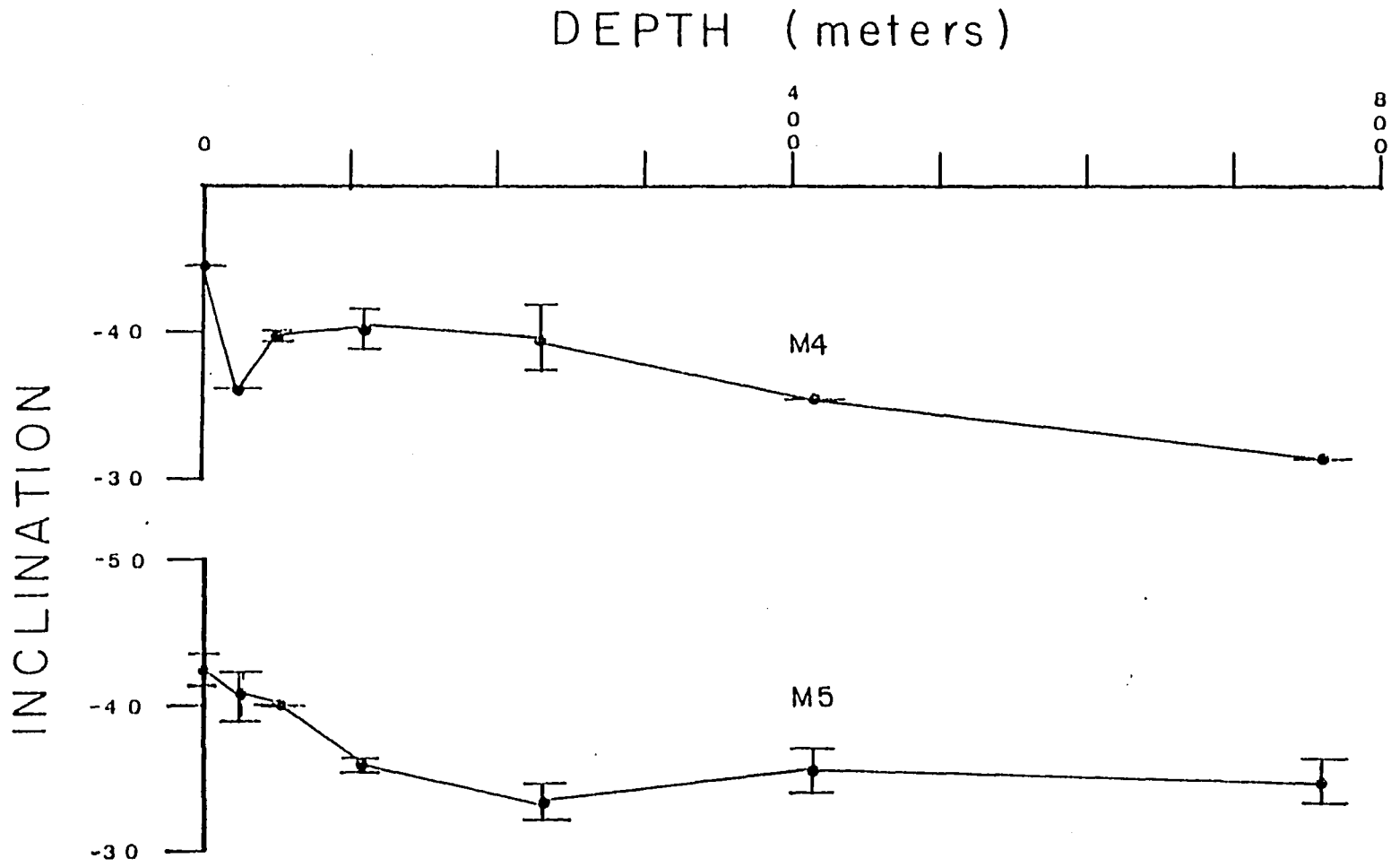
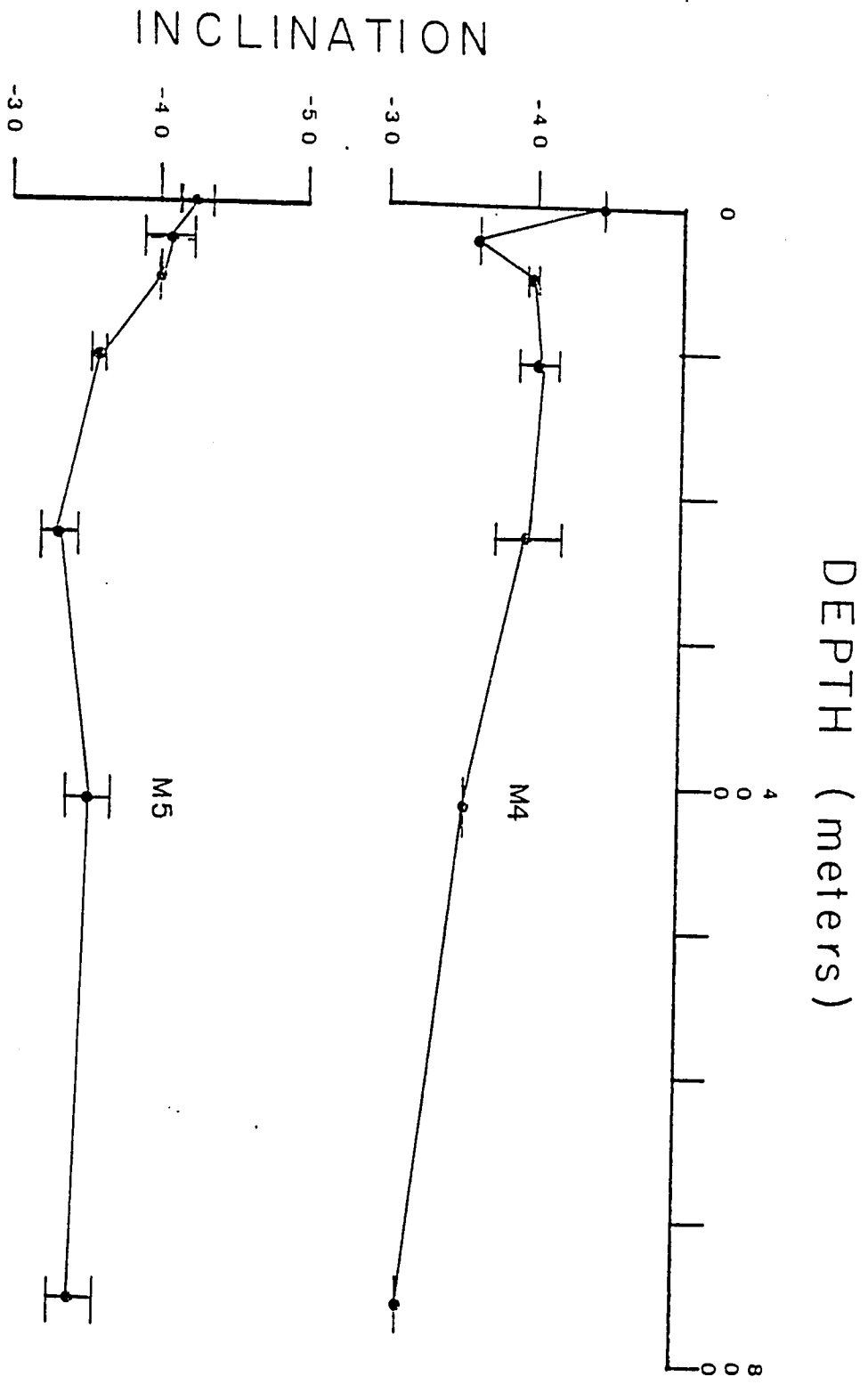


Figure 21 - Inclination (degrees), Declination (degrees), and Intensity (10^{-10} Am²) vs. Depth of Burial (marine sediment).

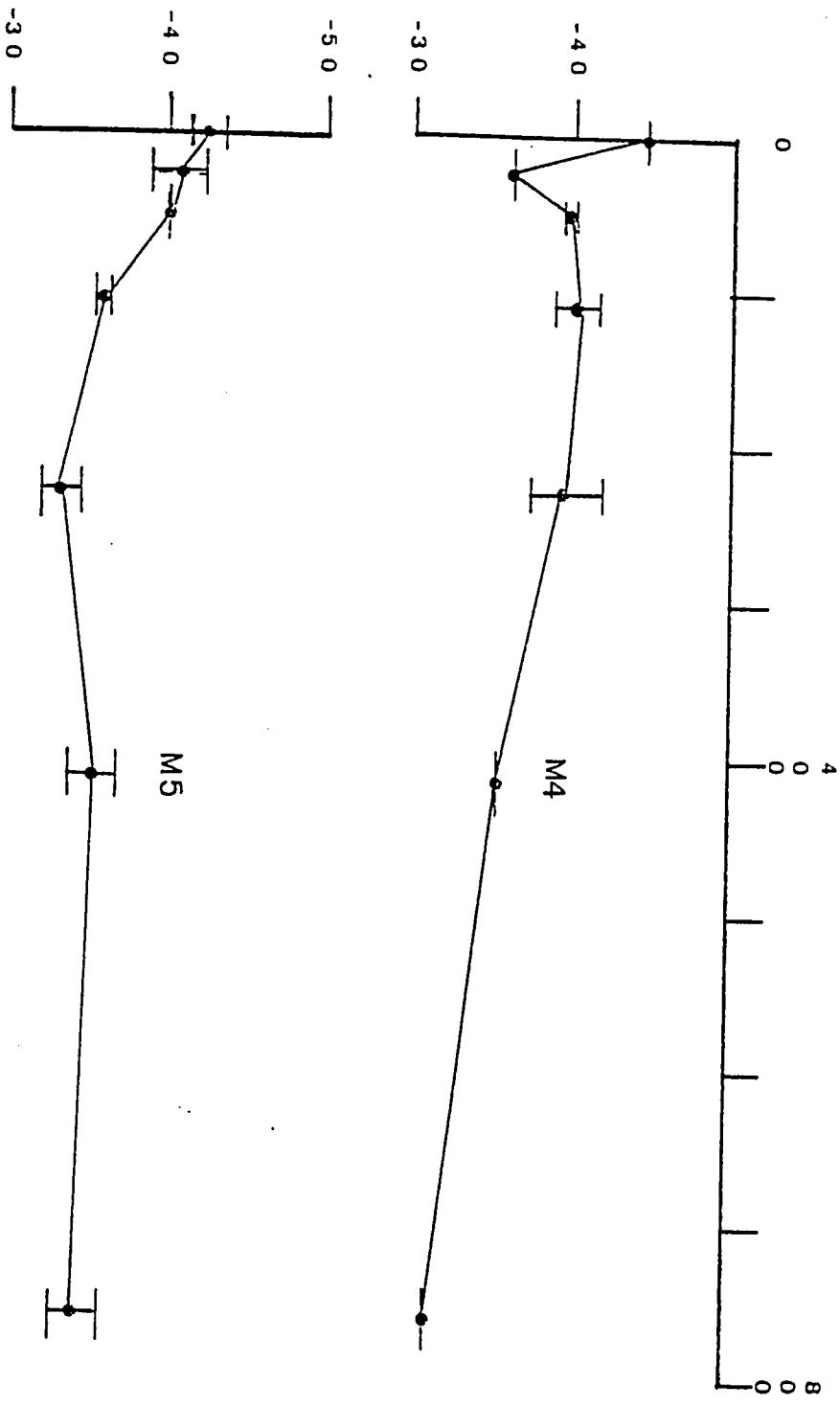
These were prepared in similar fashion to Figures 13, 14, and 15. Because of the different pattern of change in inclination, linear regression analysis was not performed on these data.

84





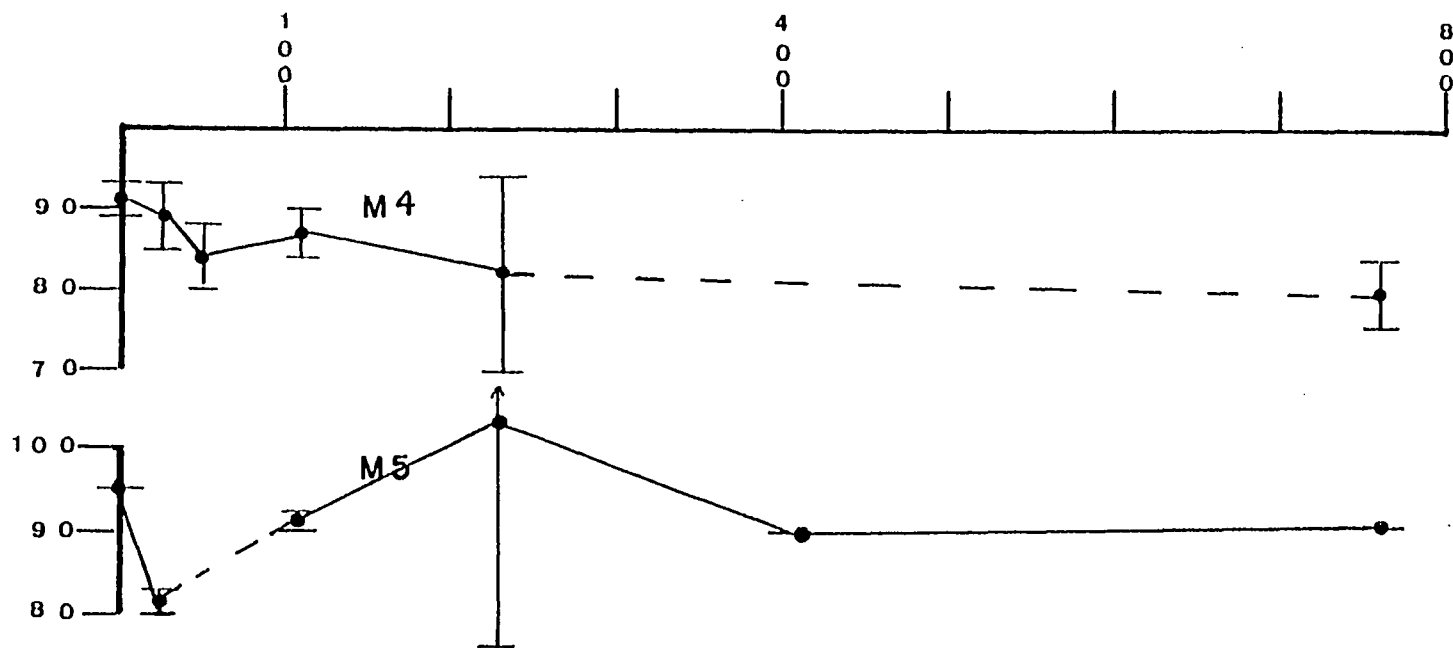
INCLINATION



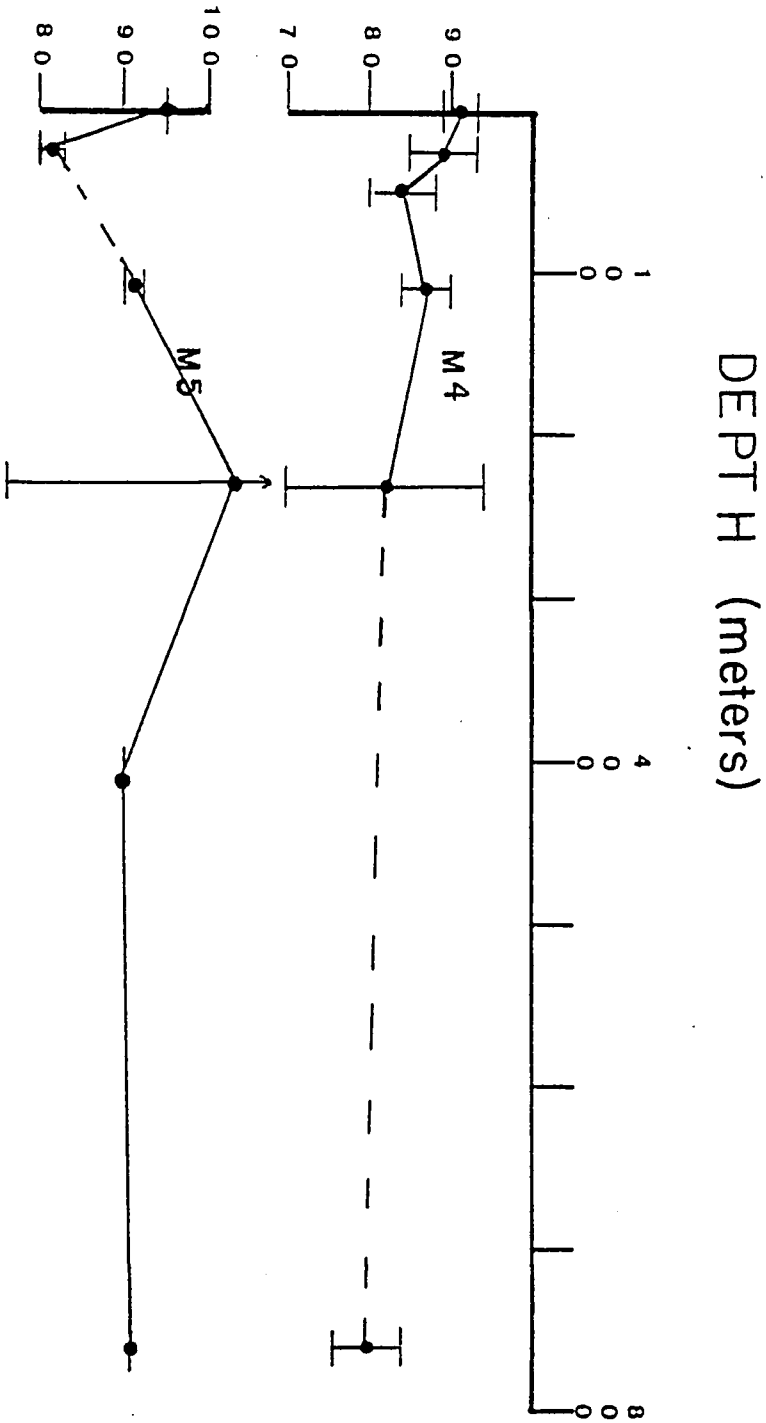
88

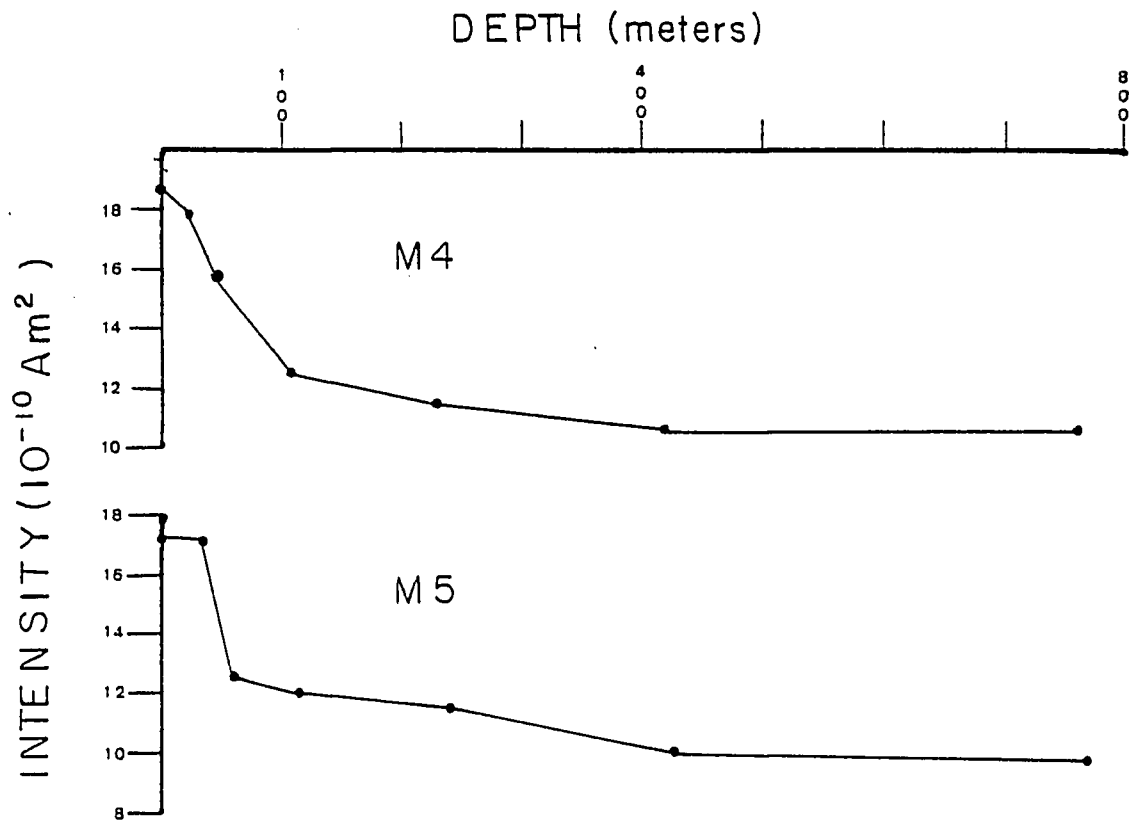
DECLINATION

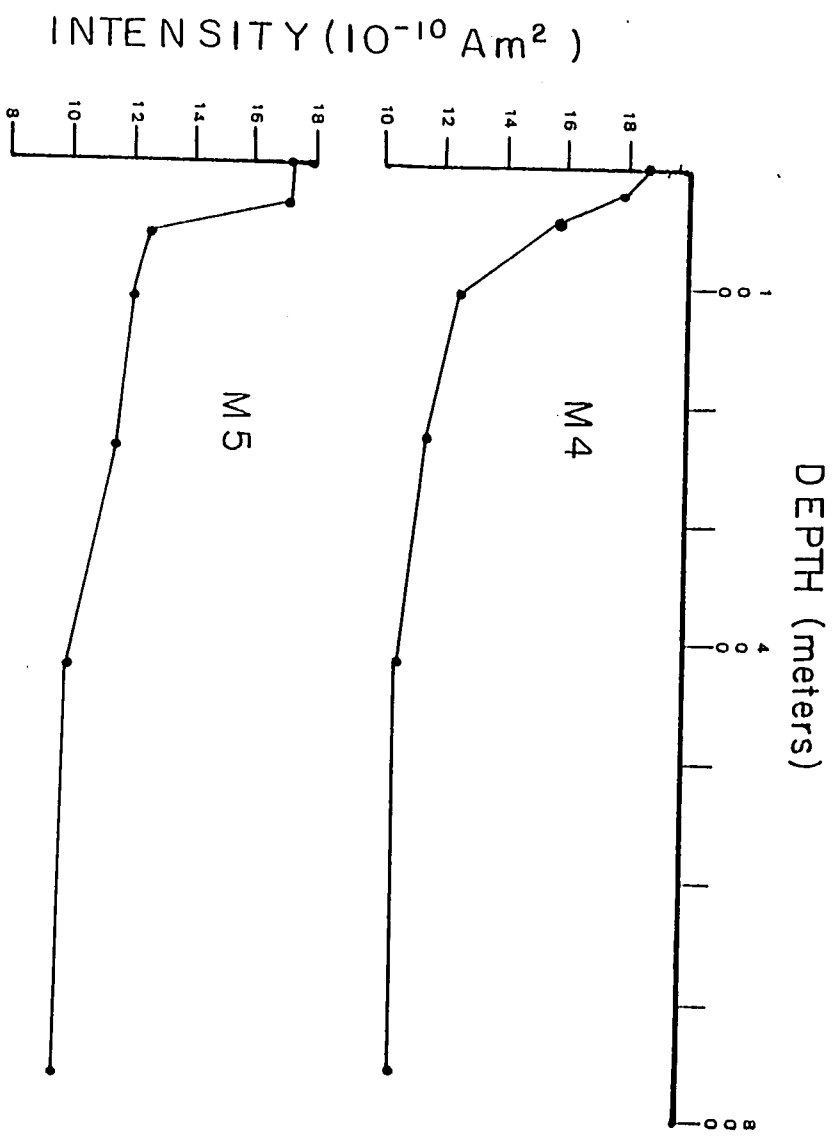
DEPTH (meters)



DECLINATION







Modeling the Compaction Effect

The rotational grain model proposed by Tucker (1980) and further supported by Hamano (1981) is used to explain the data collected with this experiment.

Initially, when the sediment is deposited, it has a high enough porosity to allow magnetic grains to move towards the magnetic field in the interstices. As the sediment settles, under its own weight, enough water is expelled to prevent the grains from moving with the earth's field, thus locking in the field.

As overburden is applied to the sediment, the intergranular contact between the grains increases causing the grains to rotate into the horizontal plane. The pushing of magnetic grains to the horizontal results in a shallowing of the magnetic vector.

The intensity of magnetism decreases during compaction. Interactions between magnetic grains as they are brought closer together probably results in magnetic particles pointing in the same direction, interfering with each other (Figure 22). As compaction continues, and water content decreases, it becomes more difficult to compact sediments, and the volume change associated with each load decreases, thereby decreasing the amount of change in magnetic intensity.

As shown in Figure 14 (intensity vs. depth), the largest change in intensity occurs in the first 300 meters of sediment. After this, the curve flattens out. This suggests that perhaps the largest change in magnetic remanence will occur in this zone.

Magnetic declination does not change because the net force is in the downward direction and there is nothing to cause the magnetic grains to rotate in any other direction. Hence, there is no force present to cause the movement necessary for a change in declination.

This model can be used to explain the results associated with the synthetic sediment, but not the marine sediment. The fact that the marine sediment contains 53% CaCO_3 while the synthetic sediment has none, makes the marine sediment a more complicated system. The 4ϕ size fraction of the marine sediment is composed entirely of foraminifera and foraminiferal fragments. The less than 4ϕ size fraction has a high coccolith content. The consolidation model associated with this type of material has not been developed and is beyond the scope of this thesis.

Summary

Two different sediments were given an anhysteretic remanent magnetization and consolidated in a Karol-Wagner 350 consolidometer to test the effects overburden pressure would have on remanent magnetism.

The first sediment was a synthetic clay, with an admixture of fine grained magnetite. The second was a calcareous ooze cored near Timor Island, with an initial calcium carbonate content of 53%.

The results of this experiment show a net shallowing of magnetic inclination, a decrease in magnetic intensity, and a constant magnetic declination.

Alternating field demagnetization analysis of three of the synthetic samples supports the idea of Tucker (1980) that compaction may only effect larger, low coercivity grains.

A rotational grain model, initially proposed by Tucker (1980) and supported by Hamano (1981) is used to explain the results of the synthetic sediment analysis. The results of the marine sediment analyses are too complex, and cannot be explained by a rotational grain model alone. The body effects of consolidation on this sediment is required to explain the results of this

Bibliography

- Aylmore, L.A.G. , and Quirk, J. P., Domain or Turbostatic Structure of Clays, *Nature*, v. 183, pp 1046-1048, 1959.
- Barton, C.E. and McElhinny, M .W., Detrital Remanent Magnetization in 5 Slowly Deposited Long Cores of Sediment, *Geop. Res. Let.*, v.6, no. 4, pp 229-232, 1979.
- Blow, R. A. and Hamilton, N., Effect of Compaction on the Acquisition of Detrital Remanent Magnetization in Fine Grained Sediments, *Geop. J. Roy. Ast. Soc.*, v. 52 pp 13-23, 1978.
- Bowles, J. E., "Engineering Properties of Soils and Their Measurement", McGraw-Hill Pub., New York, N.Y., p. 187, 1970.
- Bowles, F. A., Microstructure of Sediments: Investigation with Ultrathin Sections, *Science*, v. 159, pp 1236-1237, 1968.
- Bryant, W. R., Delflache, A. P. and Trabant, P. K., Consolidation of Marine Clays and Carbonates, in Inderbitzen, A. L. (ed.), "Deep Sea Sediments: Physical and Mechanical Properties", Plenum Press, New York, N. Y., pp 209-244, 1974.
- Carson, B., Tectonically Induced Deformation of Deep-Sea Sediments off Washington and Northern Oregon: Mechanical Consolidation, *Marine Geology*, v. 24, pp 289-307, 1977.
- Griffiths, D. H., King, R. H., Rees, A. I., and Wright, A., Remanent Magnetization of Some Recent Varved Sediments, *Proc. Roy. Soc., London, Ser. A.*, v. 246, pp 359-383, 1960.
- Hamano, Y., "An Experiment on the Post-Depositional Remanent Magnetization in Artificial and Natural Sediments", *Earth and Plan. Sci. Let.*, v. 51(1), pp 221-232, 1980.
- Hamilton, E. L., Thickness and Consolidation of Deep-Sea Sediments, *Bull. of Geol. Soc. Am.*, v. 70, pp 1399-1424, 1959.
- Variations of Density and Porosity with Depth in Deep Sea Sediment, *J. Sed. Pet.*, v. 46, no. 2 pp 280-300, 1976.

- Harrison, C. G. A., Paleomagnetism of Deep Sea Sediments, J. Geop. Res., v. 71, pp 3033-3043, 1966.
- Irving, E., Origin of the Paleomagnetism of the Torridonian Sandstones of Northwest Scotland, Phil. Trans. Roy. Soc. London, Ser. A., v. 250, pp 100-110, 1957.
- Evidence for Paleomagnetic Inclination Error in Sediment, Nature, v. 213, pp 483-484, 1967.
- Keller, G. H., "Marine Geotechnical Properties: Interrelationships and Relationships in Depth of Burial", in Inderbitzer, A. L. (ed.), "Deep Sea Sediments", Plenum Press, New York, N. Y., pp 77-100, 1979.
- Kent, D. V., Post Depositional Remanent Magnetization in a Deep Sea Sediment, Nature, v. 246, pp 32-34, 1973.
- King, F., Remanent Magnetism of Artificially Deposited Sediments, Mon. Not. Roy. Ast. Soc. Geop., Sup., v. 7, pp 115-134, 1955.
- King, R. F., and Rees, A. I., Detrital Magnetization in Sediments: An Examination of Some Theoretical Models, J. Geo. Res., v. 71, pp 561-571, 1966.
- Kramov, A. N., Orientational Magnetization of Firmly Dispersed Sediments, Izu. Acad. Sci. USSR Phys. Solid Earth, no. 1, pp 63-66, 1968.
- Larsen, G. and Chilinger, G. V. (eds), "Diagenesis in Sediments", Elsevier, Amsterdam, 551p.; 1967.
- Løvlie, R., Post Depositional Remanent Magnetization in a Redeposited Deep Sea Sediment, Earth and Planetary Science Letters, v. 43, pp 315-320, 1974.
- McElhinny, M. W., "Paleomagnetism and Plate Tectonics", London: Cambridge University Press, 358 p, 1973.
- McNish, A. G. and Johnson, E. A., Magnetization and Unmetamorphosed Varves and Marine Sediments, Terr. Mag. Atmos. Elec., v. 43, pp 401-407, 1938.
- Meade, R. H., Compaction Characteristics of Sediments from Central California, U. S. G. S. Prof. Paper no 497-D, 90 p, 1968.

- Müller, G., Diagenesis in Argillaceous Sediments, in Larson, G. and Chilingar, G. V. (eds.), "Diagenesis in Sediments", Elsevier Publ., Amsterdam, pp 127-177, 1967.
- Noel, M., Retallick, W. G., and Bull, P.A., Further Paleomagnetic Studies of Sediments from Agen Allwedd, Trans. Brit. Cave Res. Assoc., v. 8, 178-187. 1981.
- Opdyke, N. P., The Paleomagnetism of New Jersey Triassic: A Field Study of the Inclination Error in Red Sediments, J. Geop. Res., v. 66, pp 1941-1949, 1961.
- _____ and Henry, K. W., A Test of the Dipole Hypothesis, Earth and Planetary Sci. Let., v. 6, pp 139-151, 1969.
- Otofujii, Y., and Sasajima, S., A Magnetization Process of Sediments: Laboratory Experiments on Post Depositional Remanent Magnetization, Geop. J. Roy. Ast. Soc., v. 66 (2), pp 241-259, 1981.
- Rees, A. J., The Effects of Water Currents on the Magnetic Remanence and Anisotropy of Susceptibility of Some Sediments, Geop. J. Roy. Ast. Soc., v. 5, pp 235-251, 1961.
- Reike, E. and Chilingarian, G. V., "Compaction of Argillaceous Sediments", Elsevier Pub., Amsterdam, 425 p., 1974.
- Skoog, D. A., and West, D. M., "Principles of Instrumental Analysis", Holt, Reinhart, and Winson, Inc., New York, 710 p., 1971.
- Stacey, F. D. and Banerjee, S. K., "The Physical Properties of Rock Magnetism", Elsevier Publications, Amsterdam, 200 p., 1974.
- Stow, A. A. V., "Late Quaternary Stratigraphy and Sedimentation of the Nova Scotia Outer Continental Margin", unpublished Ph. D. Dissertation, Dalhousie University, Halifax, Canada, 1977.
- Tucker, P., A Grain Mobility Model of Post Depositional Realignment, J. Geophysics, v. 48 (3), pp 153-157, 1980.
- _____ Stirred Remanent Magnetization: A Laboratory Analogue of Post-Depositional Realignment, J. Geophysics, v. 48 (3), pp 153-157, 1980.

Verosub, K. L., Depositional and Post-Depositional Processes of Magnetization of Sediments, Reviews of Geop. and Space Physics, v. 15, no. 2, pp 129-143, 1977.

_____, Ensley, R. A., and Ulrich, J. S., The Role of Water Content in the Magnetization of Sediments, Geophysical Research Letters, v. 6, no. 4, pp 266-268, 1979.

APPENDIX A

Scanning Electron Micrographs of Sedimentary
Particles



PLATE 1

SEM of a cluster of magnetite grains
(Magnification 20,000X)



PLATE 2

The only SEM of a magnetite particle discovered in the synthetic sediment. Note the euhedral shape of the grain. This is not considered to be the average shape of the particles and the size of this particular particle is larger than the anticipated size of the average magnetic grain in the sediments. The smallness of the average particle of magnetite in the sediment may be the primary reason as to why no other particle was discovered. Magnification 900X.



marine sediment (300X)

PLATE 3

SEM of marine sediment (300X). Notice the high concentration of coccolith plates.

PLATES 4,5, and 6

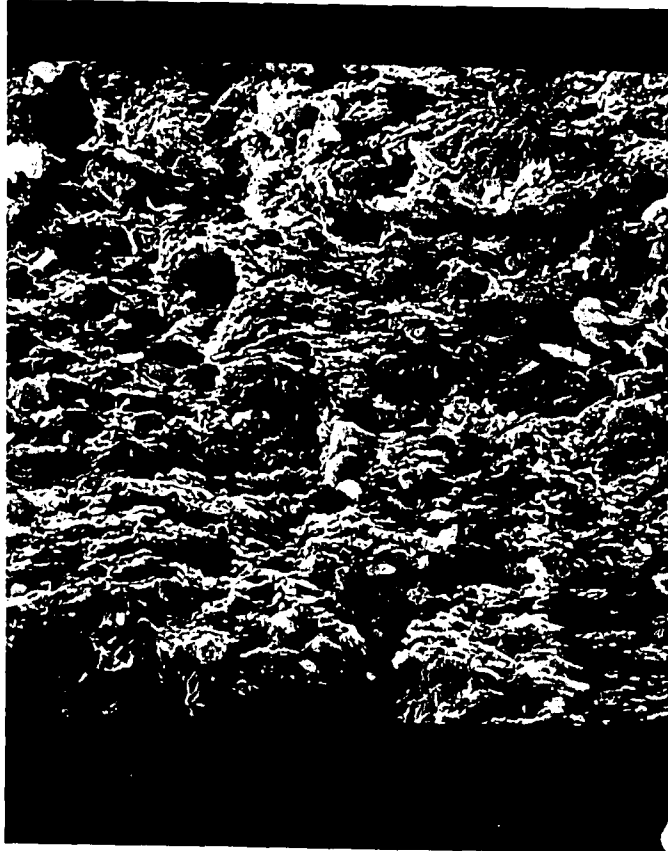
SEM's of the synthetic sediment (1,000X)

Plate 4 has clay that was not subjected to pressure.

Plate 5 has clay compacted to 14.34 kg/cm^2 .

Plate 6 has clay compacted to 57.3 kg/cm^2 .

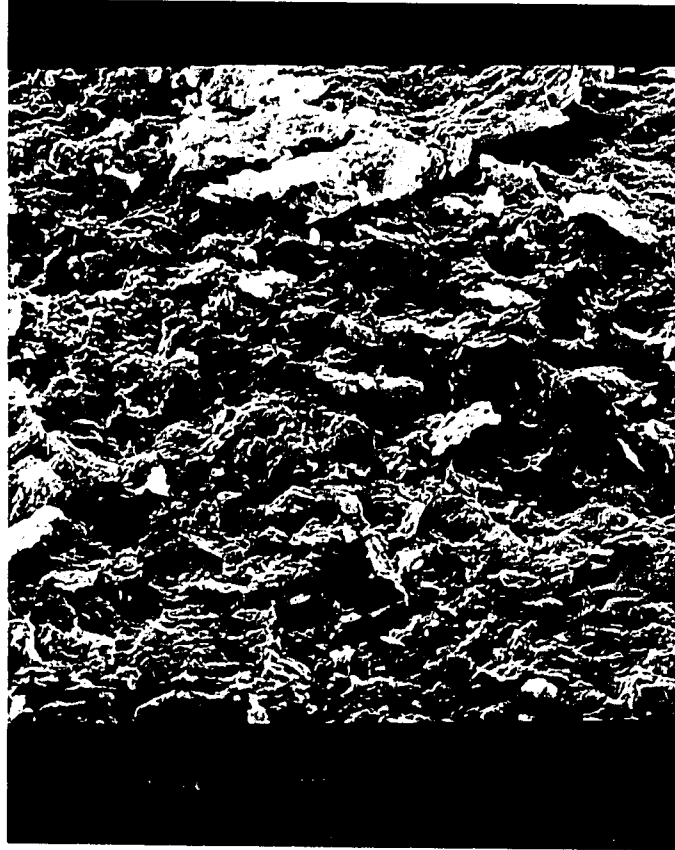
Clay grains will align themselves by the drying process alone. It is difficult to differentiate between the three plates.



Synthetic sediment (no load) (1000x)

PLATE 4

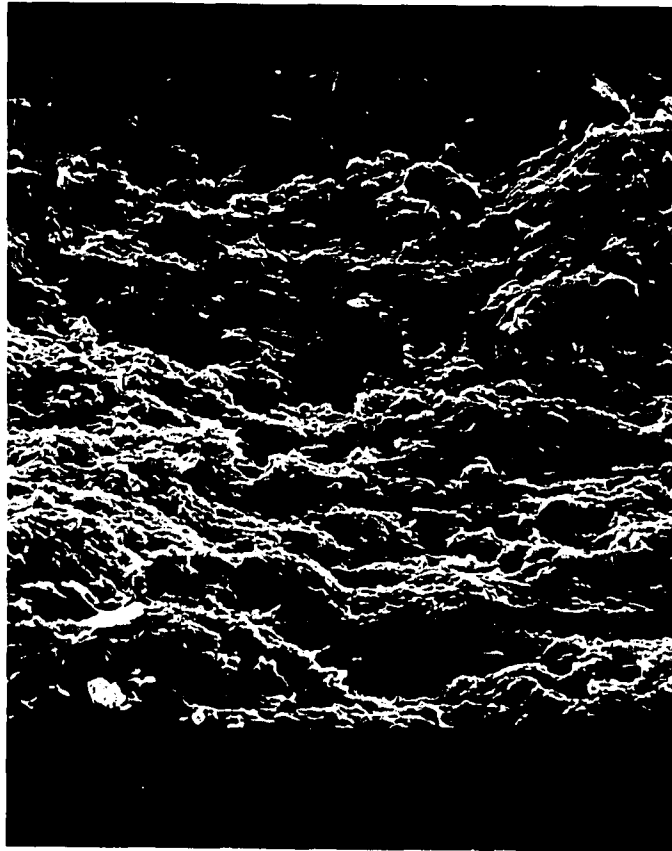
SEM of synthetic sediment that was not subjected to pressure (1,000x). Clay grains align themselves by the drying process alone. It is difficult to differentiate between Plates 4, 5, and 6



Synthetic sediment at 14.34 kg/cm² (1000X)

PLATE 5

SEM of the synthetic sediment compacted to 14.34 kg/cm²
Magnification 1,000X.



Synthetic sediment after 57.3 kg/cm² (1000X)

PLATE 6

SEM of the synthetic sediment compacted to 57.3 kg/cm² .
Magnification 1,000X.

APPENDIX B

DEPTH VS. PRESSURE TABLE (FROM HAMILTON, 1959)

TABLE OF DEPTH OF BURIAL AND PRESSURE
(from Hamilton, 1959)

<u>Depth of Burial (meters)</u>	<u>Pressure (kg/cm²)</u>
0	0
10	0.35
20	0.83
30	1.34
40	1.88
50	2.44
60	3.03
100	5.51
150	8.8
200	12.3
250	15.9
300	19.6
400	27.2
500	35.3
600	43.6
700	52.2
800	60.9
900	69.8

APPENDIX C

CONSOLIDOMETER CALIBRATION TABLE

CONSOLIDOMETER CALIBRATION TEST

<u>CONS. GUAGE READING</u>	<u>FORCE (1) (lbs)</u>	<u>FORCE (2) (lbs)</u>	<u>FORCE* (lbs)</u>
0.00	0.00	0.00	0.00
1.00	17.5	17.0	17.25
2.00	44.0	43.5	43.75
4.00	96.5	95.00	95.75
7.00	175	173.5	174.25
10.0	251	250.5	250.75
15.0	382	378	380
20.0	508.25	509	508.625
25	636	634	635
30	763	763	763

* Force averaged over two runs

APPENDIX D

TABLES OF EXPERIMENTAL DATA

Initial Height: 5.5 cmInitial Water Content: 100%Sample Name: S3Final Water Content: 35%

Load	Inclination *SD (degrees)	Declination *SD (degrees)	Intensity 10^{-9}Am^2	Δ Sample Height No Rebound cumil. cm	Δ Sample Height Rebound cumul. cm	% Δ Height NoRebound	% Δ Height Rebound
0	-46.8/0.28	265.9/2.05	14.22				
1	-32.4/0.51	273.7/0.42	12.20	1.52	1.35	27.6	24.4
2	-31.4/0.31	275.5/0.7	11.64	2.03	1.78	36.9	32.3
3	-30.5/0.32	272.3/0.62	11.29	2.13	1.98	38.7	35.9
4	-29.7/0.55	272.3/0.40	10.90	2.39	1.91	43.3	34.6
5	-27.4/0.44	272.3/0.27	10.72	2.62	1.96	47.5	35.5
6	-25.9/0.57	272.9/0.70	10.22	2.79	1.83	50.7	33.7

*SD = Standard Deviation

Sample Name: S4

Initial Height: 5.5cm Initial Water Content: 98%

Final Water Content: 36%

Load No.	Inclination *SD (degrees)	Declination *SD (degrees)	Intensity 10^{-9}Am^2	Δ Sample Height No Rebound cumul. cm	Δ Sample Height Rebound cumul. cm	% Δ Height NoRebound	% Δ Height Rebound
0	-25.5/0.0	276.3/0.0	13.23				
1	-16.8/0.56	274.9/0.30	11.97	1.52	1.46	27.6	26.5
2	-16.4/0.69	274.5/0.42	11.49	2.06	1.82	37.4	33.1
3	-15.5/0.40	275.0/0.59	11.32	2.45	2.01	44.4	36.6
4	-15.2/0.44	274.9/0.94	11.10	2.71	1.95	49.1	35.5
5	-13.0/0.62	275.8/0.61	10.93	2.90	1.84	52.5	33.4
6	-12.6/0.62	274.9/0.47	10.61	3.03	1.66	54.9	30.1

*SD = Standard Deviation

Sample Name: S5

Initial Height: 5.7cm Initial Water Content: 100%

Final Water Content: 37%

Load	Inclination *SD (degrees)	Declination *SD (degrees)	Intensity 10^{-9} Am^2	Δ Sample Height No Rebound cumul. cm	Δ Sample Height Rebound cumul. cm	% Δ Height No Rebound	% Δ Height Rebound
0	-35.0/0.0	266.15/035	11.18				
1	-21.4/0.4	270.13/1,01	10.39	1.46	1.35	27.6	26.4
2	-20.0/0.64	270.2/0.61	10.03	1.83	1.63	35.9	31.9
3	-19.0/0.59	270.3/0.96	9.86	2.09	1.75	40.9	34.4
4	-18.2/0.95	270.4/0.67	9.67	2.361	1.85	46.2	36.2
5	-16.9/0.27	270.7/0.57	9.55	2.57	1.78	50.3	34.9
6	-16.2/0.25	270.7/0.43	9.33	2.76	1.61	54.0	31.5

*SD + Standard Deviation

Initial Height: 5.5 cm. Initial Water Content: 94%

Sample Name: L1 Final Water Content: 22%

Load No	Inclination *SD(degrees)	Declination *SD (degrees)	Intensity $10^{-9}Am^2$	ΔSample Height No Rebound cumul. cm	Δ Sample Height Rebound cumul. cm	%ΔHeight NoRebound	%Δ Height Rebound
0	-66.1/0.0	171.0/0.0	21.3				
1	-63.8/0.7	182.5/1.7	20.0	1.52	1.45	27.6	26.3
2	-60.9/0.9	176.5/3.8	18.36	2.11	2.06	38.4	37.4
3	-61.0/0.25	183.7/0.37	17.10	2.60	2.53	47.4	45.9
4	-60.1/0.41	178.6/0.2	16.33	3.03	2.88	55.1	52.4
5	-59.7/0.04	183.1/5.6	16.09	3.40	3.15	61.8	57.3
6	-58.5/0.10	174.2/2.0	15.25	3.85	3.62	70.0	65.7

*SD = Standard Deviation

Sample Name: L2

Initial Height 5.7 cm Initial Water Content: 94%

Final Water Content: 29 %

Load No	Inclination *SD (degrees)	Declination *SD (degrees)	Intensity 10^{-9}Am^2	Δ Sample Height No Rebound cumul. cm	Δ Sample Height Rebound cumul. cm	% Δ Height NoRebound	% Δ Height Rebound
0	-72.8/0.7	111.8/2.8	16.1				
1	-69.5/0.46	108.1/1.86	15.5	1.52	1.37	26.7	24.0
2	-66.3/0.52	108.5/1.76	13.4	2.13	2.07	37.4	36.6
3	-66.5/0.55	106.9/1.47	13.0	2.64	2.50	46.3	44.0
4	-65.4/0.20	110.1/4.44	12.4	3.02	2.85	52.9	50.0
5	-65.3/0.54	108.3/3.11	12.0	3.39	3.08	59.5	54.1
6	-63.8/0.14	114.8/2.82	11/7	3.66	3.37	64.2	59.1

*SD = Standard Deviation

111

Sample Name: L3

Initial Height: 5.5 cm Initial Water Content: 125%

Final Water Content: 41%

Load-	Inclination *SD (degrees)	Declination *SD (degrees)	Intensity 10 ⁻⁹ Am ²	Δ Sample Height No Rebound cumul. cm	Δ Sample Height Rebound cumul. cm	%Δ Height NoRebound	%Δ Height Rebound
0	-55.3/0.22	178.0/1.6	14.77				
1	-36.7/0.76	172.3/0.2	10.95	1.52	1.47	27.6	26.8
2	-35.3/0.0	169.0/0.0	10.22	2.17	2.09	39.5	38.1
3	-34.1/0.15	178.1/2.9	9.92	2.53	2.50	46.0	45.5
4	-33.1/0.84	169.0/1.0	9.57	2.88	2.82	52.3	51.2
5	-29.1/0.0	170.1/0.0	9.23	3.30	3.09	60.0	56.2
6	-29.8/0.37	171.4/0.8	8.72	3.62	3.32	65.9	60.3

*SD=Standard Deviation

Initial Height: 5.6 cmInitial Water Content: 127%Sample Name: L4Final Water Content: 30%

Load No	Inclination *SD (degrees)	Declination *SD (degrees)	Intensity 10^{-9} Am^2	Δ Sample Height No Rebound cumul. cm	Δ Sample Height Rebound cumul. cm	% Δ Height NoRebound	% Δ Height Rebound
0	-59.7/1.31	175.8/2.4	12.51				
1	-47.8/0.76	189.5/0.9	9.77	1.52	1.44	27.1	25.7
2	-45.5/1.15	187.5/0.61	8.94	2.25	2.18	40.1	38.8
3	-44.5/0.13	188.8/0.6	8.63	2.70	2.59	48.1	46.3
4	-42.0/0.96	187.3/0.95	8.31	3.10	3.06	55.4	54.6
5	-40.2/0.05	189.1/1.97	7.91	3.62	3.35	64.6	59.8
6	-38.9/0.42	189.0/0.41	7.64	3.95	3.62	70.5	64.6

*SD = Standard Deviation

Initial Height: 5.6 cm Initial Water Content: 172%

Sample Name: M4 Final Water Content 53%

Load	Inclination *SD degrees	Declination *SD (degrees)	Intensity 10^{-9}Am^2	Δ Sample Height No Rebound cumul. cm	Δ Sample Height Rebound cumul. cm	% Δ Height NoRebound	% Δ Height Rebound
0	-44.8/0.21	91.0/0.7	186.4				
1	-36.2/0.15	89.7/0.9	178.3	1.52	1.46	27.1	26.0
2.	-39.6/0.56	84.3/1.09	157.1	1.93	1.68	34.4	30.0
3.	-40.3/0.64	87.7/0.6	123.1	2.71	2.54	48.4	45.3
4	-39.6/1.07	82.0/3.2	115.1	2.85	2.631	50.9	46.9
5.	-35.7/0.32	169.1/0.65	107.4	3.22	3.00	57.4	53.5
6	-31.7/0.36	80.1/1.05	106.2	3.58	3.34	64.0	59.7

*SD=Standard Deviation

Initial Height: 5.6 cm Initial Water Content: 164%

Sample Name: M5 Final Water Content: 44%

115

Load No	Inclination *SD (degrees)	Declination *SD (degrees)	Intensity	Δ Sample Height No Rebound cumml. cm	Δ Sample Height Rebound cumml. cm	%Δ Height NoRebound	%Δ Height Rebound
0	-42.7/0.51	95.8/0.52	172.0				
1	-40.8/0.58	80.9/1,06	172.8	1.52	1.30	27.1	23.0
2	-40.0/035	188.9/0.65	126.6	2.20	2.10	38.9	37.3
3	-36.1/0.49	92.2/1.24	120.6	2.61	2.53	46.1	44.8
4	-33.7/073	104.1/14.2	116.5	2.96	2.85	52.4	50.4
5	-35.8/0.60	90.1/0.23	100.3	3.31	3.15	58.6	55.8
6	-30.1/0.60	91.6/0.35	95.6	3.60	3.42	64.2	60.4

SAMPLE NAME: M_c

Load No.	Inclination *SD (average)	Declination *SD (average)	Magnetic Moment *SD (average)
M ₆			
Initial	45.3667/0.21	186.4667/0.54	177.33/1.61
Final	47.9667/0.65	82/9667/0.42	22.6/1.77
M ₇			
Initial	44.1/0.36	184.67/0.38	154.133/1.96
Final	41.8/0.10	177.0/0.30	140.4/0.56
M ₈			
Initial	45.55/0.59	181.6/2.63	158.62/1.17
Final	41.70/0.26	192.8/0.78	103.7/0.56
M ₉			
Initial	44.23/0.40	177.6/3.73	162.56/4.92
Final	42.62/0.84	175.24/0.98	167.52/1.07
M ₁₀			
Initial	45.5/0.85	175.67/0.17	150.07/1.83
Final	39.33/0.49	164.43/0.91	75.96/0.77
M ₁₁			
Initial	44.51/0.62	171.27/1.07	152.633/2.96
Final	33.67/1.70	158.09/0.94	86.52/1.34

*SD = Standard Deviation

Sample M (combined)

<u>Sample No.</u>	<u>%Change In Height (Rebound Excluded)</u>	<u>% Change in Height (Rebound Included)</u>
M6	42.287	39.688
M7	27.570	24.698
M8	51.751	50.014
M9	54.051	51.474
M10	60.276	57.385
M11	63.872	58.782

Vita

Frank Reginald Hall, son of Alexander and Warrenie Hall, was born in Albany, Georgia, August 9, 1956. He attended grade school in East Orange, New Jersey and was graduated from Essex Catholic High School, Newark, New Jersey, in June 1974. His undergraduate studies were completed at Kean College of New Jersey, Union, New Jersey, where he received a B.A. degree in Earth Science (Geology) in June, 1978.

As an undergraduate, Mr. Hall twice received the American Geological Institute Scholarship for minority students. He served as a research assistant under Dr. A. Lee Meyerson and served as the student representative on the Earth Science Department Curriculum Committee. He was president of the O.M.E.G.A. Club and captain of the wrestling team.

In September 1978, Mr. Hall entered the Department of Geological Sciences at Lehigh University under the tutelage of Dr. Kenneth P. Kodama as a Gotshall Fellow. As a graduate student, he was inducted into Sigma Xi in 1980. Mr. Hall was employed as a geophysicist by the U.S. Geological Survey; August 1979-August 1980. In January 1980, he began working as a research assistant at Lamont Doherty Geological Observatory of Columbia University.

His publications include:

Tidal and Seasonal Variations of Sulfate Ion in a
New Jersey March System, *Estuaries* 1982.

The Effects of Consolidation (Compaction) On Remanent
Magnetism in Argillaceous Sediments. (Abstract) *EOS*,
Trans. of the AGU, 1983.

PROXIMITY SENSING
FOR
ADAPTIVE ROBOT CONTROL

by
Paul Lindsey Hays

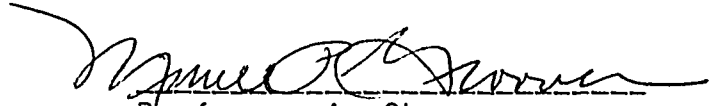
A Thesis
Presented to the Graduate Committee
of Lehigh University
In Candidacy for the Degree of
Master of Science
In
The Department of
Industrial Engineering

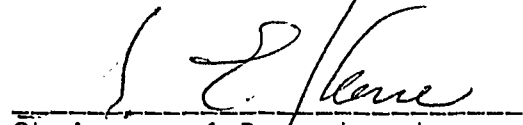
Lehigh University

1983

This thesis is accepted and approved in partial fulfillment of the requirements for the degree of Master of Science in Industrial Engineering.

May 12 1983
(date)


Professor in Charge


Chairman of Department

ACKNOWLEDGEMENTS

I wish to thank Dr. Mikell P. Groover, my major thesis advisor, and Dr. Roger N. Nagel, my minor thesis advisor, for their guidance and suggestions.

TABLE OF CONTENTS

Chapter	Page
ACKNOWLEDGEMENTS	iii
ABSTRACT	1
I INTRODUCTION	3
II CURRENT TECHNOLOGY	4
III OPTICAL SENSOR TECHNOLOGY	5
IV TEST MODEL CONFIGURATION	7
V SYSTEM DEVELOPMENT APPROACH	8
VI TEST RESULTS: ROBOT/SENSOR RESPONSE	8
VII TEST RESULTS: CONTROL LANGUAGES	10
VIII INTRODUCTION TO DEMONSTRATION PROGRAMS	12
IX CORNER PROGRAM DESCRIPTION	13
X CORNER PROGRAM ANALYSIS	16
XI HOLE PROGRAM DESCRIPTION	18
XII HOLE PROGRAM ANALYSIS	21
XIII CONCLUSION	22
XIV REFERENCES	24
APPENDICES	25
APPENDIX A. Sensor and Robot Sensor	25
Sensor Specifications	25
Sensor Bracket for Puma Robot Gripper	29
Sensor/Robot Interface Schematic	30
Pictures of Complete System	31
APPENDIX B. Robot/Sensor Tests	34
Test 1. Repeatability vs. Speed	34

	Page
Test 2. Position Feedback Test without Reposition Move . . .	34
Test 3. Position Feedback Test with Reposition Move	35
Test 4. Actual Position Repeatability Test	35
Test 5. Robot/Sensor Sensitivity Analysis	36
Test 6. Axial REACT to White Paper Test	38
Test 7. Edge Detect Test	39
Test 8. Count and DRAW Test	41
Test 9. Speed vs. Line Target Width Test	41
APPENDIX C. Corner Finding Routine Path Diagram	42
APPENDIX D. Corner Finding Routine Flowchart	43
APPENDIX E. Corner Finding Routine Program Listing	45
APPENDIX F. Hole Finding Routine Path Diagram	51
APPENDIX G. Hole Finding Routine General Flowchart	52
APPENDIX H. Hole Finding Routine Detail Flowchart	53
APPENDIX I. Hole Finding Routine Program Listing	54
VITA	58

ABSTRACT

With the growing interest in robotics, there has been an increasing need for better visual sensing techniques to provide feedback to the robot for better adaptation to an unpredictable environment. The main emphasis of work to solve this problem has been with the use of computer and camera based vision systems. The research of this thesis developed a less expensive and less complex method, using a proximity sensor, consisting of a light source, a photo transistor and fiber optics, to sense a part's location and adjust the robot's frame of reference. A light emitter and a light detector were attached to the robot arm, and worked in conjunction with the position of the arm to locate reference points on a flat plate. A new frame of reference was determined and the robot's frame of reference was transformed to match. A second program was developed to locate the center of round holes in a flat part. To demonstrate that the centers were found, the sensor was inserted through the holes.

The prime application for this arrangement would be to find the orientation of a flat part such as a sheet metal part fixtured close to the desired position. This part may need work performed on it at precise locations such as riveting, although its exact location is not known ahead of time. Therefore, its position must be sensed by the robot. The larger more common articulated arm type robot is the prime candidate to take advantage of this capability since it typically has poor accuracy, although the repeatability is normally quite good. The lack of accuracy is one of the major reasons why off-line programming methods, similar to those used in N/C machine tool programming, have

not been marketed for robots. A robot is typically programmed by physically moving it to the desired points and recording those points. Position accuracy is not especially important in this programming method although repeatability is important. By being able to verify and correct the robot's positioning, the effective accuracy is improved and off-line programming becomes feasible.

The Puma robot at Lehigh was used for this work, although it did not have all of the characteristics for which this thesis was designed. The accuracy of the Puma was better than that of the larger robots for which this sensor would be more useful. Both the accuracy and repeatability of the Puma were tested and found to be very good. Position addressability was found to be a minor limiting factor. The Puma's controller has no means of extracting the robot's wrist coordinates for use in math calculations and converting them back into point coordinates. This among other VAL language characteristics was found to limit the full effectiveness of the search techniques.

The majority of the work involved evaluating and deciding on the best sensor for the research, testing the response characteristics of the sensor and the robot, and developing two programs that demonstrate how this system works. Further development steps have been identified to improve upon the existing system.

INTRODUCTION

The objective of this thesis was to develop a simple optical type feedback system and a program to provide optical servo control that would find reference points on a part. There are a number of benefits that a vision system like this can provide a blind robot. One is to "eliminate precise positioning requirements"⁷ by accurately locating a part that is out of position. Another benefit is in the system's capability to verify and adjust a program that is developed off-line. Off-line programming has many advantages, such as improved robot utilization, although the lack of accuracy inherent in most robots, is a major reason why off-line programming has been difficult to take advantage of.

There are a few different approaches to this vision problem that are currently being developed and improved upon. They include a vision system that utilizes a camera and a computer. Another system utilizes a laser beam in addition to the camera and computer.⁹ Work has also been done with the direct scan or through scan type of optical sensors located in the gripper fingers.^{8,10} This thesis takes a different approach by using a proximity sensor attached to the hand and uses reflected light from the part to determine its presence.

Thesis tasks were defined and broken down into two major phases. Phase I involved the preliminary research on the topic, to determine current work being done and areas in need of development. With this input, Phase II proceeded with the development of the system.

The preliminary research emphasized three major topics: sensor research, robot control capability, and a literature search. The

system development phase emphasized the sensor's response, the robot's response, the sensor/robot interface, and the programming language. The response of the sensor/robot system was critical in developing the proper techniques to find the part and its orientation. Many tests were made to determine that response. From the test results, application programs were developed.

CURRENT TECHNOLOGY

Artificial vision systems for robots are improving at a very fast rate. The more complex computer and camera based systems are getting the most attention. Companies like Automatix, Inc., Westinghouse, and General Motors, and research organizations like the National Bureau of Standards, Stanford Research Institute, and MIT, to name only a few, have developed vision systems for different uses. Some are mounted in a fixed position and are used to verify parts or part position for assembly, material handling, and related tasks. MIT's Artificial Intelligence Laboratory is working on stereo vision to produce depth perception.³ In other systems the camera is attached to the robot arm for visual servo control. Automatix has developed a weld seam tracking system that uses a laser to project a straight line of light across the weld path, and a camera and a computer to interpret the shape of the line reflected off the part. The weld path is identified and the robot's hand, holding a welding torch, is guided along the path.⁹

Stanford Research Institute developed an algorithm, in 1974, that is being used to identify a part and its orientation by knowing a few fundamental properties about the parts to be seen and comparing them

with what the camera sees. These properties included area, moment of inertia, perimeter, and principal axis. Automatix improved upon this process by using a solid state camera and a more advanced video processor. The solid state camera provides more accuracy than the original electron beam camera, and the improved video processor has an increased processing speed that reduces the amount of decision data to a more manageable amount. It also takes advantage of the gray-scale feature of the camera by using different threshold levels to find the best images.⁶ "The key areas of research are finding ways to reduce the amount of data the computer needs to make a decision and attempting to convert successful laboratory systems to function in an industrial environment."¹

At the other end of the vision system spectrum lies the single element binary sensor. This sensor has been used in both experimental robot systems⁵ and industrial robot applications.¹⁰ Applications have been documented where the emitter and detector were placed in direct scan arrangement, in opposite fingers of the gripper. When the gripper is moved around a part and the light path is broken, the detector is tripped to indicate that the part has been found. This system is normally used to find one or more location pins that are used to reference the position of a fixture or a part. This thesis uses a proximity sensor arrangement where the emitter and the detector send and receive co-axially through a fiber optics bundle. In this case, a flat surface can be approached perpendicularly and detected.

OPTICAL SENSOR TECHNOLOGY

Optical sensor technology is a science by itself, with different

types of light sources, different types of light detectors, the use of fiber optics to direct the light path, and amplifiers and interface equipment. The light can be modulated or non-modulated, can be from an incandescent lamp or a light emitting diode, and it can be ambient light or infrared. The type of light used depends upon the environment, which includes the amount of ambient light, the target make-up and particles in the air. In the worst conditions, infrared, modulated light from a light emitting diode would provide the best results, since the light is of a different frequency than ambient light and pulsed at a known frequency that the receiver can detect.¹¹

Fiber optics play two major roles in this application. They make it easier to place the sensor at a remote protected location, if this is necessary, and they allow for precision control of the direction of the light. A dual spot scanner, which places two spots of fiber ends close together, is effective at following a line or an edge. The two spots lead to two different detectors, and a single light source.¹⁰

The light detector comes in different sizes, speeds, sensitivities and output voltages. Most of them can be categorized as conventional pn photodiodes, avalanche photodiodes, p-i-n photodiodes or phototransistors. The pn photodiodes are probably the most common because of the low price and the high sensitivity. The avalanche photodiodes are larger but handle larger voltages and have a higher switching speed. The p-i-n photodiode is also faster than the pn type and has a wider spectral response, although it is more expensive. The phototransistor is the fastest, most temperature and light stable¹ and delivers more current, so that it can perform control functions more

easily. With all this in mind, it is important that the detector's operating wavelength range match that of the emitter.^{2,4} A Modulated Light Source/ phototransistor combination can work in a highly lighted area equivalent to a 500 watt light bulb shining axially towards the detector.¹¹

TEST MODEL CONFIGURATION

The test model consisted of a Unimation Puma 600 robot, and a Scan-A-Matic Mini-Scan fiber optic scanner series S3010-3-1 and an R40100 relay type scanner control. See Appendix A for more specifics. The scanner is a proximity type sensor with the detector signal running co-axially through the center of a short fiber optic bundle. The light source was chosen to be an incandescent lamp for ease of human visibility in the experiment and because of the good working conditions. The light detector was a phototransistor. A relay type control was chosen over the solid state high speed control because of its compatibility with the robot's input ports. The robot was programmed to stop its arm from moving when the sensor was tripped. The difference in response time between the high speed control and the relay type did not significantly affect the overall time to stop the arm. The control was wired to the robot through two input ports: one to indicate that the sensor was operating and one for sensor release. The robot control reacts only to closed contacts at its input ports and not open contacts. The sensor was mounted on a bracket and clamped to the side of the gripper.

SYSTEM DEVELOPMENT APPROACH

After the sensor was determined and the sensor/robot interface was developed, the next major phase began. This was the system response testing phase. The final stage was for software development and testing.

The system response testing phase was a very important step. It was done to better understand the characteristics of the system, prior to developing the application software. Some of the tests evaluated the sensor's sensitivity to black versus white, the sensor's operate and release point, the robot's repeatability versus speed and the robot's REACTI function. The REACTI program function was used to interrupt an arm movement command when the voltage of the indicated input port became high. The distance the arm traveled beyond the sensor trip point was tested under different conditions.

From a statistical point of view, the data was gathered more in breadth than in specific. The objective of the experiments was to get a good feel for the response of the system. The number of data points taken depended upon the variance in the data being collected along with some assumptions on what was expected. For example, a slower approach speed to a point being sensed resulted in less overtravel and less variation in overtravel.

This data was used to develop and evaluate different search techniques and improve upon existing ones. The details of the tests can be found in Appendix B and a summary of the results follow.

TEST RESULTS: ROBOT/SENSOR RESPONSE

The robot was first tested to determine its accuracy and repeat-

ability. The results clearly showed that the Puma 600 robot rated fairly high in these two categories and the sensor would not improve its ability to find an edge or a hole that was already in position. From Test 1, the Puma had a better than .002" repeatability for a speed of less than 50% of normal, and an accuracy of between -.002" and -.004", comparing where it was programmed to go and where the display said it went. In Test 4, the actual position was tested by moving the gripper towards and away from a dial indicator, a distance of 2 and 18 inches. Similar results were found in this test. The position repeatability for speeds up to 75% of normal ranged up to $\pm .0025$. In both cases the figures got worse as the speed increased. The very slow speeds were not tested although it is reasonable to believe that the slowest speeds may not have had the best repeatability due to the reduced momentum factor and the small size of the control signals.

Tests 2 and 3 were performed to see how stable the arm was and how effective the position feedback was. There was only a slight difference in the two results, although Test 3, in which the arm was repositioned before its position was displayed, had better results.

Test 5 showed that as the sensitivity increased, so did the axial detection range, the lateral detection range and the distance to the operate point and the release point. This meant that with maximum sensitivity the sensor would need less light to respond and would respond closer to the light/dark transition line, although the axial distance from the target must be greater.

Test 6 tested the REACT! function with respect to speed. It showed how far the sensor would travel past the operate point while

ability. The results clearly showed that the Puma 600 robot rated fairly high in these two categories and the sensor would not improve its ability to find an edge or a hole that was already in position. From Test 1, the Puma had a better than .002" repeatability for a speed of less than 50% of normal, and an accuracy of between -.002" and -.004", comparing where it was programmed to go and where the display said it went. In Test 4, the actual position was tested by moving the gripper towards and away from a dial indicator, a distance of 2 and 18 inches. Similar results were found in this test. The position repeatability for speeds up to 75% of normal ranged up to $\pm .0025$. In both cases the figures got worse as the speed increased. The very slow speeds were not tested although it is reasonable to believe that the slowest speeds may not have had the best repeatability due to the reduced momentum factor and the small size of the control signals.

Tests 2 and 3 were performed to see how stable the arm was and how effective the position feedback was. There was only a slight difference in the two results, although Test 3, in which the arm was repositioned before its position was displayed, had better results.

Test 5 showed that as the sensitivity increased, so did the axial detection range, the lateral detection range and the distance to the operate point and the release point. This meant that with maximum sensitivity the sensor would need less light to respond and would respond closer to the light/dark transition line, although the axial distance from the target must be greater.

Test 6 tested the REACT1 function with respect to speed. It showed how far the sensor would travel past the operate point while

the REACTI function was stopping the movement. As assumed, the faster the speed, the more the overtravel. Test 7 showed that a lower sensitivity reduces the overtravel.

Test 8 tested the DRAW and count technique and found it to be extremely accurate. The DRAW function moves the robot arm a predefined distance and direction. When used in a program loop containing a counter that increments a variable by the value of the distance traveled, the variable represents the distance traveled. This technique was used to control the distance traveled as explained in section E of the Corner Program Description. Test 9 determined the maximum speed that the sensor could travel and still respond to a narrow line.

TEST RESULTS: CONTROL LANGUAGE

This project utilized the robot's control language to its limit and was hampered by some of the shortcomings in the area of defining a point location.

The primary weakness of the VAL language was its inability to extract the coordinates of a point's location for mathematical use, and the opposite function of assigning a point's coordinates through VAL only, without using the keyboard or human intervention. A typical use for this capability would be to calculate the coordinates of a point, given the coordinates of one or more other points. The center of a hole could be found this way by knowing three points on its edge, and the corner of a part could be calculated by knowing the coordinates of two points on each of the two intersecting edges. A slower, alternate method was developed to find the center of a hole,

although no accurate method was found that could find a corner.

There is no capability to DRAW in a transformed direction. This would be helpful if it was necessary to move a set distance and direction from a sensor found point on a part, whose position is referenced through a transformation. A MOVE statement will work in a transformation although it is only effective when the destination point can be referenced from the origin of the transformation.

A number of minor deficiencies were also found. There is no way to set limits on the work envelope. The REACTI function only responds to a high signal on an input port and cannot be set to monitor for a low signal. The REACTI function calls a subroutine when the indicated input port voltage becomes high. If the main program is to be returned to, a RETURN n function is used at the end of the subroutine. This returns to the line, n lines after the line in the main program from which the program was called. It would also be helpful to have the REACTI function or the RETURN function able to jump to a line number in the program. This would simplify the programming technique. An example of this is in PROGRAM HOLE, section B. SEARCH FOR HOLE and is described in the program description. If there was a feature that allowed the operator or programmer to manually step through a program one statement at a time and have those statements displayed on the screen, it would be much easier to debug a complex program. In the demonstration programs, a different method was used to aid in debugging. Each path point was given a number, and the TYPE function was used frequently to display the point numbers as they were completed and to display program status messages.

There are at least two more advanced robot control languages that solve some of these problems. IBM's A Machine Language (AML) is more complex to program than VAL, but it is more flexible and can manipulate point coordinates and DRAW in a transformation. Automatix's RAIL language is an improved successor to VAL. It has a MOVE PART: (X, Y, Z) function where X, Y and Z are predefined values as in the DRAW function. RAIL is an interpretive language written in PASCAL, although parts of it are rewritten in machine language. The PASCAL software is available to users for flexibility beyond that of RAIL.⁷

INTRODUCTION TO DEMONSTRATION PROGRAMS

In order to demonstrate some of the uses of a binary proximity sensor attached to a robot arm, two example programs were developed. The first one, called CORNER demonstrates how a part with a flat surface, a straight side and a corner can be located, and the reference frame of the robot altered to match the part. Pre-programmed work can be performed on this part even though the part isn't exactly where it should be. The second program called HOLE, finds a hole in a predetermined area and locates the center. This program will demonstrate its hole finding capacity by inserting the sensor into the found hole. Holes in a part could also be used as reference points to locate the part.

In order to improve the system's accuracy as much as possible, the programs were designed to compensate or cancel out any sensor or robot response characteristic that led to reduced accuracies. These include characteristics that may vary from day to day such as varying warm-up conditions, and different operating speeds. A good example of

this compensation is in the hole center search technique. The edges were located by traversing the edge, always from the hole center to the plate and always at the same speed. The overtravels of the sensor would be opposite in direction and cancel each other out.

CORNER PROGRAM DESCRIPTION

The objective of this program was to demonstrate that the sensor, attached to the robot gripper, could find a surface and then locate two edges and a corner on that surface. With three reference points located on the part, the new frame of reference could be defined. The FRAME function was used to define the reference frame of the part. Three points were needed to define the reference frame: they were the origin, a point on the X-plus axis and a point in the X-Y plane. The robot's frame of reference was transformed to that of the part. In order to prove that this procedure worked, the part was traced, by moving to pre-defined points around the part, and to a point in the middle.

The following is a description of the program steps. Refer to the path diagram, the program flow chart and the program listing in Appendix C, D, and E for further clarity.

A. FIND SURFACE OF PART

The program must be initialized by first defining the location of point A within the perimeter of the part to be found. The sensor must also be located with respect to the tool mounting flange by means of a TOOL transformation. The program starts by APPROACHing point A and then DRAWing towards the part until it is stopped by the sensor sensing the part and triggering the REACTI function through an input

port. The sensor is then moved closer to the part (P3), to get into the middle of the sensor range.

B. FIND POINT CLOSE TO EDGE ONE

The sensor then looks for the edge one (P4), where the height above the part is adjusted to the maximum sensing height (P5, A3). point A3 is recorded. This is the point in the X-Y plane of the parts reference frame and therefore doesn't have to be on the edge.

The three reference points are recorded at the same distance above the part, found by first DRAWING Z+ beyond the maximum sensing height. The REACTI 2 function is used to sense when the sensor turns off. A DRAW Z-, towards the part, with a REACTI 1 function, is then used to stop the sensor at the maximum sensing height. A slow speed is used to improve the accuracy. The sensor is moved back to point A where the middle of the sensing range is relocated (P6.3). This procedure is done to compensate for any small deviations in the plate being out of level.

C. FIND FIRST POINT ON EDGE TWO

The sensor is next moved in the minus Y direction in search of edge two. This edge must be located exactly in order to define the X axis. The edge is sensed at P7 and then found more precisely in a slow motion towards the edge (P8). The height is adjusted to the maximum sensing height by moving 4Y and then 10Z, over the plate and then up just above the sensing height (P9), then drawing towards the plate until it is sensed (P10), and then -4Y towards the edge. A2 is recorded here.

D. FIND TEMPORARY ORIGIN POINT ON EDGE TWO

A second point on edge 2 is searched to act as a temporary origin point for the reference frame. P11 and P12 search for this second point. Once found, the same search routine is used to find A1 as was used for A2. At this point a temporary reference frame called TEMP is defined using points A1, A2, and A3, so the orientation of the part can temporarily be defined and the sensor can be moved in a straight line towards the corner. A MOVE TEMP: B is used, where point B is 0, 3, 0, to move the sensor to 0, 3, 0 in the TEMP reference frame. MOVE TEMP: C, where C is -100, 3, 0, moves the sensor parallel to the edge two towards the corner. The movement is stopped at P14 when the edge is sensed. The edge and the middle of the sensing height is relocated (P15.1) at a slower speed. DRAW 3, -3, 0 moves the sensor in the direction of the adjacent edge and a counter is initiated at X = 3.

E. LOCATE CORNER

E1. MEASURE DISTANCE ACROSS CORNER

This routine DRAWS across the corner while incrementing a counter in a loop until the adjacent edge is found. By doing this, the distance traveled across the corner is measured by the variable X. The distance half way back is calculated by SETTING $X1 = X/2$.

E2. DRAW HALF WAY BACK ACROSS CORNER

DRAW -1, 1, 0 and a SET $X = X - 1$ are repeated in a loop function until $X = X1$. This DRAWS diagonally back across the corner and decrements the counter until it is half way back.

E3. DRAW TOWARDS CORNER

The corner is approached by DRAWING in a direction, perpendicular

to the last move, towards the corner and stopping on the edge. If the distance traveled across the corner (X2) is less than 12, then it is assumed that the corner has been found with enough accuracy and no further searching is necessary. A jump to line 200, section G is made.

F. PREPARE TO RELOCATE CORNER

If X2 is greater than 12, then the paths to P20 and P21 search for the edge and stops at P22 on the edge, where the program jumps back to section E, to refind the corner.

G. REFINDE SENSE HEIGHT

Once the corner is found, with $X2 < 12$, then the maximum sensing height is refound and Point A1 is recorded at the new origin.

H. TEST NEW FRAME

With the new frame of reference found, the robot moves through a test path of pre-programmed points around the part to display how accurate the part was found.

CORNER PROGRAM ANALYSIS

There are a few safety features and limiting factors that have been programmed into the corner program, and there are a few factors that are inherent in the VAL language that restrict the effectiveness of the program.

The initial APPRO A, 10 and DRAW 0, 0, -10, in section A was designed to protect against running into the part in case the sensor doesn't see the part, as in the case where the sensor approaches a hole in the part. This also limits the height range in which the surface is searched to between 15 mm and 22 mm (.59" to .86") depend-

ing on the part material reflectivity.

The middle of the sensing height range, where the sensor is located when searching for an edge is also dependent upon the material reflectivity. White paper has a 5.5 mm maximum sensing height and the aluminum has between a 10 mm and a 12 mm maximum height, depending upon the surface condition. In order that this program works on both surfaces, the middle of the sensing height range must be based on the 5.5 mm maximum height, and therefore 2 mm below the maximum. This 2 mm distance creates a limit on how much the part could be tilted from the robot's horizontal plane. If the part is tilted too much in one direction, the sensing height may be exceeded, and the program assumed that the edge has been found. If the part is tilted too much in the other direction, the sensor will run into the part and the sensor may also turn off, as if it found the edge. In order to compensate for this, during the first move across the part, from point A3 to A2, the height is readjusted at point A. This point was also found in section A, and identified as point P3. If in section A, at point P3, a HERE function was used to record that point, a MOVE statement could have been used here to move directly back to that point. More check points would increase the range. There may also be another method, such as incorporating the FRAME function and a MOVE statement, to move parallel to the surface.

After the TEMP reference frame was found and point P14 was found near the corner, the TEMP frame was not effective in guiding the sensor closer to the corner because there is no DRAW function oriented in the TEMP transformation. Another frame of reference may be

effective in improving the corner search technique in sections E and F.

The method of finding the corner in section E is not as effective as it should have been. The VAL language lacks some important features such as DRAWing in a transformed reference frame, and being able to extract the location coordinate values from a defined point and to perform mathematical analysis on those values. Also it would have been helpful to be able to reintroduce those new values into a point's coordinate values. As a result, the DRAW and count technique was the only method found that could find the corner with reasonable accuracy.

Another method that would improve the accuracy would be to control the sensor's sensitivity from the robot's controller. The sensor has a potentiometer that is used to adjust the sensitivity and also has some external contacts for remote adjustment. These could be interfaced with the output ports of the robot's controller. See Appendix B, Test 5, for the Robot/Sensor Sensitivity Test to determine how much the lateral detection range is reduced by reducing the sensitivity. The disadvantage is that the axial detection range is also reduced, requiring that the sensor travel closer to the part, and the travel speed may have to be reduced.

HOLE PROGRAM DESCRIPTION

The objective of this program was to demonstrate how the binary optical proximity sensor attached to the robot's gripper could be used to find a round hole in a part and then find the center. To prove that the hole was found, the sensor was inserted into the hole which

has a clearance of .002" on each side. The path diagram, the program flowchart and the program listing are in the Appendix F through I for reference. The program must be initialized by teaching points H1 and up to nine locations near the holes so the initial search technique has a starting point. The main program that sequences the other programs is PROGRAM PLATE. It assigns the hole locations (H1 through H9) to location HOLE, calls PROGRAM FIND and then assigns the locations of the holes found to locations J1 through J9. PROGRAM FIND first calls PROGRAM HOLE to find the hole, and then inserts the sensor into the hole with a DELAY function part way through the insertion, in case there is interference with the part, so the program can be stopped. Programs S1 through S9 are called by the REACTI function. They cancel the REACTI monitoring, they may TYPE a message on the screen and they will RETURN to the calling program at a point a defined number of lines from the interrupted line.

PROGRAM HOLE contains the logic to find the hole and then find its center. The program first cancels out any TOOL mode previously defined as in the PROGRAM CORNER, since the TOOL SENSOR transformation is not needed and not used, and no tool rotation or FRAME reassignment is used.

A. APPROACH AND FIND PART

This section APPROACHes the part to 15 mm above the pre-defined hole location and then DRAWs 12 mm toward the part until the surface is sensed. A larger draw distance was not used, in case the sensor approached near the center of the hole and did not see the part. The sensor would have crashed into the part if the draw distance was

greater than the approach distance.

A1. IF PART NOT FOUND GOTO SUBROUTINE REFINO

If the part's surface is not found on the first approach, the program jumps to PROGRAM REFINO to search for the surface. This is done by DRAWing up and over to find the edge of the hole and then adjusting the height to within the sensing height range.

B. SEARCH FOR HOLE

Once the surface has been found, at the proper height, the sensor searches for the hole in a zig-zag pattern at a high rate of speed. If the hole is sensed, the REACTI function stops the motion. If the hole is not sensed, the program stops.

C. HOLE SENSED - BACK UP AND STOP ON HOLE

Since the search pattern is performed at a high rate of speed, the hole will most likely be passed by the time the sensor stops. A slow back-up move is made to refind the hole, the direction of travel being dependent upon the direction of travel in the zig-zag pattern when the hole was sensed.

D. REFINO HOLE EDGE AND THEN CENTER

Lines 70 through 90 of the program find the X-plus edge of the hole and then moves 2 mm in the X-minus direction to move off the edge. A counter is initialized at $X = 2$. Lines 90 to 95 DRAW and count across the hole in the X-minus direction until the opposite edge is found. The distance moved and the counter variable, X, are incremented by .19 mm (.0075"). By SETting $XC = X/2$ the X-direction center point is calculated. This SET function defines a mathematical equation. Lines 95 to 100 move the sensor to that center point.

greater than the approach distance.

A1. IF PART NOT FOUND GOTO SUBROUTINE REFIND

If the part's surface is not found on the first approach, the program jumps to PROGRAM REFIND to search for the surface. This is done by DRAWING up and over to find the edge of the hole and then adjusting the height to within the sensing height range.

B. SEARCH FOR HOLE

Once the surface has been found, at the proper height, the sensor searches for the hole in a zig-zag pattern at a high rate of speed. If the hole is sensed, the REACTI function stops the motion. If the hole is not sensed, the program stops.

C. HOLE SENSED - BACK UP AND STOP ON HOLE

Since the search pattern is performed at a high rate of speed, the hole will most likely be passed by the time the sensor stops. A slow back-up move is made to refind the hole, the direction of travel being dependent upon the direction of travel in the zig-zag pattern when the hole was sensed.

D. REFINDE HOLE EDGE AND THEN CENTER

Lines 70 through 90 of the program find the X-plus edge of the hole and then moves 2 mm in the X-minus direction to move off the edge. A counter is initialized at $X = 2$. Lines 90 to 95 DRAW and count across the hole in the X-minus direction until the opposite edge is found. The distance moved and the counter variable, X, are incremented by .19 mm (.0075"). By SETTING $XC = X/2$ the X-direction center point is calculated. This SET function defines a mathematical equation. Lines 95 to 100 move the sensor to that center point.

Lines 100 to the end perform the same function in the Y-direction.

HOLE PROGRAM ANALYSIS

This hole program is simpler, more efficient and more accurate than the corner program. The VAL language was more effective in this program since the FRAME function was not needed and DRAWING in a transformed reference frame was not necessary. The hole is easier to find than a corner, and can be found with more accuracy.

The method used, to approach and sense the surface, limits the sensing range to about +3 mm/-7 mm in the Z-direction about the predefined hole location. This limit is inherent in the method used to protect against running into the part if the hole is approached near its center where the part is not sensed.

In section B, a REACTI function that jumps to a line number in the program would have been helpful. As a result, a series of GOTO statements had to be incorporated into the program to achieve the same result.

Other search techniques or area dimensions could have been used in section B to increase the search area either as part of the main pattern or as a secondary pattern if the first one failed. The pattern used demonstrates that the pattern works effectively.

In section D where the center of the hole is searched for, a 0.19 mm increment was used. A 0.20 mm was initially tried but it wasn't accepted. It was converted to .19 mm. Since the rated repeatability is $\pm .10$ mm, the .19 mm is apparently to be the prime incremental distance the robot can move, based on the joints rotational resolution, and the robot's addressability.

CONCLUSION

This project successfully demonstrated that a simple optical type feedback system attached to a robot's hand can find a part, its position, and adjust the robot's reference frame to match.

Two programs were developed to demonstrate this technique. One program was used to find a rectangular part by locating its surface, an edge and a corner, and then, to demonstrate that the robot found the part, the robot traced the perimeter of the part and then moved to a dot near the part's center. The part dimensions had been taught prior to this part finding operation. A second program demonstrated that the center of a round hole could be found in a given search area. The sensor was inserted into the hole to show that the hole was found.

If a surface must be located in two dimensions, a hole is a more accurate reference point and takes less time to find, than a corner. This optical feedback system is much slower than a camera/computer vision system and would not be practical where speed is important and this process was used frequently, but the camera/computer system is about 100 times more expensive.

System response testing was very important to the development of this system. The robot, the sensor and the complete system were tested. The Puma 600 robot was found to have a high degree of accuracy and repeatability so the sensor would not improve its ability to find an edge or a hole that was already in position. The system would be more effective on some of the larger articulated arm type robots that are not as accurate.

Further development areas were identified in the program analysis

sections, such as controlling the sensor's sensitivity and adjusting the height over the part more frequently. Different types of light such as modulated or infrared light could be tested, and even a dual spot sensor should improve the corner searching technique.

This sensor system has several potential applications and with further development it could become even more useful. An example would be as an aid to promoting the use of off-line programming for robots.

REFERENCES

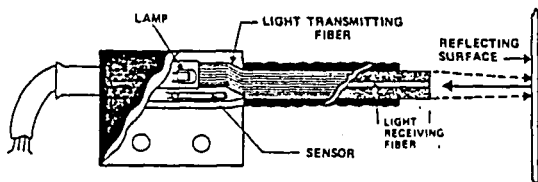
1. Aronson, R. A. "The Robot Boom Is On." Machine Design, 22-24.
2. Green, T. "The Fine Points of Sensing Light." Machine Design, 124-128, Sept. 11, 1980.
3. Hapgood, F. "Inside a Robotics Lab: Looking for Stereo Vision." Technology Illustrated, 44-49, June 1983.
4. Inglesby, T. "Fiber Optic Data Links Become Cost Effective." Assembly Engineering, 18-20, June 1983.
5. Lechtmar, H. "Connecting the PUMA Robot with the MIC Vision System." Robots VI Conference Proceedings, March 2 - 4, 1982, Detroit, Michigan, 447-466, 1982.
6. Reinhold, A. G. "Robot Vision For Industry: The Autovision System." Robotics Age, 22-28, Fall 1980.
7. Schreiber, R. R. "Robotics In the Eighties." Robotics Today, 39-42, October 1982.
8. Stauffer, R. M. "IBM Advances Robotic Assembly In Building a Word Processor." Robotics Today, 19-23, October 1982.
9. Villers, P. "One Vision System Handles Parts Assembly and Weld Seam Tracking." Sensor Review 2.3, 122-125, July 1982.
10. Wilson, K. "Fiber Optics: Practical Vision for the Robot." Robotics Today, 31-32, Fall 1981.
11. _____ No-Touch Controls Handbook: Applying Photoelectric and Proximity Control. Freehold, Illinois: Micro Switch, a Honeywell Division, 1981.

APPENDIX A



P.O. BOX 5 or ROUTE 5 WEST
ELBRIDGE, N.Y. 13060 U.S.A.
TELEPHONE (315) 689-3961
TWX: 710-545-0220 SAM WELB

MINI-SKAN
FIBER OPTIC SKANNER
S3010-3 SERIES



DESCRIPTION

Light from the lamp or LED located in the back body is transmitted coaxially to the target through the outer diameter of glass fibers in the threaded barrel. Light or IR energy then reflects from the target back through the inner fiber optic bundle to the phototransistor in the backbody. This provides maximum light to dark contrast and the most efficient return of light to the sensor.

Fiber optic illumination is not dependent on filament image and therefore changes over lamp life have minimal effect. Since tip of barrel is away from lamp, it remains cool and does not attract dust. Lamp units S3010-3 and S3010-3B differ only in body style. LED unit S3010-3 LED has the advantage of infinite life and shock & vibration resistance. A current limiting resistor is required and is shipped with each LED device.

APPLICATION SPECIFICATIONS

Designed to detect extremely small targets with exceptional accuracy. At optimum distance from target surface of .030", object definition of .003" can be obtained. At same distance the field of view is .030". Unit can detect white bond paper as far away from target surface as .250". Repeatability of object position of $\pm .0001$ " is possible.

The unit can reliably read a ladder chart of .012" width lines spaced .012" apart.

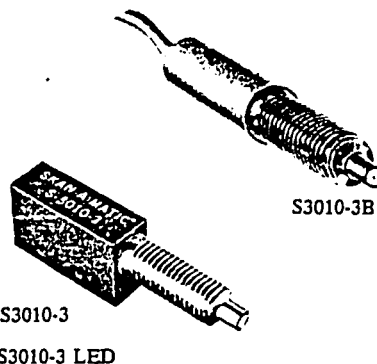
TYPICAL APPLICATIONS

1. Integrating, counting, code generation, using ladder charts, marks, holes, slots, etc.

FOR INSTANCE



2. Semi-conductor, IC and other small part automation, for inspection, sorting, proof.
3. Accurate edge and position control.
4. Line tracing, for fine control.
5. Detect shades or density of micro-sized area.



TECHNICAL SPECIFICATIONS AT 25°C

LIGHT SOURCE	Lamp	LED
Input	5.0 volts AC or DC, 115 milli-amps	100 ma max w/resultant voltage drop of 1.1 to 1.7 VDC
Life	40,000 hours	Infinite
Spectral Emission	—	940 nanometers peak

PHOTOTRANSISTOR⁽¹⁾

Bias Voltage	30 volts DC max.
Power Dissipation	50 milliwatts
Rise Time ⁽²⁾	1 microsecond typical
Fall Time ⁽²⁾	15 microseconds max.

BODY Anodized aluminum (black for lamp, red for LED units) with passivated brass barrel

TEMP. Max. operating temp. 70°C.

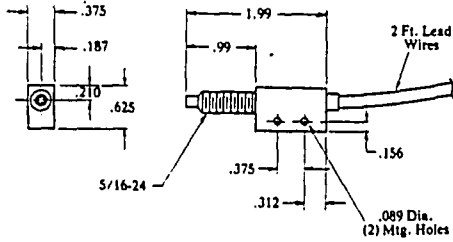
LEADS 4 conductor teflon covered cable, 2 ft. long. For additional length see Price List (type D).

Color Coding: Lamp - blue and white - no polarity
LED - blue (+) white (-)
Sensor - red (+) blk (-) twisted pair with aluminum/kapton shield

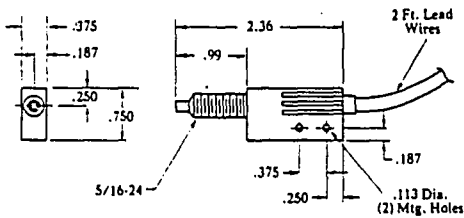
(1) For associated electronics to obtain a functional output, see R- or T-controls in this catalog, pages 27 thru 38.

(2) As obtained by laboratory testing of phototransistor. Response time of complete sensor with amplifier may be found on page 34.

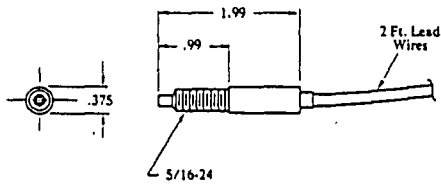
DIMENSIONS



S3010-3



S3010-3 LED



S3010-3B

OPTIONS

CONNECTOR suffix -P or -F

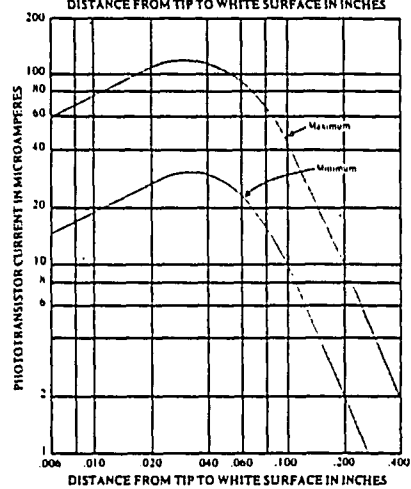
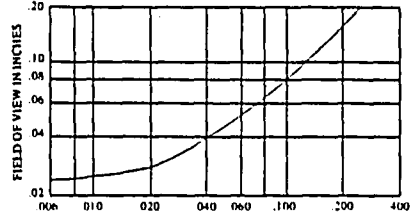
All skanners are available with multi pin cable connector. Male portion is terminated to skanner leads at factory. Female portion furnished for customer connection. Add "P" suffix to part number. Example: S3010-3-P. See Options, pg. 40 and Price List, pg. 42.

PROTECTIVE SHEATH suffix -M or -A

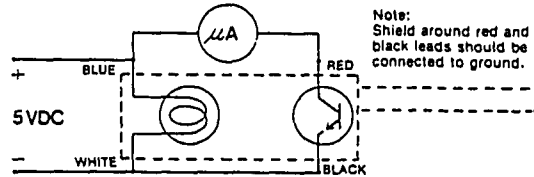
A protective sheath can be factory installed over skanner leads on all units by adding a suffix as follows: see page 42 for prices.

- M: square locked galvanized steel with black PVC jacket, 9/32" O.D. Example: S3010-3B-M
- A: square locked stainless steel, 3/16" O.D. Example: S3010-3B-A.

SKANNER PERFORMANCE
[Per Test Circuit Conditions]
For Lamp and LED Units

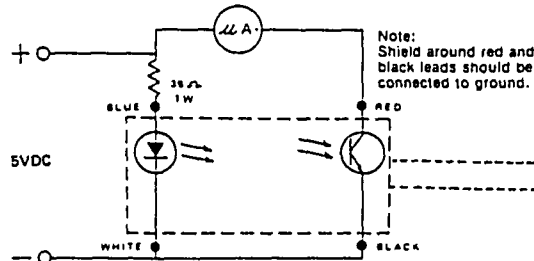


TEST CIRCUIT FOR LAMP UNITS



Note: Shield around red and black leads should be connected to ground.

TEST CIRCUIT FOR LED UNITS



Note: Shield around red and black leads should be connected to ground.

With the skanner looking entirely at white bond paper and then looking entirely at flat black for light to dark change at .030" distance from target surface:

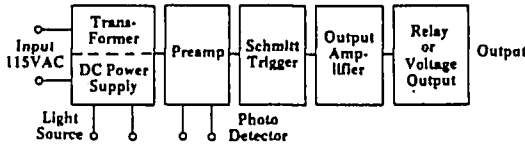
- WHITE: IL 50 micro amps, typical
IL 30 micro amps, minimum
- BLACK: ID will in all cases be at least 10 times less than IL



P.O. BOX 5 or ROUTE 5 WEST.
ELBRIDGE, N.Y. 13060 U.S.A.
TELEPHONE (315) 689-3961
TWX: 710-545-0220 SAM WELB

**INDUSTRIAL PHOTOELECTRIC
CONTROLS R40 and T40 SERIES
and HIGH SPEED CONTROL T41300**

BLOCK DIAGRAM



DESCRIPTION

The R40/T40 Series and the T41300 are complete photoelectric controls, designed to operate with one reflective scanner or thru-beam pair. Each unit amplifies the photodetector signal, provides light source power and functions as an output switch. Only standard 115VAC input is required. The R40 Series has a relay output while the T40 and T41 units have voltage output. Each is equipped with a red LED output indicator light.

CATALOG PART NUMBERS: R40/T40 SERIES

In order to properly specify a control, the part number must consist of a type letter and five digits. Select the desired output and construct the number as follows:

X	40	X	00
Output Type		Output Option	
Relay output R		5 amp Relay (R40 only) 1	
Voltage output . . . T		Open Collector (T40 only) . . . 3	
Series		Diode Protected NPN 5	
		Collector (T40 only)	

Example: T40300 describes a voltage output control with an open collector output.

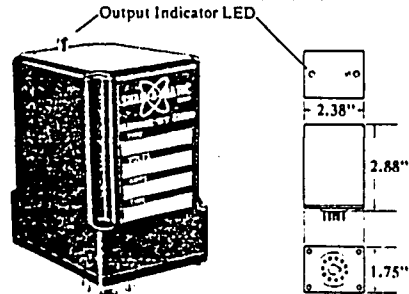
HIGH SPEED PHOTOELECTRIC CONTROL

Standard unit available only with open collector output.
Order as T41300.

OPTIONS

Remote DPDT Relay

If a two pole relay is needed or if the load is too large for the SPDT, 5 amp relay in the R40 control, the T40 Series may be used to drive an external DPDT relay. The following are available: R00030 rated 5 amps at 115VAC, 3 amps at 230VAC or 28VDC resistive load; life is 100,000 operations at rated load. R00031 rated 10 amps at 115VAC or 28VDC resistive load; life is 25,000 operations at rated load. Both are 8 pin, plug-in modules. Sockets are not included.



TECHNICAL SPECIFICATIONS FOR R40 SERIES

Power Input ⁽¹⁾	115VAC ± 10%, 50-500 HZ, 2VA
Lamp Power	5VDC at 125 ma max supplied by unit
LED Power	Use external resistor. See next page.
Sensor Excitation	5VDC supplied by unit
Output ⁽²⁾	Relay, SPDT, 5 amp 115VAC, 3 amp 230 VAC or 28VDC resistive loads
Sensitivity Adjust	Internal 15 turn potentiometer. Remote pot may be connected.
Response Time	25 millisecc. (counting rate 40 cps max)
Operation Mode	Either light energized or dark energized
Life	100,000 actuations at rated load, 1 million at 1/5 rated load
Temperature Range	0° to 50°C (32°F to 120°F)
Enclosure ⁽³⁾	11 pin plug-in module. .750" pin circle dia.; black molded nylon case.

- (1) Units for 230V are available. See Price List.
- (2) Contact protection recommended for inductive loads.
- (3) Socket not included; see Accessories (pg. 39).

TECHNICAL SPECIFICATIONS FOR T40 SERIES⁽⁴⁾

Voltage Output - Same as R40 Series except as follows:
Output Open collector NPN transistor⁽⁵⁾ to switch loads up to 100 ma. Voltage on collector not to exceed +25 VDC.

Diode protected collector NPN transistor to switch loads up to 100 ma. Voltage on collector not to exceed +5 VDC.

Response Time	1 millisecc. (counting rate 500 cps max)
Life	Infinite

- (4) See catalog part numbers to select desired output.
- (5) Output protection recommended for inductive loads.

TECHNICAL SPECIFICATIONS FOR T41300

Same as R40 Series except as follows:

Output ⁽⁵⁾	Open NPN collector, capable of switching 250 milliamps or 25VDC max.
Sensitivity Adjust	Internal 15 turn potentiometer only
Response Time	See Table
Switching Time	5 microseconds typical

MANUFACTURERS OF SUBMINIATURE PHOTOELECTRIC SENSORS AND ELECTRONIC CONTROLS

COMPATIBILITY WITH SENSORS

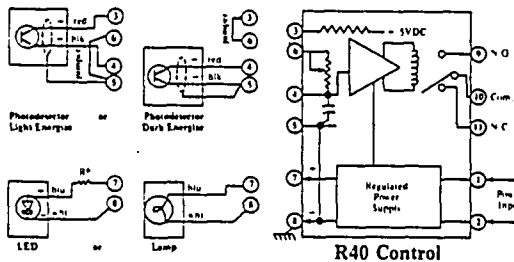
These controls are designed to be used with all Skan-A-Matic reflective skanners, thrubeam combinations, photodetectors and light sources*. The choice of unit to be used depends on the type of output and speed of response desired. If a relay output and low speed will suffice, the R40 Series is suitable. The T40 Series with open collector or diode protected collector output may be used to control voltages and give much faster response. The T41300 amplifier should be utilized wherever high speed operation is required.

The chart and curves on this page give the response time of various skanners when used with various "T" series controls. Use this data to select the desired combination.

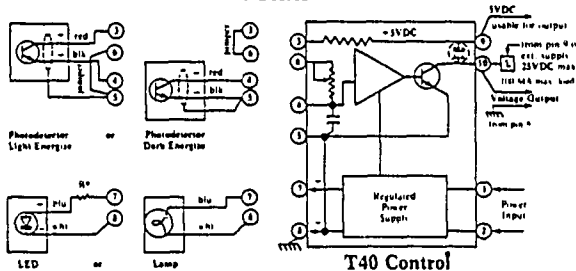
*If an LED is used, a resistor must be included as shown in the wiring diagrams. A suitable resistor is shipped with each LED device but the LED specifications should be checked before applying power.

$$\text{Calculate resistor value by } R = \frac{V_{CC} - 1.5V}{I_F}$$

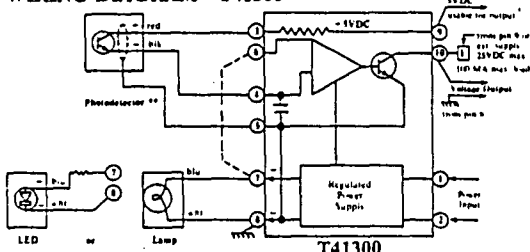
WIRING DIAGRAM - R40 Series



WIRING DIAGRAM - T40 Series



WIRING DIAGRAM - T41300



- ** for Dark Energize operation, make no connection between pins 6 and 7.
- ** for Light Energize operation, jumper pin 6 to pin 7.

All system components should have same "machine ground"
Detailed information on output connections is provided with each control unit and is also available on request.

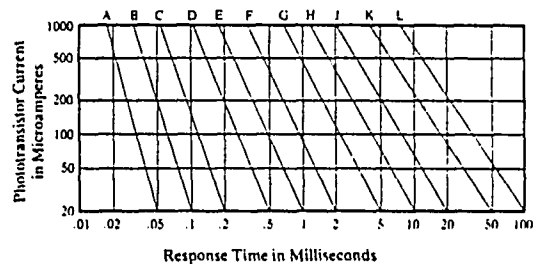
SENSOR/AMPLIFIER RESPONSE DATA

The table below denotes which curve applies to a particular sensor/amplifier combination. Each curve gives the combination's response, assuming a known phototransistor output. Since some skanners and photodetectors cannot attain the current levels at the top of the curves, their catalog pages should be consulted for maximum output.

Sensor/Amplifier Curve Reference and Typical Response Time in Milliseconds⁽²⁾

Photodetector or Scanner ⁽¹⁾ Catalog Number	AMPLIFIER ⁽³⁾			
	Standard		High Speed	
	Curve	Time	Curve	Time
P33001	G	-	D	-
P56001	J	-	F	-
S118¼, S120¼	F	.5	C	.08
S300 Series	F	.5	A	.02
S322-3 Series	F	.5	A	.02
S322-3 LED	G	1.5	D	.20
S2005-3 Series	G	1.5	D	.20
S2005-3 LED	J	7.5	F	.80
S3010-3 Series	G	2.0	D	.25
S3010-3 LED	J	8.0	F	1.00
S12001	G	.8	D	.15
S17103	G	1.0	D	.10
S17104	J	5.0	F	.50
S17105	K	15.0	F	1.50
S19 Series	F	1.0	E	.08
S20001	G	1.5	E	.35
S22 Series	G	3.0	D	.30
S24 Series	F	1.0	A	.10
S27 Series	F	.5	C	.02
S35201	L	30.0	G	1.50
S35202	H	3.0	D	.20
S35203	H	3.0	D	.20
S56401	G	1.5	D	.20
S56404	J	7.5	F	.80
S58101	H	5.0	F	.90

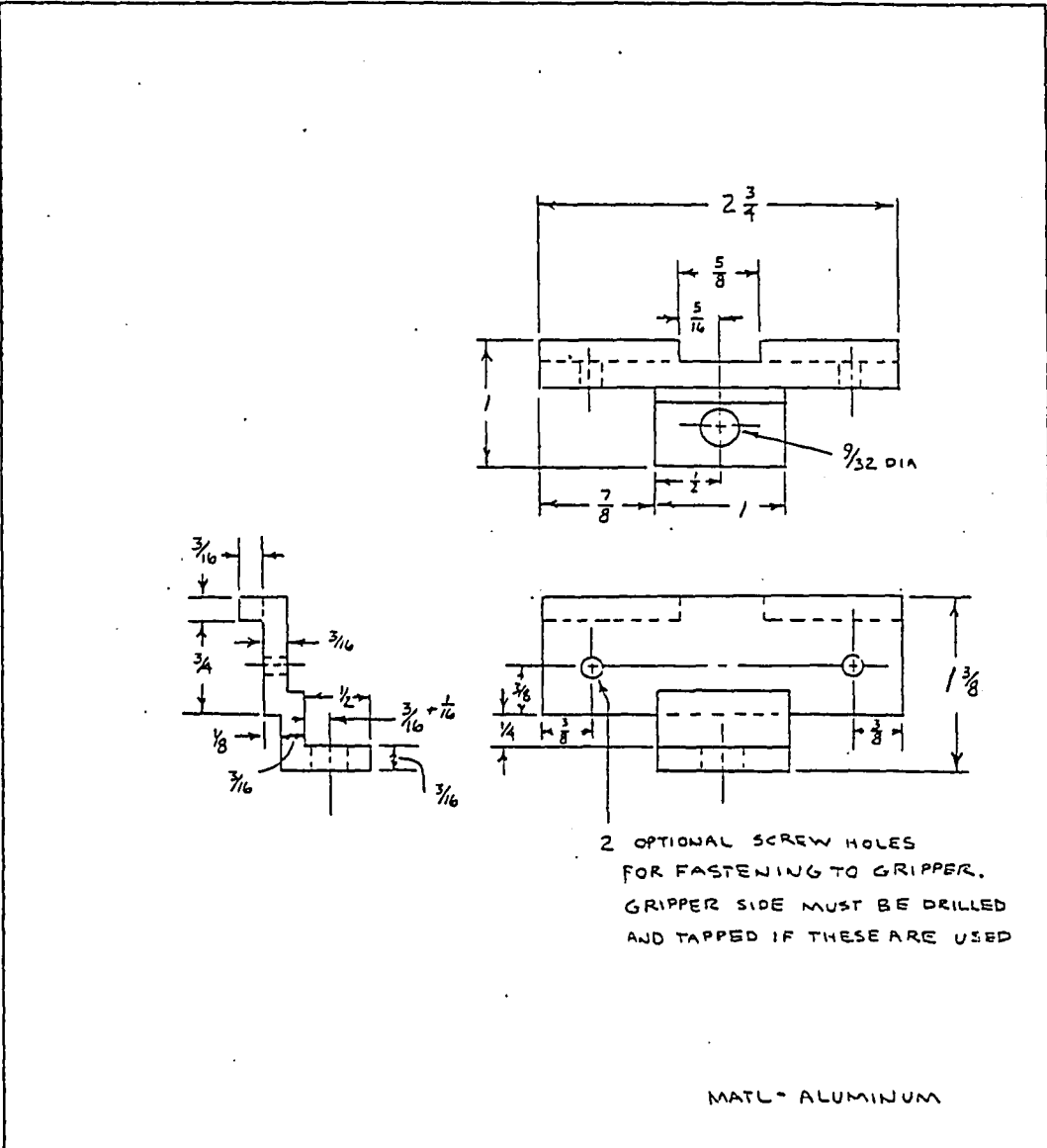
Sensor/Amplifier Response Curves⁽²⁾



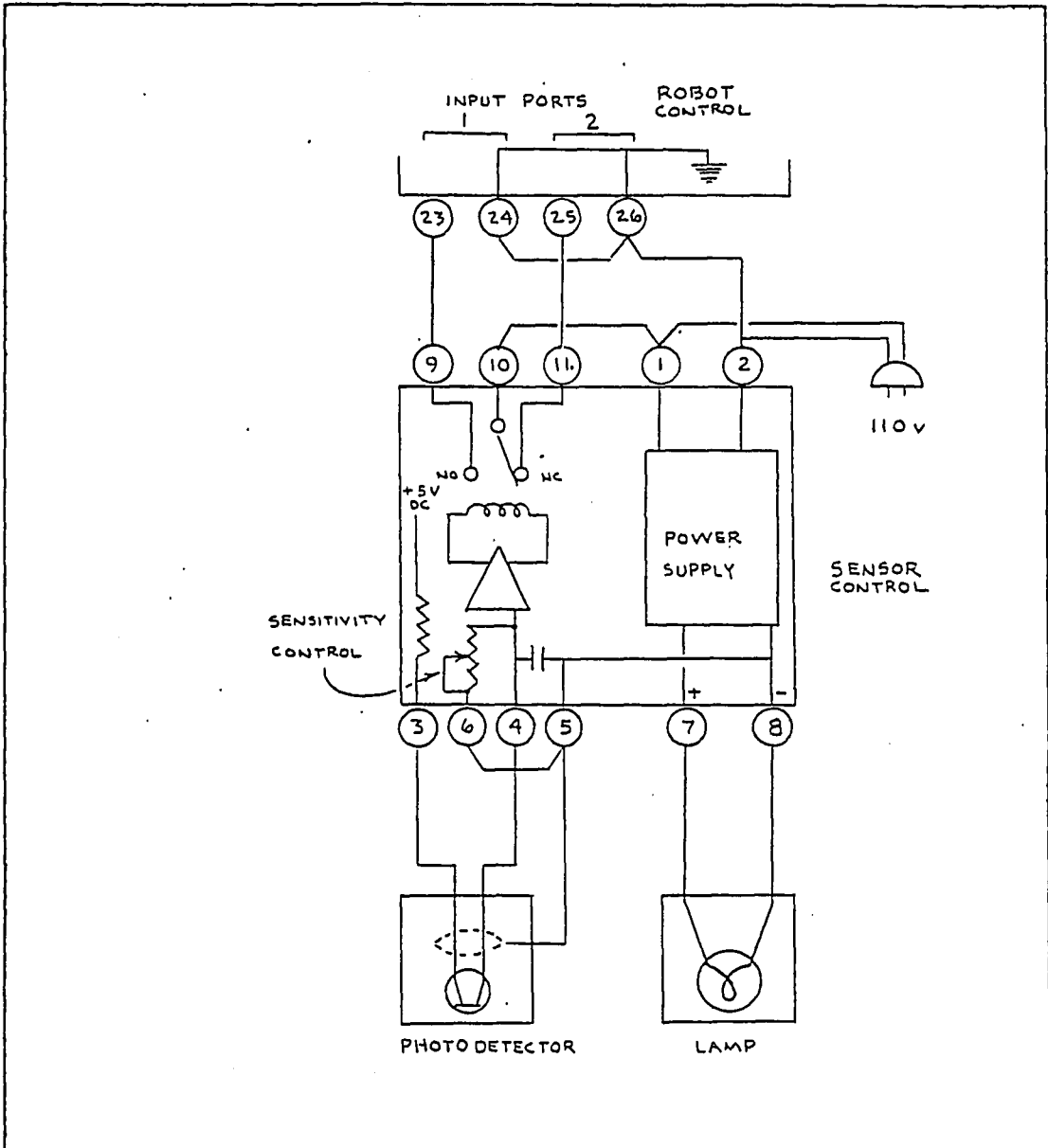
(1) Assumes a "typical" Scanner or Photodetector; deviation is possible due to manufacturing tolerances. See max. and min. performance charts on catalog pages.

(2) All data is approximate and assumes a sensor operating at its optimum distance, with a target at least as wide as its full field of view and with at least a 5:1 light to dark ratio.

(3) Since controls with relay or triac outputs have inherent speed limitations only those with transistor outputs apply in this data. Standard amplifiers include the T31/T32, T36, T40 and T46 Series, open collector versions of the R47, T51, R60 and R61 Series and the T21004 module. The high speed amplifier is the T41300 plug-in control.



REV.	DATE	APP'D.	JOB NO.	MADE BY PL HAYS	
				APP'D.	
			DATE 3 FEB 1983	SCALE FULL	
			SENSOR BRACKET FOR PUMA ROBOT GRIPPER		NO.
					29

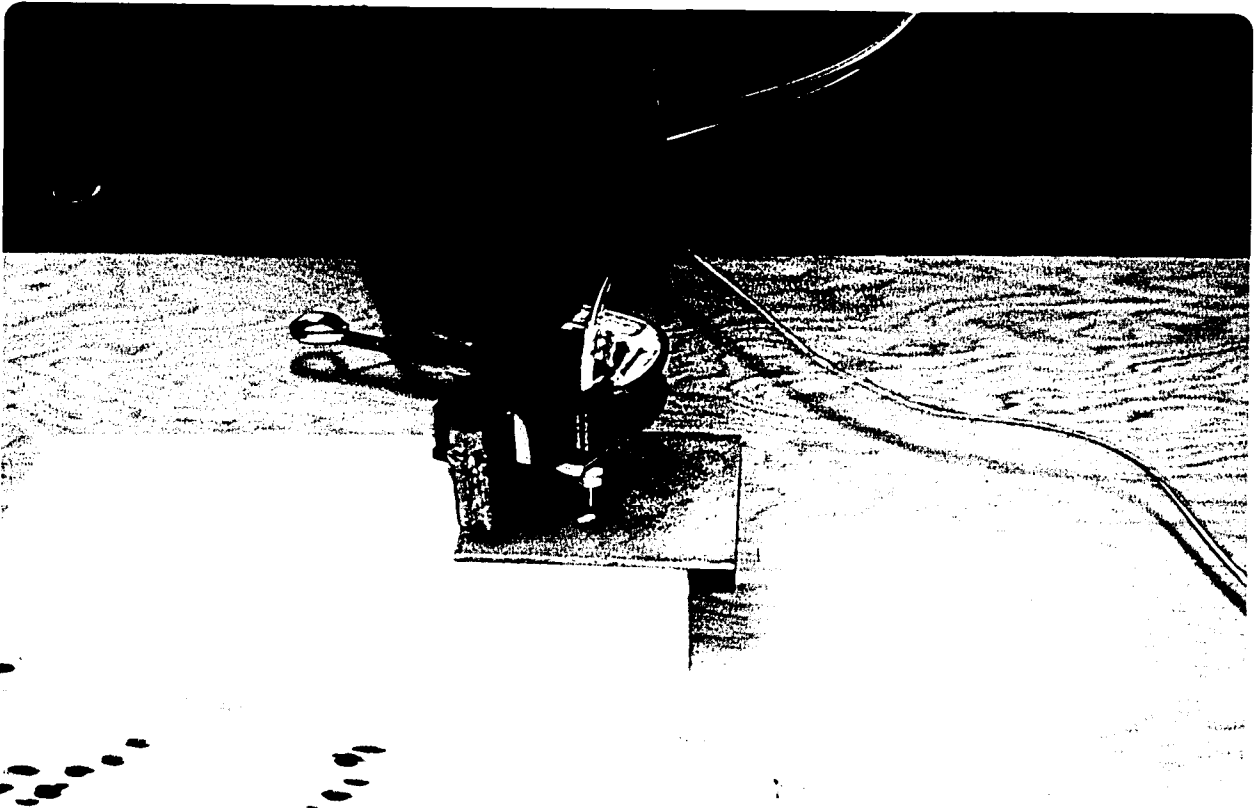


REV.	DATE	APP'D.	JOB NO.	MADE BY P L HAYS	
				APP'D.	
			DATE 10 MAY 1983	SCALE —	
			SENSOR / ROBOT INTERFACE . SCHEMATIC		NO.
					30

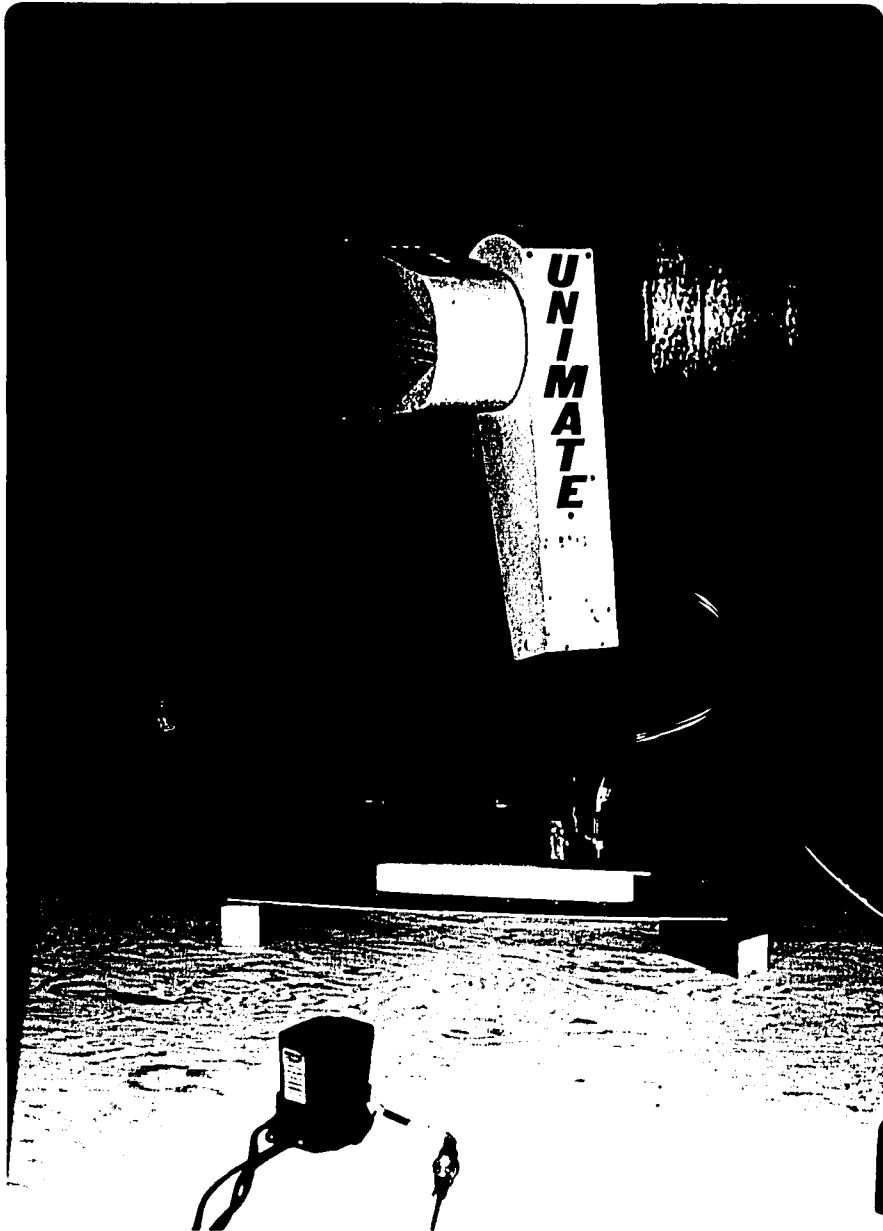
FORM 8208 (6/78)

APPENDIX A

Pictures of Complete System



The sensor clamped to the gripper by means of a bracket.



The sensor, attached to the robot's gripper, has found the surface of square plate. A part with holes in it is located in front of the square plate. The sensor control is in the foreground.



The complete system includes the control, the robot arm, the teach pendant on the table and the monitor, from left to right.

APPENDIX B

Robot/Sensor Tests

Test 1. Repeatability vs. Speed

With the sensor attached to the robot gripper, the sensor was moved between programmed locations of (0, 0, 0), (200, 0, 0 and (0, 175, 0) at different speeds. The positions were recorded after each point was moved to, using a HERE statement. This test was repeated 3 to 4 times.

Travel distance: 200 mm (8") X

175 mm (7") Y

Results:

<u>Speed</u>	<u>Total repeatability (mm)¹</u>			<u>Accuracy²</u>		
	X	Y	Z	X	Y	Z
10	0	0	0	-.09(-.0035")	-.06	-.06
20	.00	.06	0	-.06(-.0023")	-.06	-.06
50	.00	.06	.03	-.09	-.09	-.06

1. The worse case for the test for the particular direction.
2. The difference between the programmed and the recorded locations.

Test 2. Position Feedback Test without Reposition Move

In this test the position of the arm was repeatedly displayed, using the WHERE command, without commanding any repositioning of the arm. A variance of position was observed.

X	Y	Z
.03 mm	.06 mm	.06 mm

Test 3. Position Feedback Test With Reposition Move

Same as Test 2 except move A was repeated before each WHERE command position variance.

X	Y	Z	J3	J4
0	.06	.01	.012	.012

No movement in J1, J2, J5, J6.

Conclusion of Tests 2 and 3

The displayed position varies less when the position is re-established with a MOVE statement. From the data collected, it was not apparent what the cause was. It may be that the arm droops due to gravity or a calculation error causes this variance.

Test 4. Actual Position Repeatability Test

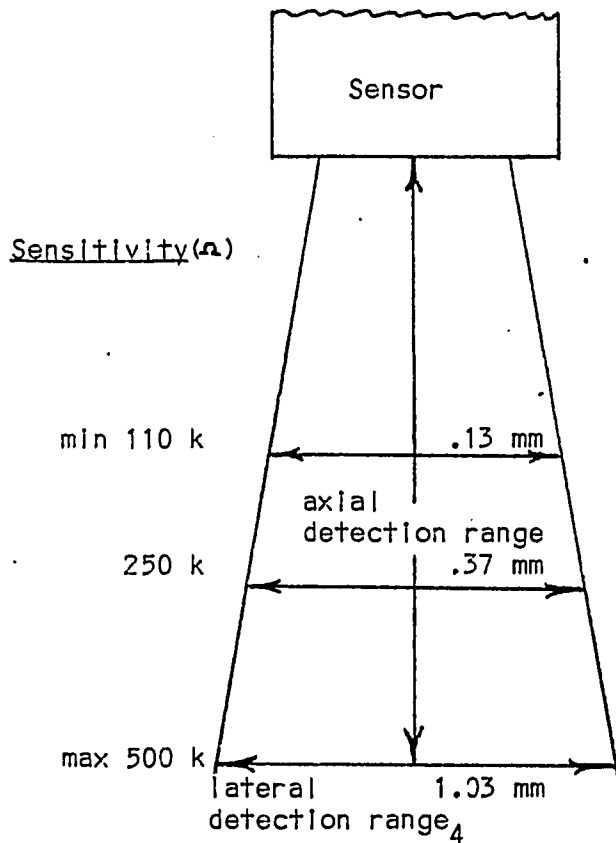
In this test the arm was moved via a MOVE statement in the X-direction, to and from a dial indicator, at various speeds and distances. The dial reading was recorded to determine the actual repeatability, as follows:

<u>Distance</u>	<u>Repeatability at different speeds (inches)</u>				
	<u>Sp 20</u>	<u>50</u>	<u>75</u>	<u>90</u>	<u>100</u>
2 in.	± .002	± .002	±.0025		
18.5 in.	± .0005	± .0025	-.001	-.003	-.003

Conclusion

As the speed and/or the distance increases, the repeatability gets worse.

Test 5. Robot/Sensor Sensitivity Analysis



Axial response to white paper

<u>Operate Point₁</u>	<u>Release Point₂</u>	<u>Axial de-tection range₃</u>
----------------------------------	----------------------------------	---

mm	mm	mm
3.31 none*	3.478 none*	.168
4.54 none*	4.85 none*	.31
5.47 1.38*	6.84 2.22*	1.37 .84*

*black paper

The purpose of this test was to determine some of the static response characteristics of the sensor. The sensor was moved axially towards and away from a white and a black paper target and the sensor trip point locations, as indicated by use of the WHERE function, were recorded. The sensor was moved laterally across the black/white transition line to determine the distance between the operate point and the release point, and the actual trip locations with respect to the line. The sensitivity was also adjusted from maximum to minimum to determine the effect.

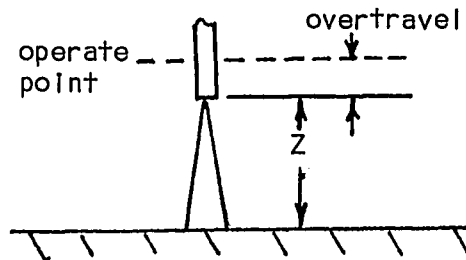
Footnotes

1. When approaching white paper axially, the sensor was triggered by the reflected light at this distance. Therefore this was the maximum operating distance from target.
2. When departing from white paper, the sensor turned off at this distance.
3. The difference in distance between the operating point and the release point (also known as the switching differential) and due to the switching hysteresis.
4. Lateral detection range between point of turn-on when sensing white and releasing when sensing black (see diagram). If the sensor is within 2 mm of the target and the sensitivity is at maximum, the sensor won't release over the black.
5. The repeatability of the operate point is better than that of the release point. The tolerance for the operate point was found to be ± 0.00 mm and ± 0.045 mm (± 0.0018 "") for the release point.
6. The sensitivity also effected the actual lateral distance from the transition line that the sensor would respond. As can be seen in the pictorials, the more sensitive setting responded closer to the line, where less light was needed to trip the sensor.

Test 6. Axial REACT to White Paper Test

This test evaluates the response of the sensor and the REACTI function to stop the motion of the arm moving axially towards a white target. The REACTI function interrupts a DRAW 0, 0, -10 statement that starts at a point 10 mm above the target. The speed was varied to test the response as follows:

<u>Speed</u>	<u>Distance stopped above target (Z mm)</u>	<u>Overtravel (mm)</u>
.5	5.84	0
1.	5.75	.09 (.0035")
2.	5.37	.47
5.	4.73	1.11
10.	4.18	1.66
20.	1.63	4.21
30.	1.63	4.21
50.	1.63	4.21 (.166 ")



Manual Axial Response Test to White Paper

To find the sense point for the above test the sensor was manually driven to and from the white paper, using the teach pendant.

Test 7. Edge Detect Test

This test evaluates the response characteristics of the sensor and the REACTI function by moving the sensor over the transition line between a black paper target and a white paper target. Various travel speeds and distances were tested. The sensor sensitivity and the travel direction (black to white and white to black) and the sensor operating mode were also evaluated. When the sensor crossed the transition line and the sensor was tripped, and the REACTI function stopped the arm movement. Due to the response time, the arm would travel past the line. This overtravel distance was calculated and recorded as follows:

Test 7 results:

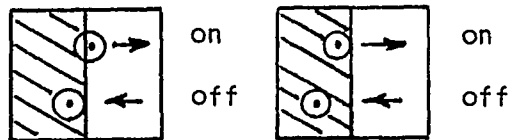
Test Specifications

<u>Test</u>	<u>Sensor Sensitivity</u>	<u>Travel Distance</u>	<u>Z Distance</u>	<u>Travel Direction</u>	
				<u>Off</u>	<u>On</u>
7.1	Max (1m)	10 mm	5.5	BL	to WH
7.2	Max	10 mm	2.5	BL	to WH
7.3	Max	20 mm	4.0	WH	to BL
7.4	Min (110 k)	20 mm	1.0	BL	to WH
7.5	Min	10 mm	1.0	BL	to WH
7.6	Min	10 mm	1.0	Wh	to BL
7.7	Max	10 mm	4.0	WH	to BL
7.8	Max	20 mm	4.0	WH	to BL

Test Results

Y Overtravel distance (mm)

<u>Speed</u>	<u>Test</u>	<u>7.1</u>	<u>7.2</u>	<u>7.3</u>	<u>7.4</u>	<u>7.5</u>	<u>7.6</u>	<u>7.7</u>	<u>7.8</u>
.5	.19	-.22	-.395±.015		0	.22	0	.15	.12
1.					0				
2.	.50	-.03		.72	.04	.48		.48	.56
5.	.87	± 0	.91	-.04					
10.	1.94	+.03		2.90	1.76	2.39	2.28	2.19	2.53
20.	3.97	-.03	4.19 ± 0	5.11	2.54	4.66	3.23	4.30	5.21
50.	9.19	±.10	12.03 ±.03	8.62	8.72	7.66	9.89	12.30	8.87



Conclusions:

1. From Test 6, the sensing distance (2 distance) must be greater for maximum sensitivity, than for minimum sensitivity.
2. Less overtravel for minimum sensitivity than maximum sensitivity (compare 7.1 vs. 7.4 and 7.6 vs. 7.7).
3. Results are not conclusive when comparing overtravel for BL to WH vs. WH to BL. (Test 7.1 vs. 7.7) and when comparing overtravel for two travel distances (Test 7.4 vs. 7.5 and 7.7 vs. 7.8).
4. The Y overtravel distance is larger for a larger Z distance as seen in the dimensional results and the pictorial for Test 7.1 and 7.2.

5. By comparing Tests 7.3 and 7.8, which were taken on different days, it can be seen that the results vary as much as a .37 (or .015 in) but do show the same general trend. This variance should be considered as a guide to the actual accuracy of these figures when comparing over a period of time.

Test 8. Count and Draw Test

Loop through a counting function and a DRAW 1, 0, 0 ten times at different speeds. Record displayed position and calculate the final position tolerance.

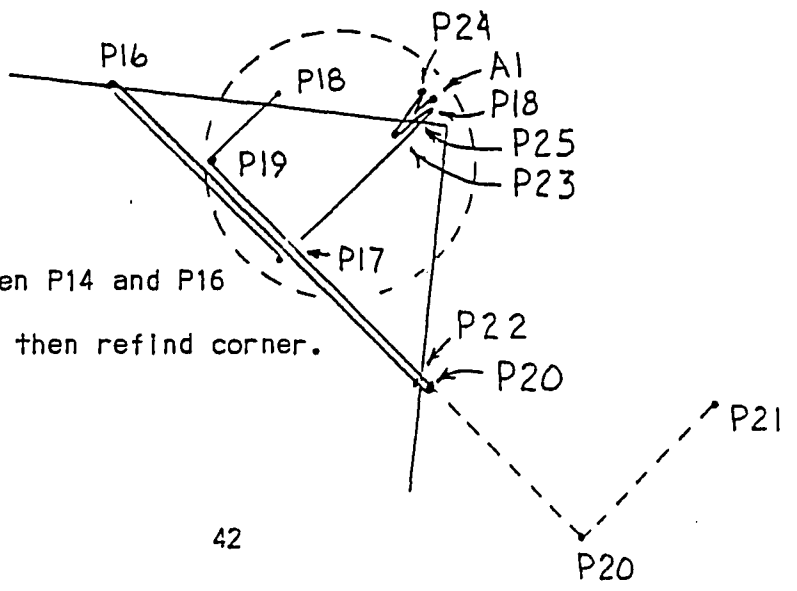
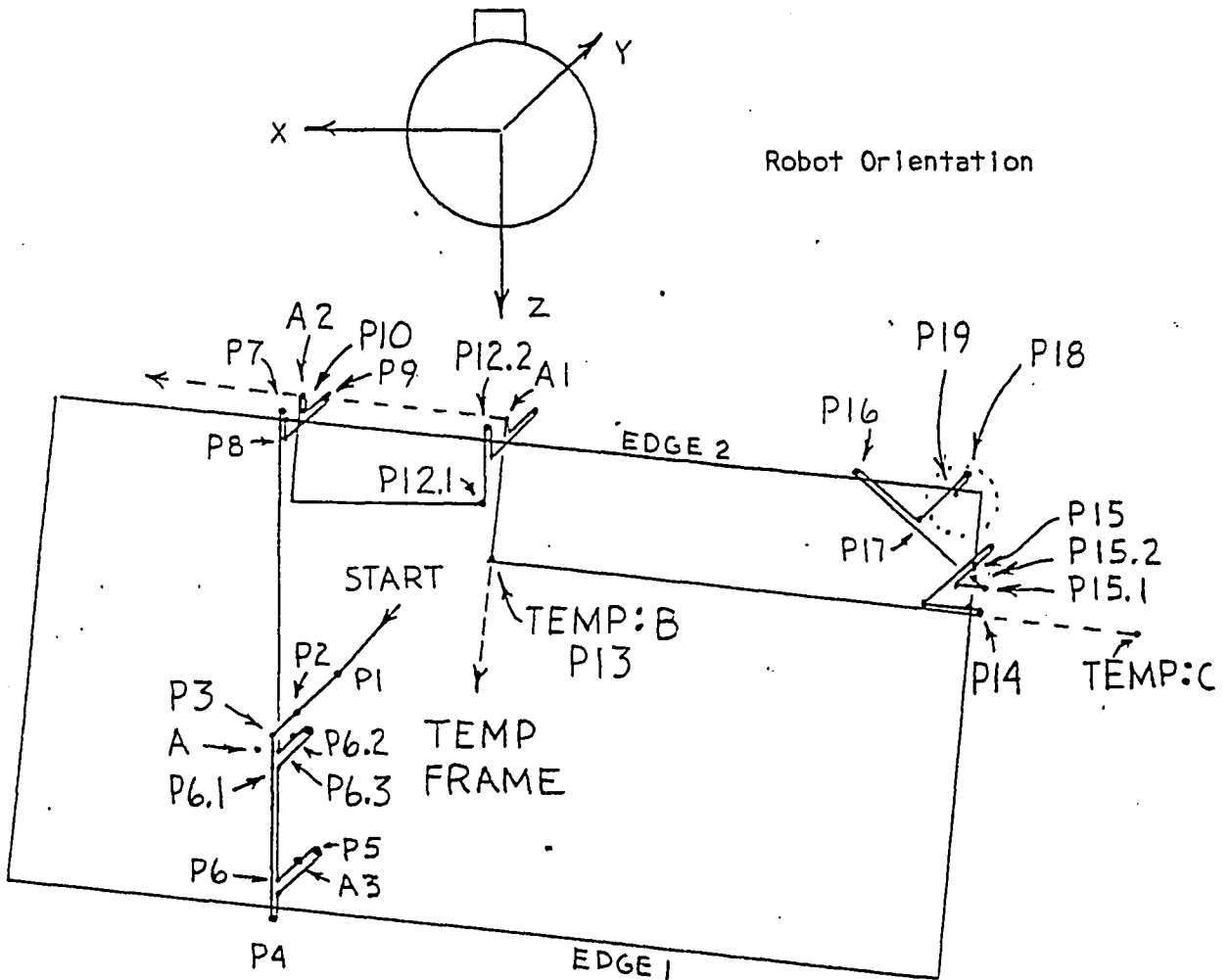
<u>Speed</u>	<u>Tol. at 10 mm X</u>	
.5	± .015 mm	(± .0006")
1.	± .015 mm	(± .0006")
2.	± .12 mm	(± .0047")

Test 9. Speed vs. Line Target Width Test

Test for the maximum speed that the sensor could respond to a white line on a black paper background. The sensor was moved over the line at a distance of 4.5 mm from the target and the sensor sensitivity was set at maximum.

<u>Line width</u>	<u>Maximum speed</u>
1/8	Between 40 and 50
1/16	Between 35 and 40

Corner Finding Routine Path Diagram



If the distance between P14 and P16
is greater than 12 mm then refind corner.

APPENDIX D

Corner Program Flowchart

A. Find Center of Part

Speed = 50
Define sensor location

Approach Part (P1)

Speed = 10

Draw towards part until sensed (P2)

B. Find Point Close to Edge

SP 40
Draw closer to part (P3)
Draw to edge (P4)

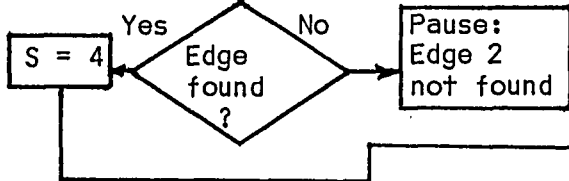
Draw back over part and find maximum sensing distance over part

Record point A3

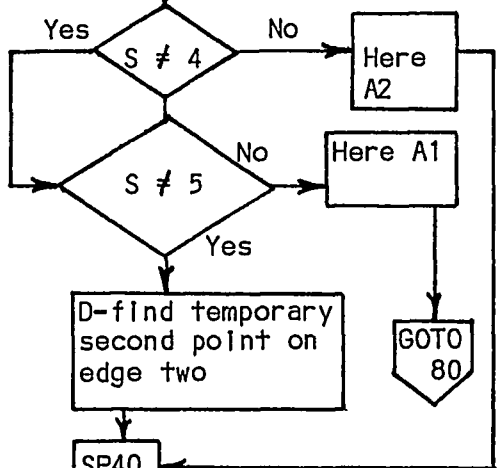
Move to A. Refind middle of sensing height.

C. Find First Point on Edge Two

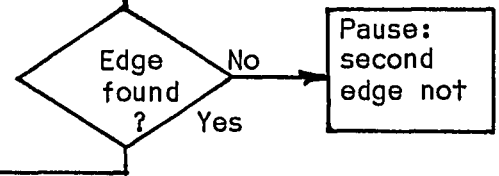
Draw to other edge. Stop when found (P7)



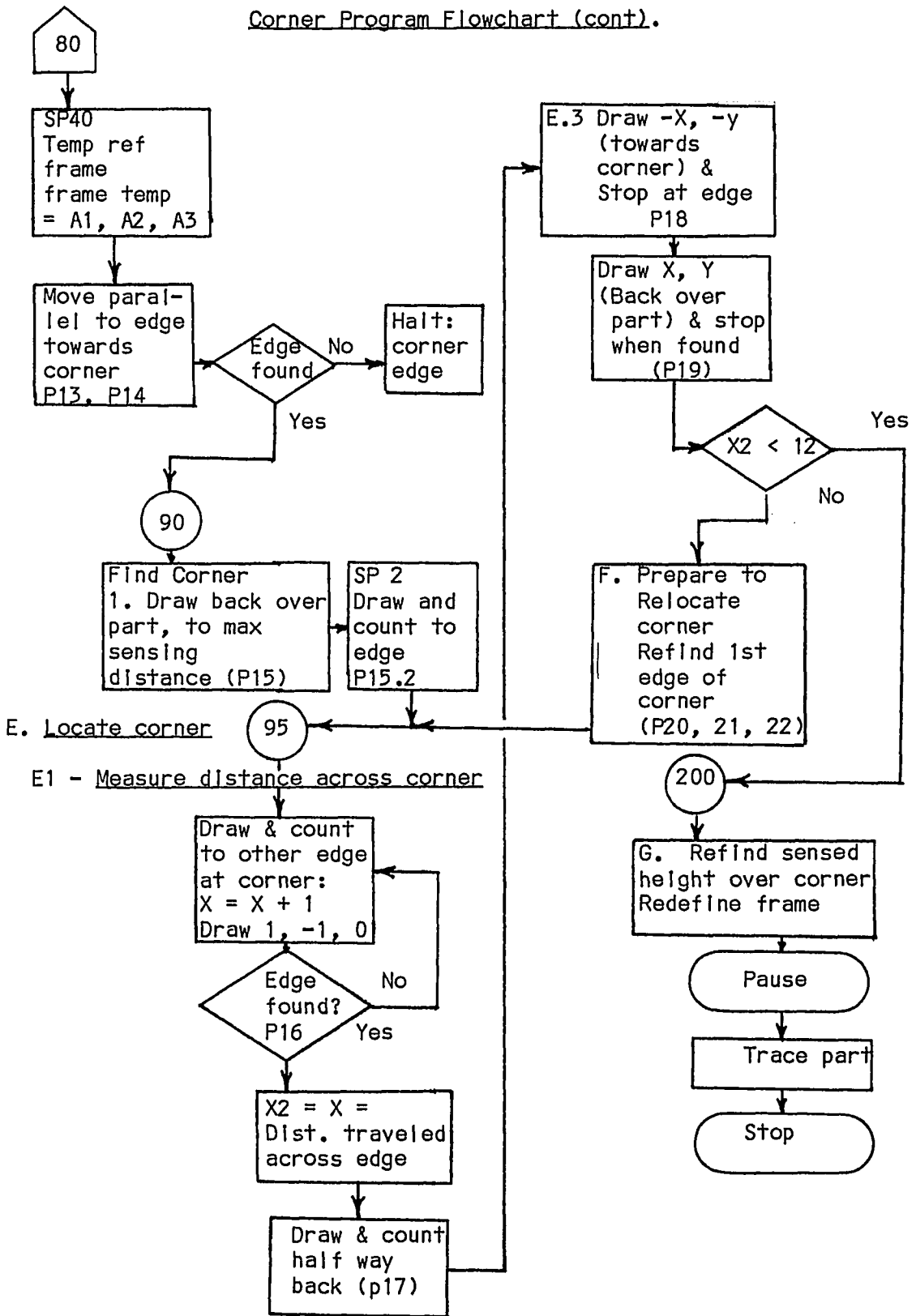
Refind edge at max sensor height
SP = 1
1. Draw back over part until edge sensed (P8)
2. Draw over then above max. height P9
3. Draw down until part sensed (P10)
4. Draw back over edge (A2)



Draw -X (toward part center)
look for another point on edge
Draw -X (P12.1)
Draw -Y (P12.1)



Corner Program Flowchart (cont).



APPENDIX E

Corner Finding Routine Program Listing

Run Procedure

1. LOAD HAYS
2. SP 25
3. TOOL SENSOR
4. DO MOVE A
5. position plate under sensor so sensor is near center of plate
and almost touching.
6. EXECUTE S

The locations in the trace routine in section G can be changed after executing the FRAME PART = A1, A2, A3 line. The locations can be reassigned by using HERE PART: P1, etc.

PROGRAM S
REM REV 10 19APR83

A *** FIND SURFACE OF PART ***

S SP 50
TOOL SENSOR
APPRD A 10
TYPE P1
REACTI 1 S1 ALWAYS
SP 10
SETI P=2
DRAW 0 0 -10

B *** FIND POINT CLOSE TO EDGE ONE ***

PAUSE TARGET NOT FOUND ON.1ST APPROACH
SP 40 ALWAYS
DRAW 0 0 -2
TYPE P3
SETI P=4
REACTI 2 S1 ALWAYS
DRAW 0 90 0
PAUSE EDGE 1 NOT FOUND
SP 40
DRAW 0 -5 0
REACTI 2 S1 ALWAYS
DRAW 0 0 15
PAUSE
TYPE P5
SP 1
REACTI 1 S1 ALWAYS
DRAW 0 0 -10
PAUSE TARGET NOT FOUND
SP 40 ALWAYS
HERE A3
TYPE A3

C *** FIND FIRST POINT ON EDGE TWO ***

C1*** MOVE TO A AND ADJUST HEIGHT

DRAW 0 0 -2
MOVE A
REACTI 2 S1 ALWAYS
DRAW 0 0 15
PAUSE
REACTI 1 S1 ALWAYS
SP 10
DRAW 0 0 -10
PAUSE PART AT P6.2 NOT FOUND
DRAW 0 0 -2
SP 40 ALWAYS
SETI P=7
REACTI 2 S1 ALWAYS
DRAW 0 -100 0

```

    PAUSE EDGE 2 NOT FOUND
    SETI S=4
40 SP 1
    REACTI 1 S1 ALWAYS
    DRAW 0 10 0
    FAUSE
    TYPE P8
    TYPEI S
    SP 10
    DRAW 0 4 0
    REACTI 2 S1 ALWAYS
    DRAW 0 0 15
    FAUSE
    SETI F=9
    REACTI 1 S1 ALWAYS
    SP 1 ALWAYS
    DRAW 0 0 -10
    FAUSE
    TYPE P10
    DRAW 0 -4 0
    IF S NE 4 THEN 50
    HERE A2
    TYPE A2
    GOTO 60
    50 IF S NE 5 THEN 60
    HERE A1
    TYPE A1
    GOTO 80

D *** FIND TEMPORARY ORIGIN POINT ON EDGE TWO ***
60 SP 40 ALWAYS
65 DRAW 0 10 -3
    TYPE P11
    SETI S=5
    TYPEI S
    SETI F=121
    REACTI 2 S3 ALWAYS
    DRAW -30 0 0
    SETI F=122
    REACTI 2 S4 ALWAYS
    DRAW 0 -50 0
    FAUSE SECOND POINT ON EDGE (P12) NOT FOUND
    GOTO 40

80 REM TEMP REF FRAME
    TYPE TEMP FRAME
    FRAME TEMP = A1 A2 A3
    SP 40 ALWAYS
    MOVE TEMP B
    TYPEI F=13

```



```

REACTI 2 S1 ALWAYS
SETI P=14
MOVE TEMP C
HALT CORNER EDGE NOT FOUND

90 REM FIND CORNER
SP 2
REACTI 1 S1 ALWAYS
DRAW 20 0 0
FAUSE
DRAW 3 0 0
REACTI 2 S1 ALWAYS
DRAW 0 0 15
FAUSE
SETI P=15
REACTI 1 S1 ALWAYS
SP 2 ALWAYS
DRAW 0 0 -15
FAUSE
DRAW 0 0 -2

REM REFINDE EDGE
SETI P=151
REACTI 2 S1 ALWAYS
DRAW -10 0 0
FAUSE P15.1 NOT FOUND
SETI X = 0
REACTI 1 S1 ALWAYS
93 SETI X = X + 1
DRAW 1 -1 0
GOTO 93
TYPE P15.2
95 SETI P=16

E *** LOCATE CORNER ***
E1*** MEASURE DISTANCE ACROSS CORNER ***
*** COUNT AND DRAW ***
REACTI 2 S1 ALWAYS
100 SETI X=X+1
DRAW 1 -1 0
GOTO 100
SETI X1=X/2
SETI X2=X

E2*** DRAW HALF WAY BACK ACROSS CORNER ***
115 DRAW -1 1 0
SETI X=X-1
IF X GT X1 THEN 115
TYPE P17
TYPE X2 = DISTANCE TRAVELED ACROSS CORNER
TYPEI X2

```

```

E3*** DRAW TOWARDS CORNER ***
  REACTI 2 S1 ALWAYS
  SETI F=18
  DRAW -10 -10 0
  FAUSE
  SETI F=19
  REACTI 1 S1 ALWAYS
  DRAW 10 10 0
  FAUSE
  REM REFINO CORNER IF DISTANCE ACROSS CORNER IS => 12
  IF X2 LT 12 THEN 200
130 REACTI 1 S5 ALWAYS

  F *** PREPARE TO RELOCATE CORNER ***
    SETI F=20
    DRAW -20 20 0
    SETI F=21
140 DRAW -20 -20 0
    FAUSE F20 21 NOT FOUND
    GOTO 145
    FAUSE
    GOTO 145
145 SETI S=6
    SETI F=22
    SETI X=0
    REACTI 1 S1 ALWAYS
150 SETI X=X+1
    DRAW 1 -1 0
    GOTO 150
    GOTO 95

  G*** REFINO SENSE HEIGHT ***
200 REM CORNER FOUND
  TYPE P = 23
  DRAW 2 2 0
  REACTI 2 S1 ALWAYS
  DRAW 0 0 15
  FAUSE
  SETI P = 24
  REACTI 1 S1 ALWAYS
  DRAW 0 0 -15
  FAUSE
  TYPE P = 25
  DRAW -2 -2 0
  HERE A1
  FRAME PART A1 A2 A3
  TYPE PART FRAME FOUND ENTER PR TO PROCEED
  FAUSE TO TRACE PART OUTLINE
  SP 40 ALWAYS
  MOVES PART P1
  HERE B1
  DELAY 2

```

```
MOVES PART P2
HERE B2
DELAY 2
MOVES PART P3
HERE B3
DELAY 2
MOVES PART P4
HERE B4
DELAY 2
TYPE PART TRACED ENTER LISTL TO DISPLAY POINTS P1 P4 RECORDEI
PAUSE ENTER PR TO REFINDE CORNER
GOTO 5
```

```
PROGRAM S1
  IGNORE 1 ALWAYS
  IGNORE 2 ALWAYS
  TYPEI P
  RETURN 2
```

```
PROGRAM S2
  IGNORE 1 ALWAYS
  IGNORE 2 ALWAYS
  TYPEI P
  RETURN 3
```

```
PROGRAM S3
  IGNORE 2 ALWAYS
  TYPEI P
  RETURN 5
```

```
PROGRAM S4
  IGNORE 2 ALWAYS
  TYPEI P
  RETURN 2
```

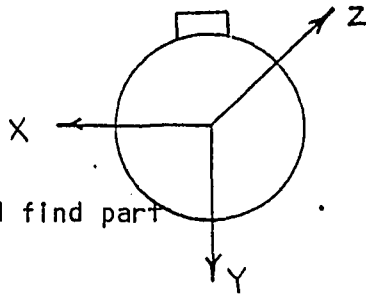
```
PROGRAM S5
  IGNORE 2 ALWAYS
  TYPEI P
  RETURN 4
```

APPENDIX F

Hole Finding Routine Path Diagram

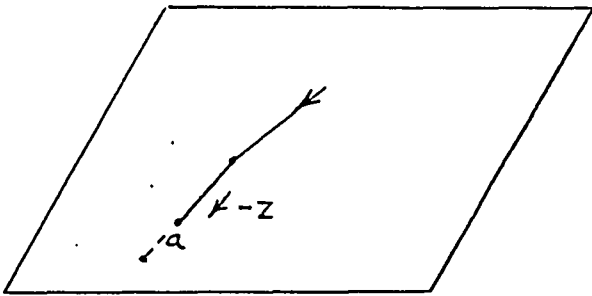
Program Hole

A. Approach and find part



Robot Orientation

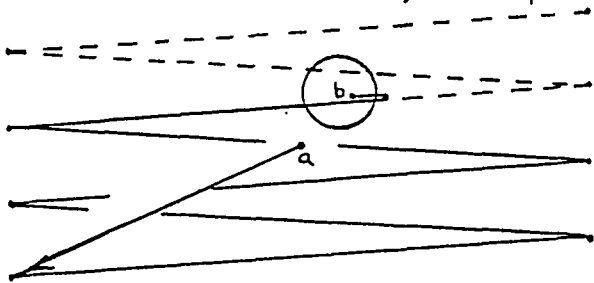
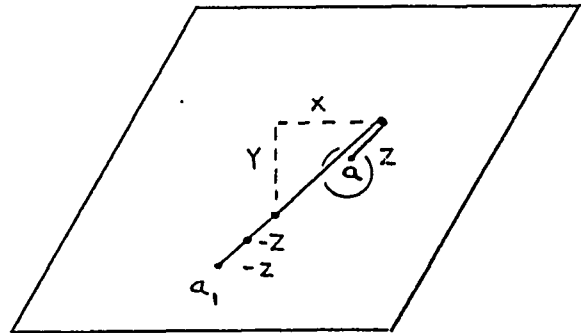
A1. If part not found, GOSUB REFIND



Point Hole (on part)

B. Search for Hole In XY plane

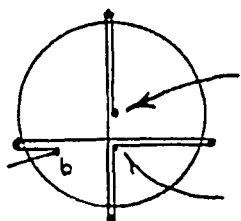
C. When hole sensed, back-up and stop on hole (b)



D. Refind hole edge, then fine hole center.

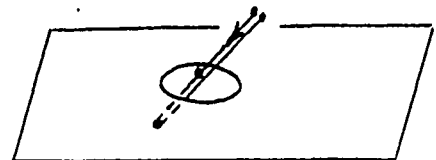
Program Find

A. GOSUB HOLE
B. Insert sensor into found hole



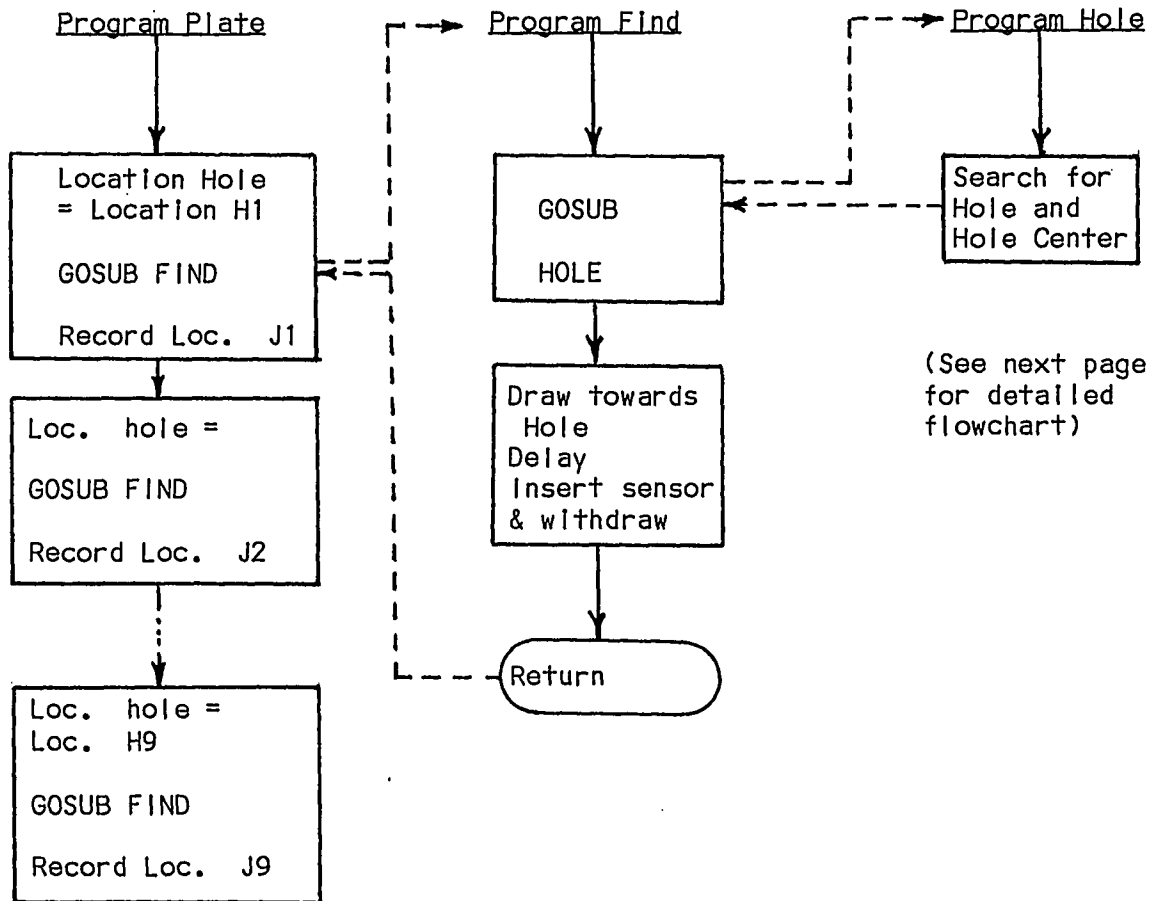
Y-Center found

X-Center found



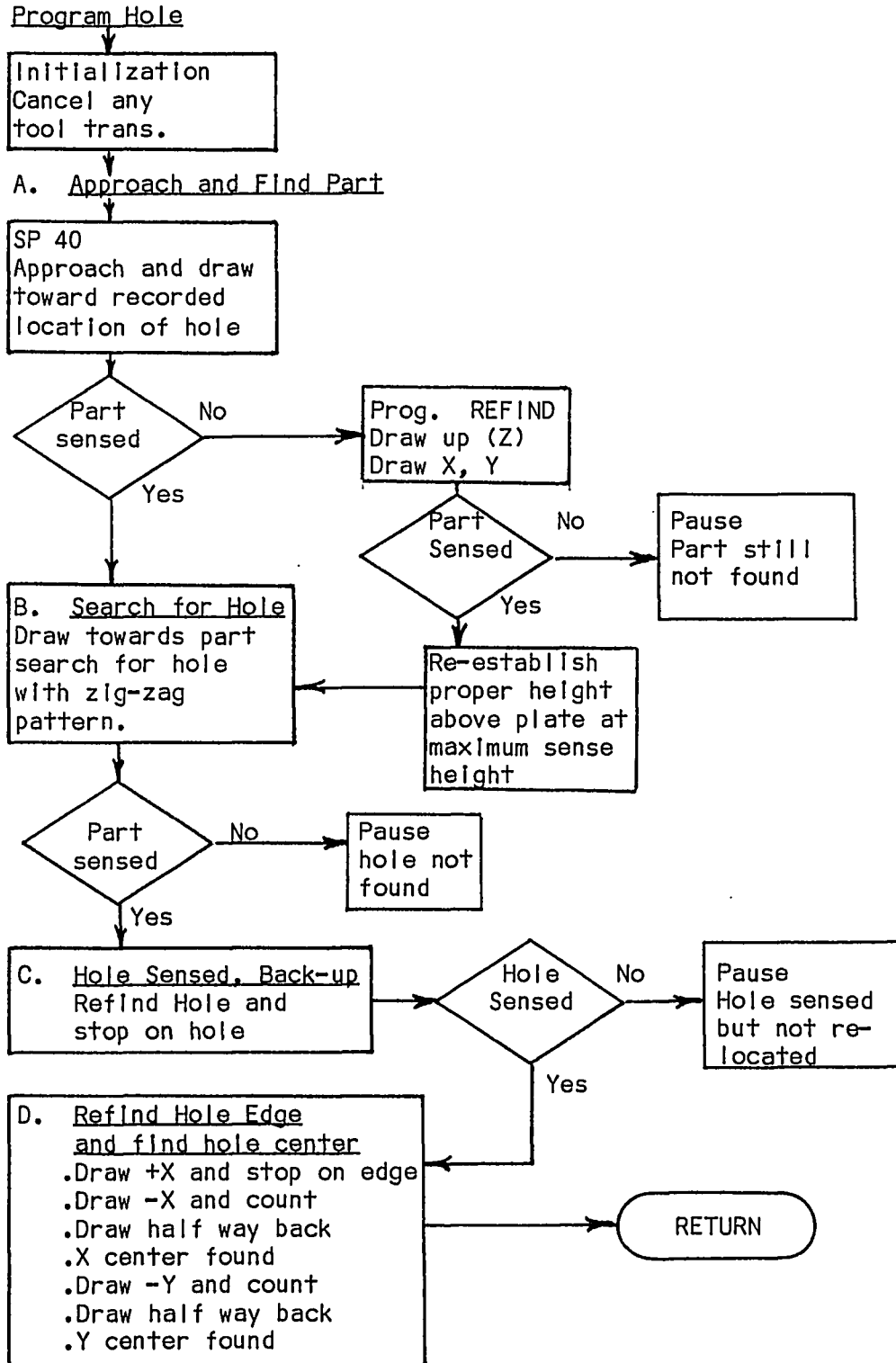
APPENDIX G

Hole Finding Program General Flowchart



APPENDIX H

Hole Finding Program Flow Chart



APPENDIX I

Hole Finding Routine Program Listing

Run Procedure

1. LOAD HAYS
2. SP 25
3. TOOL
4. DO MOVE H1
5. position the plate under the sensor with the sensor near the hole.
6. repeat 4 and 5 for hole H2
7. EXECUTE PLATE

The hole locations can be redefined by using TE H1 to teach up to 9 hole locations.

PROGRAM HOLE
REM REV 4 21APR83

TOOL

A *** APPROACH AND FIND PART ***

5 SF 40 ALWAYS
APPRO HOLE 15
SETI P=1
REACTI 1 S8 ALWAYS
SF 10
DRAW 0 0 -12

A1*** IF PART NOT FOUND (IE HOLE FOUND) GOSUB REFINO (PART) ***

GOSUB REFINO
REM SEARCH FOR HOLE
SF 10
DRAW 0 0 -10
SF 30

B *** SEARCH FOR HOLE ***

REACTI 2 S6 ALWAYS
DRAW 15 -10 0
DRAW -30 2 0
DRAW 30 2 0
DRAW -30 2 0
DRAW 30 2 0
DRAW -30 2 0
DRAW 30 2 0
DRAW -30 2 0
DRAW 30 2 0
DRAW -30 2 0
PAUSE HOLE NOT FOUND
GOTO 40
GOTO 30
GOTO 40
GOTO 30
GOTO 40
GOTO 30
GOTO 40
GOTO 30
GOTO 40

C *** HOLE SENSEO- BACK-UP AND STOP ON HOLE ***

30 REACTI 2 S7 ALWAYS
DRAW 10 0 0
PAUSE C- HOLE SENSEO BUT NOT RELOCATED
GOTO 70

40 REACTI 2 S7 ALWAYS
DRAW -10 0 0
PAUSE C- HOLE SENSEO BUT NOT RELOCATED

70 REM D *** REFINO HOLE EDGE AND FIND CENTER ***
TYPE DISTANCE TRAVELED ACROSS HOLE (MM) = X/100 (OR Y/100)

SF 1
REACTI 1 S8 ALWAYS
DRAW 10 0 0
PAUSE HOLE EDGE X NOT FOUND
DRAW -2 0 0
SETI X=200
REACTI 1 S9 ALWAYS
90 DRAW -19 0 0


```

      SETI X=X+19
      GOTO 90
      TYPEI X
      SETI XC = X/2
95  DRAW 19 0 0
      SETI X=X-19
      IF X GT XC THEN 95
100 TYPE X CENTER FOUND
      REACTI 1 S8 ALWAYS
      DRAW 0 10 0
      PAUSE HOLE EDGE Y NOT FOUND
      DRAW 0 -2 0
      SETI Y=200
      REACTI 1 S9 ALWAYS
110 DRAW 0 -19 0
      SETI Y=Y+19
      GOTO 110
      TYPEI Y
      SETI YC=Y/2
120 DRAW 0 19 0
      SETI Y=Y-19
      IF Y GT YC THEN 120
      TYPE Y CENTER FOUND
      RETURN 0
PROGRAM S6
      IGNORE 2 ALWAYS
      TYPE HOLE SENSED
      SP 2 ALWAYS
      RETURN 9
PROGRAM S7
      IGNORE 2 ALWAYS
      TYPE HOLE FOUND NOW LOCATING CENTER
      RETURN 2
PROGRAM H
      REV 1 20MAR83
      SET HOLE =H1
      GOSUB HOLE
      HERE HOLE1
      SET HOLE =H2
      GOSUB HOLE
      HERE HOLE2
      STOP      OR REM
      FRAME SHEET = HOLE1 HOLE2 HY
      SP 35
      MOVES SHEET
      MOVES SHEET H3
      DELAY 2
      MOVES SHEET H4
      STOP
PROGRAM REFINO
      TYPE PART NOT FOUND. SEARCH FOR PART
      *** MOVE UP OVER AND DOWN TO REFINO ***
      DRAW 0 0 2
      REACTI 1 S1 ALWAYS
      DRAW -10 10 0

```

```

PAUSE PART STILL NOT FOUND
REACTI 2 S1 ALWAYS
DRAW 0 0 10
REACTI 1 S1 ALWAYS
DRAW 0 0 -5
PAUSE
DRAW 0 0 -2
RETURN 0
PROGRAM PLATE
TYPE USE PANIC BUTTON AND R-ENTRY TO STOP + CONTINUE
SET HOLE=H1
GOSUB FIND
HERE J1
SET HOLE=H2
GOSUB FIND
HERE J2
SET HOLE=H3
GOSUB FIND
HERE J3
SET HOLE=H4
GOSUB FIND
HERE J4
===
SET HOLE=H9
GOSUB FIND
HERE J9
PROGRAM FIND
REM FIND HOLE AND INSERT SENSOR INTO HOLE
GOSUB HOLE
REM      OR RET
DRAW 0 0 -3
DELAY 2
DRAW 0 0 -3
DRAW 0 0 6
RETURN 0
PROGRAM S8
IGNORE 1 ALWAYS
RETURN 2
PROGRAM S9
IGNORE . ALWAYS
RETURN 3

```

VITA

Paul L. Hays was born on May 5, 1949 in Summit, New Jersey to Alfreda and James B. Hays. He earned a degree of Bachelor of Science in Industrial Engineering at Northeastern University in 1974. He is currently employed by Pitney Bowes in Stamford, CT, as a Manager of Robot Automation.